

The process of scientific discovery is, in effect, a continual flight from wonder.

Albert Einstein

University of Alberta

Analysis of Bacterial Surface Properties using Atomic Force Microscopy

by

Loredana Stefania Dorobantu

A thesis submitted to the Faculty of Graduate Studies and Research

in partial fulfillment of the requirements for the degree of

Doctor of Philosophy

in

Chemical Engineering

Department of Chemical and Materials Engineering

©Loredana Stefania Dorobantu

Fall 2009

Edmonton, Alberta

Permission is hereby granted to the University of Alberta Libraries to reproduce single copies of this thesis and to lend or sell such copies for private, scholarly or scientific research purposes only. Where the thesis is converted to, or otherwise made available in digital form, the University of Alberta will advise potential users of the thesis of these terms.

The author reserves all other publication and other rights in association with the copyright in the thesis and, except as herein before provided, neither the thesis nor any substantial portion thereof may be printed or otherwise reproduced in any material form whatsoever without the author's prior written permission.

Examining Committee

Murray R. Gray, Chemical and Materials Engineering, University of Alberta

Julia M. Foght, Biological Sciences, University of Alberta

Subir Bhattacharjee, Mechanical Engineering, University of Alberta

Janet A. W. Elliott, Chemical and Materials Engineering, University of Alberta

Nathalie Tufenkji, Chemical Engineering, McGill University

ABSTRACT

The morphology and physicochemical properties of bacterial cells at the molecular level influence their adhesion to surfaces and interfaces. In this study, atomic force microscopy (AFM) was used to explore the morphology of soft, living cells in aqueous buffer, to map bacterial surface heterogeneities, to directly correlate the results in the AFM force distance curves to the macroscopic properties of the microbial surfaces, and to model the experimental AFM force curves using classical Derjaguin-Landau-Verweij-Overbeek (DLVO) theory of colloidal stability. The surfaces of two bacterial species exhibiting different macroscopic surface hydrophobicity, measured as the oil/water contact angle (Θ): *Acinetobacter venetianus* RAG-1 ($\Theta = 56.4^\circ$) and *Rhodococcus erythropolis* 20SE1c ($\Theta = 152.9^\circ$) were probed with chemically functionalized AFM tips, terminated in hydrophobic and hydrophilic groups. All force measurements were obtained in contact mode and made on a location of the bacterium selected from the tapping mode image. AFM imaging revealed morphological details of the microbial-surface ultrastructures with about 20 nm resolution. The heterogeneity in surface morphology was directly correlated with differences in adhesion forces as emphasized by retraction force curves and also with the presence of external structures, either pili or capsules, as confirmed by transmission electron microscopy. The AFM retraction force curves for *A. venetianus* RAG-1 and *R. erythropolis* 20S-E1-c showed differences in the interactions of the external structures with hydrophilic and hydrophobic tips. *A. venetianus* RAG-1 exhibited an asymmetrical pattern with multiple adhesion peaks suggesting the existence of biopolymers with different lengths on its surface. *R. erythropolis* 20S-E1-c showed long-range attraction forces accompanied by single rupture events

indicating a more hydrophobic and smoother surface. The magnitude of the adhesion forces was proportional to the water contact angle on the two bacterial lawns. The experimental force curves between the two microbial cells and functionalized AFM probes presented discrepancies when compared to the classical DLVO theory. Therefore, an extended DLVO model incorporating an acid–base component to account for attractive hydrophobic interactions and repulsive hydration effects was used to assess the additional interactions. Extended DLVO predictions agreed well with AFM experimental data for both *A. venetianus* RAG-1, whose surface consists of an exopolymeric capsule and pili, and *R. erythropolis* 20S-E1-c, whose surface is covered by mycolic acids as well as an exopolymeric capsule. The extended model for the bacteria-AFM tip interactions was consistent with the effects of acid base and steric forces, in addition to classical DLVO theory.

ACKNOWLEDGEMENTS

First of all, I would like to acknowledge the support of my thesis supervisor, Professor Murray Gray. Thank you Dr. Gray for all the wonderful opportunities you have given me throughout my graduate studies. I truly appreciate everything you have done for me.

Special thanks go to my research committee members, Professor Julia Foght and Professor Subir Bhattacharjee for thoughtful discussions and helpful suggestions which have been invaluable in further fulfillments of my research objectives.

It gives me pleasure to thank Professor Nathalie Tufenkji for being the external member of my defense committee and for her valuable advice regarding thesis revision.

Numerous people made invaluable contributions to the progress of my research project. Many thanks deserve Tuyet Le, Dr. Xiaoli Tan, Tania Rizwan, Zenghe Kang, Maryam Zargarzadeh, Andree Koenig, and Leanne Swekla.

I wish to extend my sincere gratitude to my family for their continued support, encouragement and of course, incredible patience.

This thesis is humbly dedicated to the memories of my mother Georgeta and grandmother Victoria. I miss you both very much!

TABLE OF CONTENTS

1. INTRODUCTION.....	1
1.1 Background.....	1
1.2 Specific research objectives and thesis overview.....	4
2. LITERATURE REVIEW.....	6
2.1 Role of Microorganisms in Hydrocarbon Degradation.....	6
2.1.1 Bioremediation of Petroleum Hydrocarbons.....	6
2.1.2 Bioprocessing of Petroleum Hydrocarbons.....	7
2.1.3 Bioavailability of Hydrophobic Substrates.....	8
2.1.4 Mechanisms of Hydrocarbon Transport towards Microbial Cells.....	9
2.1.5 Advantages of Bioremediation and Bioprocesses.....	10
2.2 Bacterial Adhesion to Surfaces and Interfaces.....	11
2.2.1 Bacterial Cell Envelope.....	14
2.2.1.1 Gram-negative Bacteria.....	15
2.2.1.2 Gram-positive Bacteria.....	17
2.2.2 Cell Surface External Appendages.....	19
2.2.2.1 Bacterial Capsule and Slime Layers.....	19
2.2.2.2 Pili and Flagella.....	19

2.3	Macroscopic Cell Surface Properties.....	20
2.3.1	Cell Surface Hydrophobicity.....	20
2.3.2	Cell Surface Charge.....	21
2.4	Atomic Force Microscopy.....	21
2.4.1	Basic Theory of Atomic Force Microscopy.....	22
2.4.2	Force Curve Analysis.....	23
2.4.3	AFM in Biological Systems.....	26
2.4.4	Probe Modification.....	28
2.4.5	Immobilization of Bacteria for AFM Characterization...	29
2.5	Equations Governing the Force Interactions.....	30
2.5.1	DLVO Theory of Colloidal Stability.....	31
2.5.1.1	Electrostatic Interactions.....	31
2.5.1.2	Van der Waals Interactions.....	34
2.5.2	DLVO Theory Applied to Microbial Systems.....	37
2.5.3	Schematic of DLVO Interactions.....	38
2.5.4	Extended DLVO Theory.....	41
2.5.5	Steric Forces.....	42
2.5.6	Soft-particle DLVO Theory.....	43
3.	MATERIALS AND METHODS.....	45
3.1	Microorganisms and Growth Conditions.....	45
3.2	Cell Immobilization for AFM Measurements.....	45
3.3	Functionalization of AFM Tips.....	46
3.4	Imaging of Bacterial Cells with AFM.....	47

3.5	Force Analysis on Bacterial Surfaces Using AFM.....	48
3.6	Zeta Potential Measurements.....	49
3.7	Transmission Electron Microscopy of Bacterial Cells	50
3.8	Contact Angle Measurements.....	50
4.	Atomic Force Microscopy Measurement of Heterogeneity in Bacterial Surface Hydrophobicity	52
4.1	Introduction.....	52
4.2	Microbial Characterization: Ultrastructure and Morphology.....	55
4.3	Force Measurements.....	65
4.4	Discussion	73
5.	Analysis of Force Interactions between AFM Tips and Hydrophobic Bacteria using DLVO Theory.....	80
5.1	Introduction.....	80
5.2	Mathematical Modeling.....	85
5.2.1	Determination of Hamaker Constant	86
5.2.2	DLVO Model.....	86
5.2.3	Extended DLVO Models	88
5.2.4	Steric Model	89
5.3	Physicochemical Surface Properties Used for DLVO Interaction Calculations.....	90

5.4	Modeling of the AFM Approach Curves	92
5.4.1	Glass Interaction with the Gold AFM Tip in 0.001M KCl Solution.....	94
5.4.2	Modeling of Bacteria-Modified AFM Tip Interactions in 0.1M phosphate buffer.....	96
5.4.3	Significance of the Parameters Obtained from the Extended DLVO Fitting to the Steric Model.....	99
5.5	Discussion.....	102
6.	IMPLICATIONS OF THE CURRENT STUDY.....	110
6.1	Bacterial Positioning at the Oil/Water Interface.....	112
6.2	Separation of Bacteria from the Oil/Water Interface Revealed by AFM Experiments.....	117
6.3	Mass Transfer across the Oil/Water Interface.....	125
6.3.1	Bacterial Colonization of an Oil/Water Interface.....	125
6.3.2	Hydrocarbon Transport towards Microbial Cells.....	126
7.	CONCLUSIONS AND RECOMMENDATIONS.....	144
7.1	Conclusions.....	144
7.2	Directions for Future Work.....	147
8.	REFERENCES.....	151

APPENDIX A	167
A.1 Representative AFM retraction curves taken on <i>A. venetianus</i> RAG-1 (a) and <i>R. erythropolis</i> 20S-E1-c (b) surfaces in phosphate buffer with the hydrophobic tip.....	167
A.2 Representative AFM retraction curves taken on <i>A. venetianus</i> RAG-1 (a) and <i>R. erythropolis</i> 20S-E1-c (b) surfaces in phosphate buffer with the hydrophobic tip.....	168
A.3 Representative AFM retraction curves taken on <i>A. venetianus</i> RAG-1 (a) and <i>R. erythropolis</i> 20S-E1-c (b) surfaces in phosphate buffer with the hydrophilic tip.....	169
A.4 Zeta potential of <i>A. venetianus</i> RAG-1 measured in solutions of various electrolyte concentrations.....	170
A.5 Zeta potential of <i>R. erythropolis</i> 20SE1c measured in solutions of various electrolyte concentrations.....	171
A.6 <i>A. venetianus</i> RAG-1 length measured from AFM height images.....	172
A.7 <i>A. venetianus</i> RAG-1 width measured from AFM height images.....	173
A.8 <i>A. venetianus</i> RAG-1 height image taken in tapping mode..	174
A.9 <i>R. erythropolis</i> 20SE1c length measurements.....	175
A.10 <i>R. erythropolis</i> 20SE1c width measurements.....	176

LIST OF TABLES

Table 2.1	Surface tension components (γ_L^{LW} and γ_L^{AB}) and parameters of γ_L^{AB} (γ_L^+ and γ_L^-), mJ/m ² , for the most commonly used high-energy contact angle liquids....	36
Table 5.1	Summary of parameters used for DLVO interaction calculations.....	90
Table 5.2	Summary of quantitative data resulted from fitting the XDLVO theory to the experimental AFM force curve (approach) for <i>A.venetianus</i> RAG-1 and <i>R.erythropolis</i> 20S-E1-c interacting with both hydrophobic and hydrophilic AFM tips.....	101
Table 6.1	Parameters obtained for the case <i>A. venetianus</i> RAG-1 and <i>R. erythropolis</i> 20SE-1-c partitioning at the oil/water interface.....	142
Table 6.2	Parameters obtained for the case when <i>A. venetianus</i> RAG-1 is immersed in the water phase and <i>R. erythropolis</i> 20SE-1-c is immersed in the oil phase.....	143

LIST OF FIGURES

Figure 2.1	Critical steps involved in cell attachment - convective transport, diffusion, attachment, and resistance to detachment.....	13
Figure 2.2	Schematic representation of a typical cell envelope of Gram-negative bacteria.....	16
Figure 2.3	Typical cell envelope of Gram-positive bacteria.....	18
Figure 2.4	Force distance curve obtained on <i>A. venetianus</i> RAG-1 surface which possesses extracellular structures.....	25
Figure 2.5	AFM height image of <i>A. venetianus</i> RAG-1 showing surface detail.	27
Figure 2.6	DLVO plot showing electrostatic, van der Waals, and total potential between a flat plate and a sphere.....	40
Figure 4.1	(a) <i>A. venetianus</i> RAG-1 AFM phase image taken in phosphate buffer with the hydrophilic tip; (b) and (c) <i>A. venetianus</i> RAG-1 AFM phase and amplitude images taken in phosphate buffer with the hydrophobic tip.....	57
Figure 4.2	(a) <i>R. erythropolis</i> 20S-E1-c AFM phase image; (b) <i>R. erythropolis</i> 20S-E1-c AFM amplitude image. (c) Adhesion force map for the surface of one cell of <i>R. erythropolis</i> 20S-E1-c.....	61

Figure 4.3	Transmission electron micrographs; (a) Thin sections of <i>A. venetianus</i> RAG-1, negatively stained, with pili extending from the cell surface (scale bar = 200 nm); <i>A. venetianus</i> RAG-1 (b) and <i>R. erythropolis</i> 20S-E1-c (c) surrounded by capsule.....	64
Figure 4.4	Typical results from AFM force measurements. Panel (a) represents the approach curves while panel (b) indicates the retraction curves.....	67
Figure 4.5	Force distribution histogram for <i>A. venetianus</i> RAG-1 (a) and <i>R. erythropolis</i> 20S-E1-c (b) interacting with the hydrophobic tips in PBS.....	69
Figure 4.6	(a) Distribution of adhesion forces over <i>A.venetianus</i> RAG-1 surface on a representative cell and the corresponding bacterial image (c) showing the locations where the forces were measured. (b) Distribution of adhesion forces over <i>R. erythropolis</i> 20S-E1-c surface on a representative cell and the corresponding bacterial image (d) showing the locations where the forces were measured.....	72
Figure 5.1	Modeling of the approach curves for <i>A.venetianus</i> RAG-1 and <i>R.erythropolis</i> 20S-E1-c interacting with the hydrophobic (a and c) or the hydrophilic (b and d) AFM probes in 0.1M PBS.....	93
Figure 5.2	Approach curve between unmodified AFM probe and cleaned glass surface in 0.001M KCl solution.....	95

Figure 5.3	Modeling of the approach curves for <i>A.venetianus</i> RAG-1 interacting with the hydrophobic AFM probe.....	98
Figure 5.4	Schematic representation of the interaction between an adhering cell possessing exopolymeric capsule and pili, and the thiol coated AFM probe.....	107
Figure 6.1	Schematic showing the deformation of the interface z_i and particle height immersed in the oil phase z_0	111
Figure 6.2	<i>R. erythropolis</i> 20S-E1-c assumed to be spherical with radius r and contact angle θ in equilibrium at the oil/water interface leveled at $z = 0$ far from the microorganism.....	114
Figure 6.3	<i>A. venetianus</i> RAG-1 assumed to be spherical with radius r and contact angle θ in equilibrium at the oil/water interface leveled at $z = 0$ far from the microorganism.....	116
Figure 6.4	Representative <i>A. venetianus</i> RAG-1 approach curve used to set the lower limit for δ	118
Figure 6.5	Representative <i>A. venetianus</i> RAG-1 retraction curve used for conversion into energy.....	119
Figure 6.6	Energy vs separation distance for <i>A. venetianus</i> RAG-1.....	120
Figure 6.7	Representative approach force curve for <i>R. erythropolis</i> 20S-E1-c used to determine the lower bound for δ	122
Figure 6.8	Representative retraction force curve for <i>R. erythropolis</i> 20S-E1-c used for conversion into energy.....	123
Figure 6.9	Energy vs distance curve for <i>R. erythropolis</i> 20S-E1-c.....	124

Figure 6.10	Schematic of mass transfer resistances for transport of hydrocarbons to a bacterial cell.....	127
Figure 6.11	<i>A. venetianus</i> RAG-1 positioning at the oil/water interface based on a contact angle of 56°	131
Figure 6.12	<i>A. venetianus</i> RAG-1 immersed in water with pili extending in the oil phase.....	133
Figure 6.13	Spherical cells packed on a plane surface.....	135
Figure 6.14	<i>R. erythropolis</i> 20SE-1-c positioning at the oil/water interface based on its contact angle.....	137
Figure 6.15	<i>R. erythropolis</i> 20SE-1-c completely immersed in the oil phase.....	139
Figure 7.1	Amplitude AFM image of <i>P. florescence</i> LP6a surrounded by an extracellular capsule.....	148

1. INTRODUCTION

1.1 Background

The use of microorganisms in remediation of oil spills is an important *in situ* technology considered to be the most environmentally sound, least intrusive and cheapest of the new technologies in this field.[1] However, the very low water solubility of crude oil present challenges to bacteria using petroleum as a growth substrate.[3] A common adaptation for overcoming the poor aqueous solubility of the hydrocarbons and an important step for successful bioprocesses represents the attachment of bacteria to the oil/water interface, at the surface of oil droplets suspended in water.[4] Even though extensive research has been done on bacterial adhesion in the last decade,[5] the fundamental mechanism governing this process is not well understood and clearly defined.[6] An accurate quantification of the physico-chemical properties of microbial surfaces is fundamental to reach a better understanding of bacterial adhesion to a surface or interface.[7]

The focus of this thesis is on the nanoscale investigation of microbial adhesion towards hydrophobic and hydrophilic surfaces. The surface behavior of microbial cells has historically been described in terms of macroscopic surface properties starting with the pioneering observations by Mudd and Mudd [8, 9] of bacterial partitioning at oil/water interfaces. These studies suggest that microorganisms possessing different degree of surface hydrophobicity can position on one side or the other of the oil/water interface.

Macroscopic cell-surface properties have been commonly inferred from water contact angle measurements on bacterial lawns deposited on membrane filters [10, 11], from bacterial adhesion to hydrocarbons [12] or from zeta potential

measurements.[13] These measurements result in average cell surface properties and do not provide information about the forces governing the adhesion process at the molecular scale.[7, 14]

The electron microscopy techniques such as transmission electron microscopy (TEM) and scanning electron microscopy (SEM) have been used traditionally to observe the morphology of bacterial cells. While these approaches can provide high resolution images, the extensive sample preparation, which consists of treatments with heavy metals to enhance contrast and make structures visible and the requirement for the sample to be under vacuum, limits its application in visualization under physiological conditions.[4]

Atomic force microscopy (AFM) offers new perspectives for obtaining the morphology of biological surfaces and localized physicochemical properties by means of imaging and force-distance curves.[15, 16] For example, AFM allows probing of surface charge, hydrophobicity, and mechanical properties of living microorganisms in their physiological environments, without chemical preparation and with nanometer resolution, providing information that is complementary to that obtained using macroscopic techniques.[15, 17]

AFM also permits quantitative determination of the nanoscale interaction forces between the probe tip and a cell by means of force-distance curves.[18] In particular, force-distance curves, which record the variation of interaction forces as the AFM tip approaches the cell surface, makes contact and then retrieves from it, allow the direct measurement of surface forces in aqueous environments and determine whether classical DLVO theory of colloidal stability, or other kinds of interactions dominate force measurements.[7]

Application of the DLVO theory to microbial cells usually involves the assumption that they are inert, perfectly smooth, with no asperities or surface

structures.[19] Living organisms such as bacterial cells are capable of producing extracellular specific structures such as capsules or slime layers of polysaccharides [20] and protein-based appendages, namely pili, [21] whose structure and chemistry facilitate microorganism's adhesion to different types of surfaces and interfaces.[20]

As a result, the force curves taken on bacterial surfaces are expected to involve specific biological polymer interactions and raise the discrepancy between the experimental curves and classical DLVO theory of colloidal stability.[22]

In an attempt to account for the presence of polymeric structures on bacterial cell surfaces, polymer interactions have been introduced into the model in addition to DLVO forces for the interpretation of AFM force measurements.[23] The polymer force arises from contact between the AFM probe and the extracellular structures extending from the microorganism surface into solution; as the AFM tip pushes down on the cell, the polymers rearrange into a more compact spatial arrangement.[19, 24] These polymer interactions can be attractive or repulsive. Jucker et al.[25] have proposed that steric repulsion arises from the higher affinity of the bacterial polymers for the aqueous medium than for the solid surface (e.g., the AFM probe tip). Polymer attraction or bridging has been proposed [25] to take place when the microbial surface polymers have a higher affinity for the solid surface than for the liquid medium and are long enough to bridge the distance from the bacterial cell to the solid surface.[26] Bridging is generally observed for solids and microorganisms that are both hydrophobic.[27]

1.2 Specific research objectives and thesis overview

The overall goal of this project was to study bacteria, characterized by different degrees of surface hydrophobicity, with respect to their interactions with hydrophobic and hydrophilic modified surfaces. This work was done in two parts, with specific objectives stated as follows:

1. The hypothesis underlying the first part of this thesis was that microbial cells are heterogeneous in terms of hydrophobicity. The following approach was taken to prove this hypothesis (presented in Chapter 4):
 - Select microorganisms possessing different degrees of hydrophobicity
 - Find the right substrate for bacteria immobilization
 - Derivatize AFM tips with thiols terminated in hydrophilic and hydrophobic groups
 - Perform AFM imaging and force measurements at random locations on the microbial surfaces

2. The goal of the second part of this thesis was to model the AFM approach curves, recorded with both hydrophilic and hydrophobic modified AFM tips, such that the type of interactions involved in bacterial adhesion could be predicted (presented in Chapter 5). The following steps were undertaken to accomplish the goal of this section:

- Model the approach curves using the DLVO theory accounting for electrostatic and van der Waals interactions
- When discrepancy existed between experiment and the DLVO theory, the XDLVO model accounting for acid-base interactions was considered including an additional term to the classical DLVO theory
- In the case of microbial cells possessing long extracellular structures, EDLVO model accounting for steric interaction was added to the classical DLVO theory and fitted to the approach force curves

2. LITERATURE REVIEW

2.1 Role of Microorganisms in Hydrocarbon Degradation

Diverse environmental communities of microorganisms, including many species of bacteria and fungi, have evolved the ability to degrade hydrocarbons. Bacteria are the best described hydrocarbon utilizing microorganisms.[28] For example, *Pseudomonas* spp.[29], *Bacillus* spp.[30], *Arthrobacter* spp.[31], *Mycobacterium* spp.[32], *Acinetobacter* spp.[33], and *Rhodococcus* spp.[34] have been reported as hydrocarbon degraders. These microbes are widely distributed in soil and marine environments following oil spills. In recent years, the focus on using microorganisms in removal of oil spills and biotransformation of hydrocarbons into more valuable products has considerably increased. Bioremediation and bioprocessing are emerging as promising alternatives to conventional methods for hydrocarbon degradation due to their capabilities of being safer, less costly and more efficient.[28]

2.1.1 Bioremediation of Petroleum Hydrocarbons

The foundation of bioremediation, which has been studied since the early 1940's, has been the observation that over extended periods of time and without human intervention, nature eliminates both natural and most man-made pollution through natural processes.[35] The largest, most successful and thoroughly studied application of bioremediation to date is the cleaning of the *Exxon Valdez* spill in Prince William Sound, Alaska, where the spillage of more than 41 million liters of crude oil contaminated the marine environment and approximately 2,000 km of the shorelines causing severe ecological damage to the surrounding communities.[36] The initial approach to the cleanup of the oil spills in Prince

William Sound was physical and it turned out to be expensive and not efficient. Consequently, bioremediation was considered as an alternative method. The use of microorganisms as a treatment method for oil pollutant removal restored the rocks to their original whiteness, which provided a contrast to the black oily untreated shorelines and gave visual credence to its effectiveness [28, 36].

Microorganisms carry out biodegradation in many different types of environments; of particular relevance for pollutants or potential pollutants are soils, groundwater, surface waters, and oceans.[37, 38] Crude oil is recognized as a major marine pollutant and petroleum products, such as gasoline and diesel, are the most frequent organic pollutants of soils and ground-waters.[39] It is estimated that the petroleum hydrocarbons entering the world's oceans range from 1.9 to 11.8 million tonnes each year.[40] Petroleum entering an ecosystem provides an important source of carbon and energy necessary for microbial growth, being actively transformed into cell biomass and carbon dioxide that can be readily accommodated in the environment.[41, 42]

2.1.2 Bioprocessing of Petroleum Hydrocarbons

Bioprocesses represent a promising biotechnological tool for the production of fine chemicals.[43] Environmental bacterial communities possess oxidative enzymes capable of degrading various types of hydrocarbons for assuring their carbon and energy requirements and concomitantly transforming them into valuable products.[35] It is well documented that several strains of yeast belonging to the genus *Candida* produce α,ω dicarboxylic acids which are versatile chemical intermediates useful as raw materials for the preparation of adhesives, fragrances, polyamides, polyesters, and antimicrobials.[44] Even though non-enzymatic syntheses of such chemicals exist, the process is very

complicated and results in a mixture of dicarboxylic acids which require extensive purification steps. [44]

Other chemicals which have been successfully produced by alkane biodegradation include amino acids, organic acids, carbohydrates, lipids, nucleic acids, vitamins, enzymes, co-enzymes and antibiotics [45], polyhydroxyalkanoates [46], and biosurfactants [47, 48].

Whereas some microorganisms degrade alkanes (normal, branched and cyclic paraffins), or use aromatics, others use both paraffinic and aromatic hydrocarbons.[28, 49, 50]. The normal alkanes in the range C₁₀ to C₂₆ are considered to be the most readily degraded of all hydrocarbons. However, the low-molecular-weight aromatics, such as benzene, toluene and xylene, which are among the toxic compounds found in petroleum, are also easily biodegraded by many microorganisms.[51] More complex structures such as asphaltic fractions are more resistant to biodegradation and the most persistent in different ecosystems. Relatively little is known of the metabolism of individual compounds in this fraction. Gibson [52] has provided brief reviews of the degradation of individual hydrocarbons in petroleum.

2.1.3 Bioavailability of Hydrophobic Substrates

Petroleum is a naturally occurring, highly complex mixture of organic compounds containing gaseous, liquid and solid hydrocarbons with varying degrees of water solubility, chemical structure, volatility, and toxicity.[53] A majority of these molecules is indeed composed solely of carbon and hydrogen, but most oils contain a small percentage of organic sulfur, organic nitrogen, and trace amounts of metallic constituents.[53]

As a major component of petroleum, alkanes have become an important source of pollution in the environment because of their massive utilization.[54] Their low solubility in water causes separation in a two-phase system.[55]

Utilization of alkanes by microorganisms poses the problem of contact between the immiscible substrate and the microbial cell.[56] Therefore, the major problem to be overcome by microorganisms in hydrocarbon degradation is to make the hydrophobic carbon source accessible to them.[55, 57]

2.1.4 Mechanisms of Hydrocarbon Transport towards Microbial Cells

In order to find an efficient method of supplying hydrocarbons to microbial cells, it is important to understand the mechanism of hydrocarbon transport towards them.[58, 59] Cell-substrate contact is obviously essential for substrate uptake by microorganisms. As the hydrocarbons have a low solubility in water, the substrate must be transported through the aqueous phase in such a way to achieve the cell substrate contact. At least three modes of hydrocarbon transport towards microbial cells have been emphasized throughout the literature:

- Interaction of cells with hydrocarbon dissolved in the aqueous phase;
- Contact of cells with pseudosolubilized hydrocarbon droplets much smaller than the cells;
- Direct contact of the cells with large hydrocarbon droplets;

It is generally accepted that the first mechanism cannot support the observed rate of growth of microorganisms on long-chain alkanes due to their low solubility in the aqueous medium.[60] Even though, this mechanism has been reported as valid for aromatics and gaseous hydrocarbons, whose solubility in aqueous medium is slightly higher, the microbial growth is restricted in this case.[61]

The second mechanism relies on microbial production of emulsifiers or surfactants that increase the concentration of hydrocarbon in the aqueous phase by producing hydrocarbon micro-droplets which attach to the microorganism's surface, facilitating the uptake process. This mechanism has been observed by various research groups. [62, 63]

Direct contact of cells and oil droplets appears to be the mechanism through which most hydrocarbon substrates are taken up by the cells.[64]

Microbial cells can use either one or a combination of the above described mechanisms for the hydrocarbon transport. It was reported that during the growth of *Candida lipolytica* on *n*-hexadecane, both the second and third mechanisms played important roles in substrate transport.[61, 64]

2.1.5 Advantages of Bioremediation and Bioprocesses

The application of hydrocarbon microbiology to solve pollution problems in water and soil has an enormous economic and environmental importance promising an improved substitute for ineffective and costly physicochemical remediation methods.[65] Contaminated land is costly to clean up using traditional remediation methods. For example, in the USA, the remediation cost is expected to exceed US \$1 trillion [66] for petroleum polluted sites.[67] The use of microbial biodegradative abilities in restoration of oil-polluted environments has

been proven to have advantages over conventional treatments, offering a low-cost permanent solution and a much safer alternative in removal of oil pollutants.[68] The cost effectiveness emerges especially through elimination of transportation expenses by treating oil pollutants on-site and by using biological systems which are very cheap compared to some chemicals used in traditional remediation techniques.

Other benefits include the reduction of contamination risks in other areas as well as the positive public acceptance.[65] The preference for using bioremediation over traditional methods also arises from the safety of its ultimate end products, CO₂ and biomass; bioremediation representing an extension of natural processes that can be accelerated by optimizing key variables. Traditional methods, such as incineration, tend to create new waste often more harmful than the initial substrate. A multi-disciplinary approach is fundamental for the investigation of the bioremediation of polluted soils and contaminated aquifers as well as for hydrocarbon bioprocessing. [42, 69, 70]

2.2 Bacterial Adhesion to Surfaces and Interfaces

It is generally accepted that microbial attachment to a surface or an interface is a primary ecological strategy for the survival of species and the development of specific activity and function within different environments having impact on a variety of fields.[70] Bacteria adhesion at oil/water interfaces, for example, has been extensively studied since the early work of Mudd and Mudd. [8, 9] In this case, as the oil is immiscible in water, it gives a distinct boundary phase to which microorganisms with more hydrophobic surfaces tend to be attracted.[71]

Although bacterial adhesion results from the same underlying physico-chemical mechanisms that govern the adhesion of nonliving particles, the complexity of bacterial surfaces have defied simple rules that rely on surface-averaged properties, such as surface charge or hydrophobicity.[72]

Initial microbial attachment to a substrate is a net result of attractive and repulsive forces and the chemical properties of the bacterial surface which is a complex three-dimensional structure with a myriad of functional groups.[73]

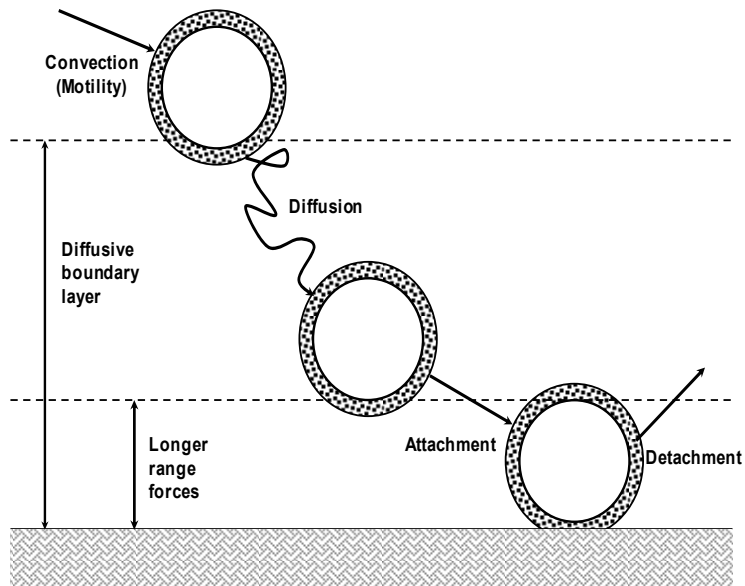


Figure 2.1 Critical steps involved in cell attachment - convective transport, diffusion, attachment, and resistance to detachment. Long-range interaction forces govern the rate of attachment and short-range interaction forces govern the strength of adhesion. Adapted from reference [1].

The transition of a bacterium from a planktonic to an adherent state involves a number of steps, as illustrated in Figure 2.1. The microorganism must first reach the proximity of a surface by fluid convection or motility. Then, it must

cross the diffusive stagnant boundary layer by Brownian motion to reach a separation distance where interaction forces between the bacterium and surface become significant compared to thermal forces driving the Brownian motion, which are on the order of 1 pN.[1] Finally, the bacterium must form a strong interaction with the surface that is resistant to any subsequent dislodging forces (e.g., fluid shear).[1] Conventionally, these forces are characterized based on the physico-chemical properties of the interacting surfaces and by the macromolecular structure and extracellular appendages accompanying microbial surfaces.

2.2.1 Bacterial Cell Envelope

Bacterial surfaces are structurally very complex emphasizing a layered cell envelope which consists of a plasma membrane, cell wall, often an outer polysaccharide layer, and various surface appendages. The classical differentiation of microbial cell envelope is exemplified by Gram-positive and Gram-negative strains, according to the way they stain in the Gram reaction.[70] As Geoghegan et al. reported in reference [70], this classification defines bacteria with vastly different cell surface physiologies related to significant differences in surface chemistry. Generally, the envelope of Gram-negative bacteria is structurally and chemically more complex than that of Gram-positive bacteria. Gram-positive bacterial surfaces are dominated by teichoic acids and Gram-negative surfaces by polysaccharides.[2] Both Gram-negative and Gram-positive bacteria have been shown to possess a variety of external surface layers and surface appendages of different structural and chemical nature and having various physico-chemical properties.

2.2.1.1 Gram-negative Bacteria

Gram-negative strains have a multi-layered cell envelope consisting of two lipid bilayer membranes sandwiching a thin 1 to 2 nm-thick peptidoglycan layer which is embedded in a concentrated gel-like matrix, the periplasmic space. The cytoplasmic membrane delimits the inner part of the cell from the external environment. The peptidoglycan layer makes up 8 to 15 percent of the mass of the Gram-negative cell wall and gives the bacterium shape.[2] The outer membrane of Gram-negative bacteria is composed of two types of lipids, lipopolysaccharide (LPS) and phospholipids, as well as a number of characteristic proteins and polysaccharides that serve to protect the cell.[2]

The LPS is composed of three parts:

- (a) the lipid region that forms hydrophobic interactions with the lipid region of the phospholipids;
- (b) the hydrophilic, O-antigen polysaccharide region that protrudes into the extracellular medium;
- (c) the core oligosaccharide that connects the two regions

The length of the LPS chain up through the outer core is about 2 to 3 nm, whereas the length of the O-antigen portion can reach up to 40 nm, depending upon the number of repeating units, bending of the O-antigen chain, and solution conditions such as pH and ionic strength.[187]

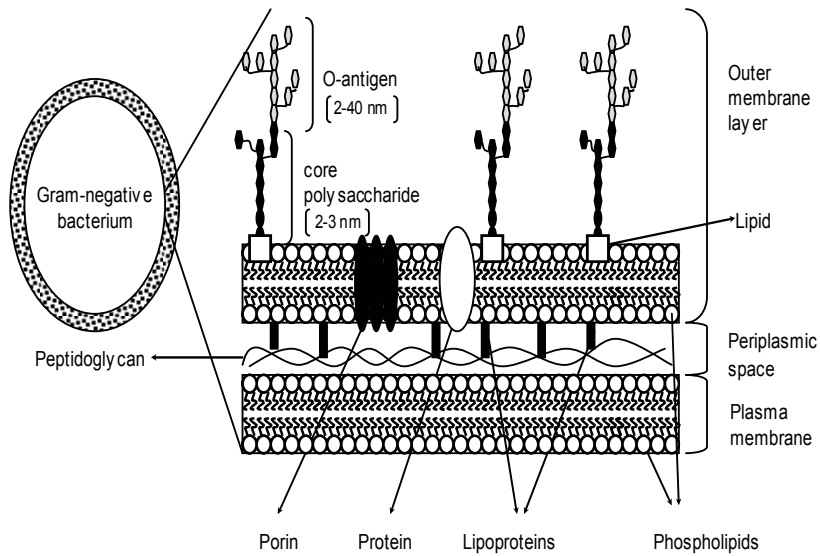


Figure 2.2 Schematic representation of a typical cell envelope of Gram-negative bacteria. Adapted from reference [2].

2.2.1.2 Gram-positive Bacteria

The Gram-positive envelope consists basically of two layers which are illustrated in Figure 2.3. The first layer is represented by the plasma membrane that is closely associated with a well-defined, rigid outer layer of 15 to 30 nm thickness consisting primarily of peptidoglycan and that can range anywhere from 50 to 80 percent of the cell wall mass.[174] The second and outermost layer serves to protect the cell from environmental factors.

The other major components of the Gram-positive wall are teichoic acids which vary in nature of the sugar backbone and type, and location of various substituents.

The walls of acid-fast Gram-positive bacteria contain mycolic acids which are complex, long-chain hydrocarbons substituted with sugars that confer hydrophobicity to the cells.[174] The protective cover of the acid-fast bacteria make them impervious to acids, as a result the name.

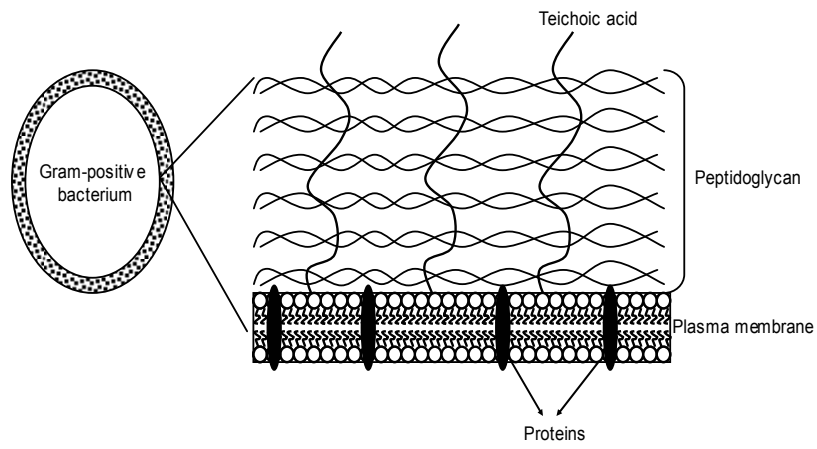


Figure 2.3 Typical cell envelope of Gram-positive bacteria. Adapted from reference [2].

2.2.2 Cell Surface External Appendages

Bacterial interactions with their surroundings are mediated by highly diverse classes of surface constituents such as capsules, pili and flagella which are present on the outside of the cell wall. These surface constituents are made of polymeric substances which consist of exopolysaccharides, proteins, lipopolysaccharides, lipoteichoic acids, and lectins.[17]

2.2.2.1 Bacterial Capsule and Slime Layers

Capsules are highly hydrated structures consisting of over 95% water.[74] The composition of the capsule is highly variable even among the strains of the same species. It mainly consists of polysaccharides and proteins [75] that contain various functional groups, including carboxyl, amino, and phosphate. Capsular polysaccharides can be either linear or branched homopolymers or heteropolymers possessing hydroxyl groups that can be substituted with both organic or inorganic molecules.[76]

2.2.2.2 Pili and Flagella

A variety of surface appendages may extend beyond the cell surface into the external environment. Most prevalent among bacteria are flagella and pili also known as fimbriae which anchor to the plasma membrane. As Touhami et al. emphasize in their study, pili can perform a variety of different functions, for example, aiding genetic transfer via conjugation (e.g., F pili of *Escherichia coli*), movement across surfaces via twitching (e.g., the type IV pili of *Pseudomonas aeruginosa*), and adherence to a variety of surfaces (e.g., type IV pili of *P. aeruginosa*).[77]

Pili are straight, thin filaments that extend to distances greater than 100 nm from the cell wall and can reach up to one μm , and are composed of more than a thousand protein subunits, pilin. The chemical analysis of pilin reveals a low number of basic amino acids, a few free carboxyl groups, and a relatively high proportion of residues with hydrocarbon side chains. Such a composition would confer hydrophobic properties to the pili.[78]

Bacterial flagella endow the microorganism with motility and are composed of one or more proteins.

2.3 Macroscopic Cell Surface Properties

The behavior of an adhering cell is governed by the physical and chemical interactions of the macromolecules in the interfacial region.[70] Macroscopic approaches such as zeta potential and hydrophobicity measurements play an important role in the progress of our understanding of bacterial surface-averaged or macroscopic physico-chemical properties. These are described in more detail in the following sections.

2.3.1 Cell Surface Hydrophobicity

Hydrophobicity is widely accepted as a determinant of bacterial adhesion.[6] Specific molecular components that have been implicated in contributing to surface hydrophobicity include surface-associated proteins such as fimbriae on Gram-negative bacteria [79] and mycolic acids on Gram-positive species. [80]

2.3.2 Cell Surface Charge

Microorganisms as well as most surfaces to which they adhere usually have a negative zeta potential under physiological conditions. The negative charge, which mainly arises from carboxyl and phosphate groups, may be uniformly distributed or alternate on a patchwork pattern with positive charge from amino groups.[81] For Gram-positive strains, net negative charge results from a predominance of phosphate groups in teichoic acids and carboxylates of the peptidoglycan layer as well as acidic polypeptides and polysaccharides in glycocalyx.[82] The negative charge of Gram-negative bacteria results mainly from acidic capsular polysaccharides and peptides and to a lesser extent from acidic lipopolysaccharides.[82] Decreases in zeta potential correlate with nitrogen-to-carbon ratio and nitrogen-to-phosphorus ratios of microbial surfaces as measured by X-ray photoelectron spectroscopy (XPS).[83, 84]

It has been observed a reduction of zeta potential of *E.coli* following trypsin treatment, suggesting a role of surface proteins, possibly associated with fimbriae, in determining surface potential.,[85] Typical zeta potential values for bacteria obtained from microelectrophoresis range from around -10mV to -50mV at neutral pH.[85]

2.4 Atomic Force Microscopy

The invention of the atomic force microscope (AFM) by Binnig and co-workers in 1986, also known as the scanning force microscope (SFM), is now recognized as one of the most important milestones of modern science.[86] The AFM is a high resolution surface imaging tool that additionally enables the manipulation and probing of surface forces at small separation distances.[87]

It can be operated in air or liquid allowing the investigation of biological surfaces or cell components, in close-to-natural conditions.[88] The main component of the AFM is the tip which has to be sharp in order to obtain high lateral resolution. The contact zone with the sample is only a few atoms across, so that only a small number of atoms and molecules on the tip are involved in generating the force profile at small separation distances.[89]

2.4.1 Basic Theory of Atomic Force Microscopy

The AFM tip mounted at the end of a flexible cantilever is brought into contact with the surface of the sample, resulting in bending of the cantilever and deflection of a laser beam reflected by the cantilever surface. The magnitude of the deflection and the displacement of the cantilever are simultaneously recorded by a position sensitive photodiode. The electronic feedback in the system is used to compensate the differences in surface relief adjusting the z-extension of the piezoelectric element.[180] More than ten different imaging modes are routinely used in AFM analysis.[180] The primarily AFM mode of operation is contact mode, where the tip remains in continuous contact with the surface while translated over the sample. Consequently, the contact mode is associated with high shear forces, which can remove the sample from the substrate or damage its surface if it is not sufficiently well immobilized.[17] As a result, this method is not suitable for delicate soft samples such as microbial surfaces.

To minimize the damage to the sample surface because of tip interactions, the dynamic AC mode or tapping mode was developed.

In this case, the AFM tip taps the sample surface at the end of an oscillation cycle instead of dragging the tip along the surface; consequently, the

destructive effects of lateral interactions are minimized or even completely eliminated.

The loading force, which represents the product of the force constant of the AFM cantilever and its attraction/retraction speed, can be controlled by the maintenance of a constant oscillation of the cantilever. The oscillation of the cantilever can be obtained in the acoustic mode which greatly reduces the likelihood of the cells being damaged.[180] Therefore, AC mode has become a very useful tool for imaging biological systems.

2.4.2 Force Curve Analysis

The AFM has evolved from an imaging tool into a powerful instrument that can probe intermolecular forces at certain locations on a sample surface. The cantilever deflection is a measure of the interaction force between the AFM tip and the sample surface. Attractive forces lead to a negative cantilever deflection whereas repulsive forces lead to a positive cantilever deflection.

When the tip is far away from the surface, forces are absent and the cantilever is not deflected. Attractive surface forces become visible when the tip approaches the surface. If the value of the positive force gradient is the same as the spring constant a mechanical instability, known as snap-in, occurs.[90] The force that the tip exerts on the surface increases as the tip displacement increases. In the case of a hard substrate, the slope of the force curve converges to -1 and sample displacement and cantilever deflection are proportional.[90] The distance between the tip and the sample remains constant along this contact line. This fact is used to calibrate the cantilever deflection in the case of force microscopes that use a laser deflection signal, which means that the deflection is directly obtained from the signal of the photodiode.[90]

The repulsive forces between the tip and the sample decrease continuously during retraction of the z-piezo up to the so-called snap-off point, where tip separation from the sample surface occurs, and which is visible immediately after the minimum of the curve where the maximum adhesion force can be measured.[188] Under appropriate conditions the snap-in or snap-off contact might vanish in liquid, the interaction between the tip and the sample being mainly repulsive.

A force curve is a plot of the measured force versus the displacement of the z-piezo device. The displacement of the piezo device can be translated into a tip-sample separation distance by subtracting the contact line from the cantilever deflection.[188] After applying this normalization a so-called force-distance curve is obtained, Figure 2.4. The AFM force-distance curves provide details on the type of interaction occurring between the AFM tip and sample surface, and consequently reveal important information on the physico-chemical properties of the studied surface.[17]

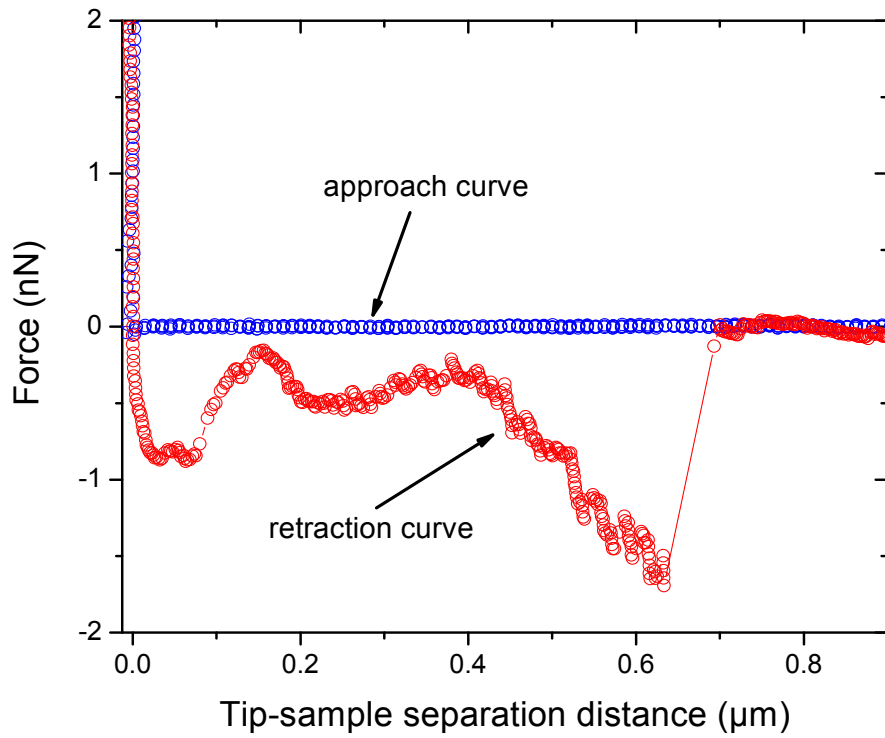


Figure 2.4 Force distance curve obtained on *A. venetianus* RAG-1 surface which possesses extracellular structures.

2.4.3 AFM in Biological Systems

Although atomic force microscopy (AFM) has traditionally been used for analyzing non-biological surfaces, it is increasingly used for imaging biological samples offering an alternative to electron microscopy techniques for obtaining morphology of microbial species with nanometer resolution (Figure 2.5). AFM allows not only imaging of biological samples but also it is becoming a more and more popular tool for probing intermolecular forces at different locations of a bacterial surface using AFM tips with well defined surface chemistry.

The AFM technique has been adapted to microbial adhesion experiments [91] and has been able to provide a new perspective on bacterial adhesion contributing to the enrichment of already known macroscopic knowledge of bacterial adhesion based on physico-chemical approaches. The AFM technique is able to analyze a single bacterium, as opposed to other techniques such as contact angle and zeta potential measurements that generate data based on the behavior of an entire population of bacteria.[91]

The most important of the microbial physico-chemical properties that can be studied with the AFM are surface hydrophobicity [92, 93], charge distribution [92], and stretching properties of long surface polymers.[94]

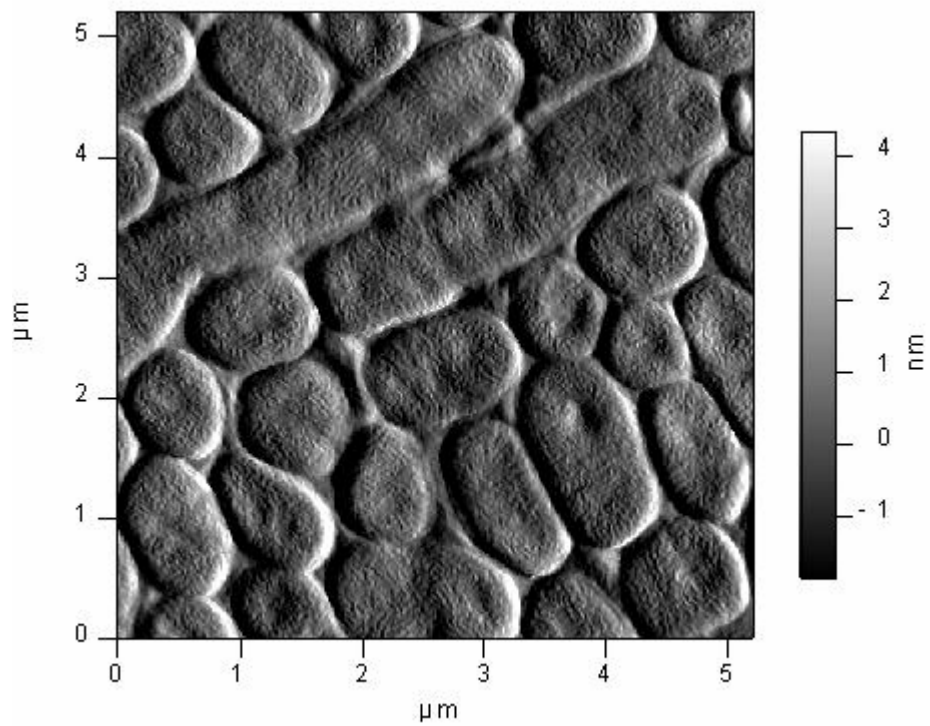


Figure 2.5 AFM height image of *A. venetianus* RAG-1 showing surface detail. The image was recorded in AC mode in air.

2.4.4 Probe Modification

Different research groups have been working on modifying the properties of the AFM tip which is often desirable when data on the composition or sample surface heterogeneity is the objective.[17] Commercially available AFM tips have a unique surface chemistry by being made of silicon or silicon nitride and therefore can probe only a limited range of interactions. Modifications of the surface properties of the tips extend this to a wide range of physico-chemical and specific functionalities.[188] The most common way of derivatizing the probe surface is by using alkanethiols.[95, 96] Alkanethiols bind to gold surfaces; consequently, the AFM tip needs to be covered with gold before thiol functionalization. The main advantage of thiol functionalization is that such tips are straightforward to prepare and a wide range of functional groups can be used (e.g. $-\text{CH}_3$, $-\text{OH}$, and $-\text{COOH}$).

An alternative method to functionalize tips is the application of silanizing agents to directly modify the tip. These surfaces are typically characterized by a higher defect density and lower degree of self-organization compared to the thiol-modified tips.[97]

Colloidal beads can also be mounted on the AFM cantilevers. Because of the large size of a typical colloidal particle, the lateral resolution of both sample structure and interaction forces is only on the order of 1 to 10 μm .

2.4.5 Immobilization of Bacteria for AFM Characterization

During the last decade, numerous methods were developed for the immobilization of bacteria in both dead and living states. Bacterial samples for AFM analysis can be prepared by using chemical fixatives like glutaraldehyde, as demonstrated by Razatos et al. [18], or by chemically cross-linking them to the substrate with 1-(3-dimethylaminopropyl)-3-ethylcarbodiimide HCL (EDC) as emphasised by Camesano et al. [98] A problem with these treatments is that they change the surface properties of the bacteria by cross-linking the proteins. These methods are not suitable when analyzing bacterial physico-chemical properties.

While most mounting procedures destroy cell viability, recent advances in substrate preparation have preserved cell integrity.[189] One of the most widespread methods, developed by Kasas and Ikai is to entrap bacteria in the pores of a microfilter (pore size typically between 0.45 and 1.5 μm).[99] The bacterial surface is then routinely analyzed on the reverse side of the filter so that only the part of the bacterium which protrudes through the surface is analyzed.[17] The advantage of this method is that it does not rely on either chemical fixatives or immobilizing agents. The main disadvantage of this technique is that it does not allow the analysis of the whole of the bacterial surface and it is suitable only for spherical cells.[17]

An alternative method involves the embedding of the bacteria in an agar gel.[100] Although the substrate is gelatinous and not suitable for imaging in AC mode, the method works as long as the bacterial surface sticks out of the agar layer.[17]

A disadvantage of this method is the need for elevated temperatures to liquefy the agar. The high temperatures could affect the viability of the bacteria and alter the bacterial surface structures.[17]

Recently, an alternative method for imaging bacteria in their native state, without affecting their surface properties, was developed by Schar-Zammaretti and Ubbink.[101] They attached negatively-charged bacteria to glass slides functionalized with poly-L-lysine. As most bacteria are negatively charged, the method is suitable for a wide range of bacteria.

2.5 Equations Governing the Force Interactions

As emphasized by Busscher in reference [101], all adhesive interactions among macroscopic bodies, colloidal particles—whether microorganisms or inert synthetic particles—and molecular entities are mediated by physico-chemical interactions.[102] There are only a few basic forces in nature able to exert these interactions including the Lifshitz-Van der Waals forces, electrostatic interactions, hydrogen bonding, and Brownian motion.[103] All other forces are direct or indirect corollaries of these basic forces.[103]

Mathematical modeling was introduced as a quantitative tool to better understand physico-chemical properties of synthetic or living entities.

2.5.1 DLVO theory of Colloidal Stability

The well-known DLVO theory —named for Derjaguin, Landau, Verwey and Overbeek— describes the stability of a colloid dispersion as a balance between the two forces: electric double layer repulsion and van der Waals attraction.[104]

The range of the electric double layer interactions extends up to 100 nm, varying inversely with the square root of the ionic strength and arising from the existence of overlapping diffuse double layers of counterions near charged surfaces in solution. The van der Waals forces arise from the specific alignment and coupling interactions of molecular dipoles and they range up to a few nanometers. In addition to these forces, there may be polymer bridging or depletion forces that extend to the radius of gyration of the polymer, and acid-base forces whose extent is not more than several molecular diameters. These four forces are the base of colloid science, and the quantitative understanding of their molecular basis has led to their widespread control and exploitation.

Direct measurement of the interactions between the AFM tip and various substrates has proven to be an essential tool in validating DLVO theory for ideal macroscopic and various microscopic systems.[105, 106]

2.5.1.1 Electrostatic Interactions

Electrostatic forces are predominant in aqueous solutions arising from dissociation of ions, ion adsorption or metal ion substitution of surfaces; they can be attractive or repulsive depending on the surface potential, ionic strength, and pH.[107] However, most surfaces possess a net negative charge and have affinity for the positively charged ions randomly distributed in the solution. Concomitantly, the negatively charged surfaces repel negative charges in the

solution. This leads to an electrical potential that forms the electric double layer, which decreases from the value at the surface to zero at infinite distance in the bulk solution.

The AFM has been shown to be a versatile instrument for measuring electrostatic forces.[108] The electrostatic interactions are characterized by the high strength, as well as long range in comparison to the other relevant surface interactions, such as van der Waals forces.[108]

Electrostatic interactions among charged surfaces in fluids can be classically treated with the Poisson-Boltzmann equation, which describes the variation of potential and charge density of the counter ions at different separation distances from a charged surface of arbitrary shape.[105] Simplified models have been developed from the fundamental relationship based on assumptions about particle surface charge and geometry.[105]

When two charged surfaces approach each other in an electrolyte solution, their diffuse double layers overlap, resulting in the electrostatic double layer interaction. Theoretical curves for electrostatic double-layer force, F_e , as a function of the separation distance, h , can be calculated using the well known expression derived by Hogg, Healy, and Fuerstenau [109] assuming constant surface potential on the substrates:

$$F_e = 4\pi\epsilon\epsilon_0(\kappa a)\left(\frac{kT}{ze}\right)^2 \psi_t\psi_s \left[\frac{\exp(-\kappa ah)}{1 + \exp(-\kappa ah)} - \frac{(\Psi_t - \Psi_s)^2}{2\Psi_t\Psi_s} \times \frac{\exp(-2\kappa ah)}{1 - \exp(-2\kappa ah)} \right] \quad 2.1$$

In the above formula, Ψ_t and Ψ_s are the scaled surface potentials ($\Psi = ze\psi/kT$) of the tip and the substrate, respectively, h is the separation distance between the two substrates, a is the AFM tip radius, and κ is the inverse Debye length, given by the following expression:

$$\kappa = \sqrt{\frac{2000N_A e^2 (Mz^2)}{\varepsilon_0 \varepsilon kT}} \quad 2.2$$

where N_A is Avogadro's constant, M the molarity (mol l^{-1}) of the ions of the electrolyte, z the valence, ε the dielectric constant of the solution, ε_0 the dielectric permittivity of vacuum, k and e are the Boltzmann constant and the electronic charge, respectively, and T is the absolute temperature. According to the above relationships, an increase in electrolyte concentration results in a decrease in Debye length and concomitant reduction in electrostatic force.

The surface potential of a microbial cell is assumed equal to its zeta potential, as calculated from experimental values of electrophoretic mobility and the Smoluchowski equation [110] :

$$\mu_E = \frac{\varepsilon_0 \varepsilon_R \zeta_{Smol}}{\mu_f} \quad 2.3$$

where μ_E refers to the electrophoretic mobility of the sample, ζ_{Smol} the zeta potential and μ_f the fluid viscosity, taken as that of water.

The counterions in the medium screen the surface charge and decrease the measured electrical potential at high ionic strength. Hence, the electrostatic interactions are low at high ionic strength and high at low ionic strength.[111]

2.5.1.2 Van der Waals Interactions

The van der Waals or London dispersion forces originate from induced dipoles in molecules and have an interval of influence ranging from about 0.2 nm to over 10 nm.

The expression for the nonretarded van der Waals force between a sphere and an infinite planar surface, based on Hamaker's approach and Derjaguin's approximation is given as [112],

$$F_{\text{vdw}} = \frac{A}{6} \left[-\frac{a}{h^2} - \frac{a}{(h+2a)^2} + \frac{2a}{h(h+2a)} \right] \quad 2.4$$

where A is the Hamaker constant, a is the radius of the AFM tip, and h is the surface-to-surface distance between the substrate and the AFM tip.

The expression for the Hamaker constant of the system can be computed in terms of the Hamaker constants of the individual components

$$A_{132} = (A_1^{1/2} - A_3^{1/2}) (A_2^{1/2} - A_3^{1/2}) \quad 2.5$$

where A_1 and A_2 are the Hamaker constant of glass and gold, respectively, and A_3 is the Hamaker constant of the solution.

The various surface tension components of a bacterial cell can be obtained through contact angle measurements using the van Oss–Chaundhury–Good equation [113]

$$(1 + \cos \theta) \gamma_L = 2 \left(\sqrt{\gamma_S^{LW} \gamma_L^{LW}} + \sqrt{\gamma_S^+ \gamma_L^-} + \sqrt{\gamma_S^- \gamma_L^+} \right) \quad 2.6$$

where θ is the contact angle, γ_L is the total surface tension of the liquid, γ_i^{LW} is the Lifshitz-van der Waals (LW), or apolar surface tension component of condensed material (*i*), γ_i^+ and γ_i^- are the electron acceptor and electron-donor parameters of the Lewis-acid base components of the surface tension of condensed material (*i*), and the subscripts *S* and *L* refer to the substrate and liquid phase. Values of γ_L for a number of liquids have been tabulated as shown in Table 2.1.

Table 2.1. Surface tension components (γ_L^{LW} and γ_L^{AB}) and parameters of γ_L^{AB} (γ_L^+ and γ_L^-), mJ/m², for the most commonly used high-energy contact angle liquids.[119]

Liquid		γ_L	γ_L^{LW}	γ_L^{AB}	γ_L^+	γ_L^-
Polar	Water	72.8	21.8	51.0	25.5	25.5
	Glycerol	64.0	34.0	30.0	3.92	57.4
	Formamide	58	39.0	19.0	2.28	39.6
Apolar	Diiodomethane	50.8	50.8	0	0	0

Knowledge of the surface free energy allows the calculation of the Hamaker constant for individual microbes, which may be used to calculate their individual interaction energies. van Oss et al.[113] formulated an algebraic method of determining the Hamaker constant based on the apolar component of the microbial surface free energy:

$$A_{ii} = 24\pi l_0^2 \gamma_i^{LW} \quad 2.7$$

where l_0 represents the minimum equilibrium distance between two parallel flat layers of material i . van Oss determined that the minimum separation distance fell within a range of $1.57 \pm 0.09 \text{ \AA}$.

2.5.2 DLVO Theory Applied to Microbial Systems

A bacterial suspension may be interpreted as a living colloidal system as a result of their small size, density, which is only slightly greater than that of water, and their negatively-charged surfaces. Consequently, many researchers have attempted to describe bacterial adhesion by colloidal theories such as the DLVO theory.[111, 114] However, it should be noted that the DLVO theory, which was derived for homogeneous, hard bodies, sometimes is only of qualitative value when applied to bacterial interactions.[7]

The DLVO theory deals with the interplay of electrostatic interactions and short range van der Waals forces. Additionally, in the case of microorganisms, hydration forces and polymer-mediated interactions can be measured at short separation distances (between 0.1 and 5 nm) for the first group and at larger

distances (up to 100 nm) for the latter. All these surface forces play an important role in predicting rates of attachment of bacteria in solution to surfaces.[115]

While useful in many situations where surfaces may be assumed uniform and relatively ideal, the DLVO theory does not account for several types of interaction forces thought to be relevant to microbial attachment, including hydrophobic interactions,[103] and steric forces,[114] as well as the effects of surface roughness.[116] As a result, discrepancies between measured interaction forces and the DLVO theory have been mentioned by a large number of researchers studying microbial attachment.[115,116,117]

2.5.3 Schematic of DLVO interactions

As illustrated in Figure 2.6, the general trend of any DLVO plot shows that the interaction energy (or force) is equal to zero at infinite separation distance so that the particles exert no influence on each other. Then, as two surfaces approach, the initial interaction between them is governed by a balance of long-range attractive and repulsive forces, primarily van de Waals and electrostatic interactions.[18] van der Waals forces draw the surfaces together, creating a gradually attractive interaction energy leading to a secondary minimum, Figure 2.6. The depth and location of the secondary minimum depends on the ionic strength. In general, an energy maximum separates two energy minima.

At a few nanometers from contact, there is a significant energy barrier due to the electrostatic repulsion becoming the dominant force. However, if through Brownian motion or some other mechanism the energy barrier is overcome, the colloids fall into a deep energy minimum with the interaction energy going to negative infinity at a separation distance of zero. This primary

energy minimum corresponds to short-range interactions at contact and it is very unlikely for a particle to detach after reaching this minimum.

In general, the attachment of a particle to a surface can be viewed as crossing into the primary minimum or into a secondary minimum that is sufficiently deep to keep them together.[83] The height of the maximum energy barrier predicts the rate at which attachment occurs. As it has been emphasized by Somasundaran in reference [83], higher electrolyte concentrations, larger Hamaker constants, or lower surface potentials all decrease the decay length of the repulsive forces (the Debye length) and reduce the energy barrier to attachment.[84]

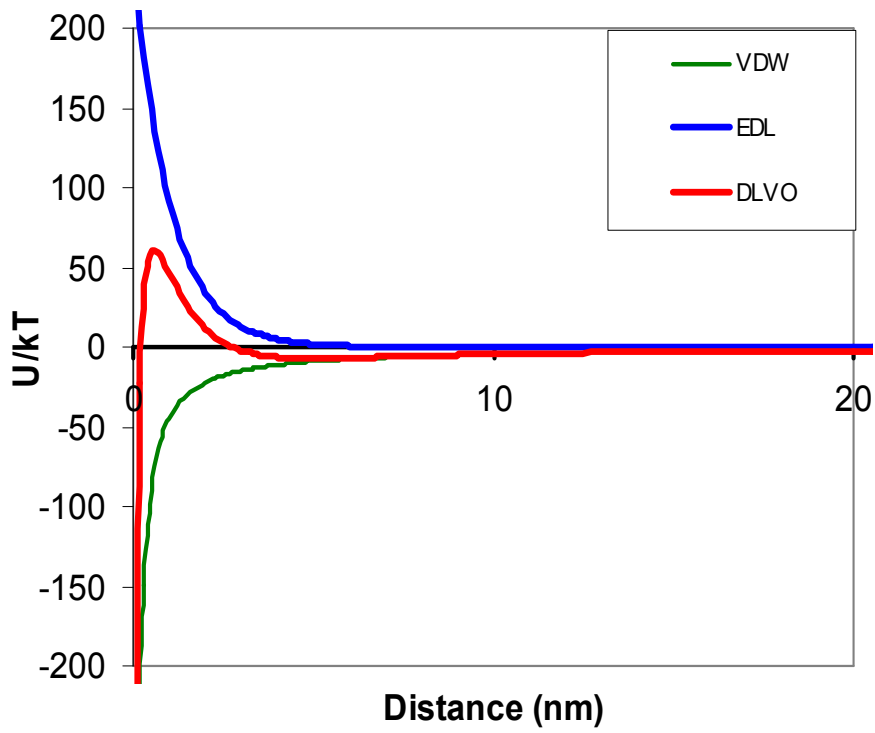


Figure 2.6 DLVO plot showing electrostatic, van der Waals, and total potential between a flat plate and a sphere.

The appearance and depth of the secondary energy minimum is dependent on the ionic strength of the solution. At high ionic strength, the electrostatic forces are not as significant, and therefore a secondary minimum exists. At low ionic strength, electrostatic interactions play a larger role preventing a secondary minimum from forming.

In the case of a suspension of *E. coli* in high ionic strength buffer, the DLVO theory has predicted an energy maximum that acts as a barrier to direct contact between the cell and the substratum, and a secondary energy minimum that is sufficiently deep to allow adhesion to occur at about 3 nm from the sample surface.[118]

2.5.4 Extended DLVO Theory

Application of the DLVO theory to microbial cells usually involves the assumption that they are inert. Living organisms are capable of producing extracellular specific structures, and have structurally and chemically more complex cell walls than the surface of synthetic colloidal particles; therefore, it is expected that the force curves recorded upon approach to bacterial surfaces would involve specific biological interactions.

The DLVO theory does not take into account short-range forces such as hydrophobic interactions that are of particular importance being considered the driving forces for the adhesion of microbes to the oil/water interface as in bioremediation and bioprocesses.

Van Oss et al. [119] have proposed an enhanced DLVO model, the extended DLVO theory, that accounts for acid-base (AB) interactions. These interactions determine the hydrophobicity (or hydrophilicity) of the involved surfaces and can range up to 5 nm from the surface into the surroundings being attractive or repulsive.[111]

The acid-base theory has had better success at modeling bacterial systems than typical DLVO.[120] In biological systems, hydrophobic interactions are usually the strongest of all long-range noncovalent interactions. It can be shown that hydrophobic attraction arises principally due to the hydrogen-bonding free energy of cohesion of the water molecules of the liquid medium in which hydrophobic molecules, sites or particles are immersed.[103]

2.5.5 Steric Forces

In general, the disagreement between the experimental results and calculated extended DLVO interactions have been attributed to interactions between bacterial extracellular structures and surfaces.[25] Jucker et al. have shown that polymer interactions can be attractive or repulsive.[25] Steric repulsion has been proposed to arise from higher affinity of the microbial polymers for the solvent than for the solid surface.[25] Inflexible polymer chains may also hinder the cell to approach the solid surface at distances where DLVO-type attraction would occur.[121] Bridging attraction occurs when the polymers have a higher affinity for the solid surface than for the liquid medium and anchor the cell to the surface across an energy barrier resulting from DLVO forces.[25] In this case, irreversible bacterial adhesion occurs that has been suggested to originate from the formation of hydrogen bonds.[113, 122]

The steric interactions between the AFM tip and a particular bacterial surface were modeled using a model developed for grafted polymers at relatively high surface coverage.[7] The force per unit area between two parallel flat surfaces, F_{St} , only one of which is coated with polymer, has been modeled following the work of Alexander [123] and de Gennes.[124] Butt et al. [125] have modified the model to describe the forces between a spherical AFM tip and a flat surface by integrating the force per unit area over the tip surface, resulting in the following formula for the interaction force

$$F_{St} = 50k_B T a L_0 \Gamma^{3/2} e^{-2\pi h / L_0} \quad 2.8$$

where k_B is Boltzmann constant, T the temperature, a the tip radius, Γ the grafted polymer density in the brush layer (m^{-2}) reflecting how much of the surface is covered by polymers, h the separation distance between the two surfaces, and L_0 the equilibrium thickness of the polymer layer. For all the calculations, the tip radius was assumed to be 40 nm. L_0 and Γ serve as fitting parameters for the model.

2.5.6 Soft-particle DLVO Theory

Ohshima [181,182] has developed the soft-particle DLVO theory to help explain the interactions between soft biological samples and various surfaces. The Ohshima's theory assumes the presence of an ion-penetrable, charged polyelectrolyte layer around the rigid core of a microorganism.[181] Since the outer membrane of Gram-negative bacteria, for example, is composed of LPS, proteins, and phospholipids [183], the surface has a non-uniform distribution of

charge, and therefore the zeta potential may not be an accurate measure of the surface potential. By fitting the soft-particle theory to the electrophoretic mobility data as a function of ionic strength, a surface potential value can be obtained for the bacterial surface.

Most of the earlier studies in literature relied only on Smoluchowski formula to calculate the surface potential of a microorganism. According to the Smoluchowski formula, the surface potential is expressed as zeta potential and depends only on the viscosity of the medium.

A comparison of the surface potentials using Smoluchowski's formula and Ohshima's soft-particle calculations showed that Smoluchowski's results always predicted higher surface potentials for the bacteria.[184] Moreover, lower energy barriers were obtained when the energy calculations were performed with surface potentials obtained from the soft-particle calculations than when zeta potential values were used.[184] However, de Kerchove and Elimelech [185] have shown that the outer surface potential of bacteria determined with Ohshima's theory for soft particles failed to predict the low attachment efficiencies of two *Escherichia coli* K12 mutants having lipopolysaccharide (LPS) layers of different lengths.

3. MATERIALS AND METHODS¹

3.1 Microorganisms and Growth Conditions.

The hydrocarbon-degrading bacteria employed in this study were *Acinetobacter venetianus* RAG-1 (formerly *A. calcoaceticus* RAG-1 [186]) and *Rhodococcus erythropolis* 20S-E1-c. *A. venetianus* RAG-1, a representative of the Gram-negative bacteria, was originally isolated by growth on crude oil by Reisfeld et al. [126] from a marine beach and has been thoroughly characterized by others.[127] *R. erythropolis* 20S-E1-c, a representative of acid-fast Gram-positive bacteria, was initially isolated from a marine sediment in Washington State [128], and is one strain of a species frequently isolated from hydrocarbon-impacted environments. This genus has long-chain hydrophobic mycolic acids exposed on the exterior of the cell wall surface.[129]

The bacterial cultures were grown in Trypticase soy broth (Difco, Sparks, MD) with incubation at 28°C and under gyratory shaking. Both microbes were harvested by centrifugation at their early stationary phase (previously determined by optical density and viable cell count) and washed twice with 0.1M (pH 7) potassium PBS. The washed cells were then resuspended in phosphate buffer.

3.2 Cell Immobilization for AFM Measurements.

Applying AFM to the examination of living microbial cells requires a robust technique for cell immobilization, while avoiding denaturation. Effective immobilization techniques must position the cells such that they are firmly

¹ Portions of this chapter have been published:

Dorobantu, L.S., Bhattacharjee, S., Foght, J.M., and Gray, M.R. 2008. Langmuir 24: 4944-4951.

attached to a support and stable to tip forces in liquid environments that favor viability. Both species of bacteria used in this study were strongly bound to the surface of glass slides coated with 3-aminopropyltrimethoxysilane (Genorama, Asper Biotech, Tartu, Estonia). A droplet of concentrated bacterial suspension (5-10 μ l) was placed onto a silanized glass slide. After 60 min of settling, the bacteria-coated glass was rinsed to remove loosely attached cells and transferred to the AFM stage. Slides were kept hydrated the entire time prior to AFM work by soaking the slide in phosphate buffer. All measurements were made at room temperature under 0.1M phosphate buffer solution.

3.3 Functionalization of AFM Tips

Olympus gold-coated cantilevers (Bio-levers) with nominal spring constants of 27-50 pN/nm, determined using the Cleveland thermal noise method [130], were purchased from Asylum Research (Santa Barbara, CA). These AFM tips were functionalized with alkanethiols terminating in OH (hydrophilic) or CH₃ (hydrophobic) groups by immersing the gold coated cantilever in 1 mM ethanol solutions of 11-mercapto-1-undecanol (Sigma-Aldrich, Oakville, ON) or octadecane thiol (Sigma-Aldrich), respectively.[93, 131] The tips were exposed to the solutions for 18 h. After self-assembly, all tips were rinsed with pure ethanol to remove any physisorbed thiols and gently dried in a stream of nitrogen. The tips were used immediately after preparation, conducting every set of measurements with a fresh tip.

3.4 Imaging of Bacterial Cells with AFM

All AFM characterization was performed using a Molecular Force Probe 3D (MFP 3D) from Asylum Research (Santa Barbara, CA) controlled with IGOR PRO software (Wavemetrics, Portland, OR). This instrument gives improved control over the z position of the cantilever relative to the sample by using an absolute position sensor. All the topographic images were acquired in AC (alternating current) mode, to avoid the surface damage accompanying contact-mode imaging of soft samples.[132] In AC mode of operation, the AFM cantilever is vibrated near its resonance frequency and scanned over the surface of interest using intermittent contact between the tip and the sample. While imaging in AC mode, the system monitors the vibrational amplitude of the cantilever and keeps it constant with the aid of a feedback system that adjusts the z-piezo in response to topographic information. It is the z-piezo movement that generates a topography data set. This mode of operation reduces friction forces and hence reduces the accumulation of cellular components on the tip being considered the best choice for imaging soft biological samples such as bacterial cells.[133]

To better resolve small surface features and borders, phase and amplitude images were recorded in addition to the more common topographic images. The scan rate ranged from 0.5 to 1 Hz and the tip velocity was maintained between 25 and 50 μms^{-1} . Typically, we began by scanning a 20 μm \times 20 μm area that would contain several bacterial cells. Gradually, the image size was reduced to isolate individual cells (2 μm \times 2 μm). Topographic, phase and amplitude images were acquired using both non-functionalized silicon nitride probes, as well as the functionalized probes. These measurements were used to determine the variations in topographic resolution due to tip modification. All measurements were performed in “wet” conditions, that is, by keeping the tip and

sample immersed in phosphate buffer. The phase and amplitude mode images were acquired employing chemically derivatized AFM tips with alkanethiols terminating in OH (hydrophilic) or CH₃ (hydrophobic) groups. These images not only provide a better resolution of the finer microstructural details of the bacterial cell surfaces, but also provide insight regarding interactions between the heterogeneous cell surface and the chemically modified tips. The amplitude image resembles a derivative of the height image, accentuating edges on the sample surface and therefore tracking bacterial roughness, at the expense of the height information.[134] The phase image is generated by mapping the phase lag of the cantilever oscillation relative to the phase of the drive oscillation. Since it is energy dissipation that directly impacts the phase signal, variations in adhesion, elasticity, viscoelasticity, and long-range forces between the sample and the tip, which all impact the energy dissipation, can be mapped in the phase image.[98]

3.5 Force Analysis on Bacterial Surfaces Using AFM

Forces were measured between individual bacterial cells and chemically modified silicon nitride cantilevers. After topographic images were recorded for at least three bacterial samples, the tip was positioned over the top of a cell, scanning was stopped and force measurements were performed at randomly selected locations around the upper surface of each bacterial cell studied. The force distance curve was obtained for both the approaching and retracting motions of the tip. The pull-off is characterized by the location where the cantilever elastic stress overcomes the adhesive interactions between the probe and the sample. In the retraction phase, the pull-off (snap-off) force was recorded, and this force was used as a key parameter to study the tip adhesion to the bacterial cell surface. Triplicate measurements were performed on each

location on the surface of a bacterial cell. At least five cells were measured with the use of fresh probes and independent preparations to ensure consistent results. Individual force curves were collected at Z-scan rates of 0.5 Hz. IGOR PRO software was used to analyze the force measurements, which were initially acquired in terms of tip deflection (V) vs. relative distance of separation (nm). The slope of the retraction curves in the region where the probe and sample were in contact was used to convert the voltage into cantilever deflection (nm). The conversion of deflection data to force was conducted employing the approach previously described by Ducker et al.[106]

3.6 Zeta Potential Measurements

A Brookhaven ZetaPALS analyzer (Brookhaven Instruments Corporation, Holtzville, NY) and disposable folded capillary cells were used to measure electrophoretic mobilities of different bacterial suspensions at room temperature. [110] Zeta potential was measured for cells that were harvested in the early stationary phase. The microbes were resuspended in phosphate buffer at several ionic strengths. Prior to using the bacterial sample, three conductance readings of the buffer solution were recorded to allow the polarization of the electrodes at the studied ionic strength.[13] The measured mobility of the bacteria was converted to zeta potential by the instrument software using the Smoluchowski equation (2.3). In this study, for each sample, the measurement was repeated three times at room temperature (22°C). The average value and standard deviation are reported on the basis of the three measurements.

3.7 Transmission Electron Microscopy of Bacterial Cells

Negative staining was used to visualize cell external structures such as pili and to measure the dimensions of the cells. A drop of the bacterial suspension was placed on a carbon-coated grid for 5 minutes without allowing the liquid to dry. Following this, the sample was stained by applying a drop of 2% (w/v) uranyl acetate solution to the grid. After staining, the grid was washed twice and examined with a Philips / FEI (Morgagni) transmission electron microscope.[101] Capsules were visualized using transmission electron microscopy (TEM) by fixing cells in 5% cacodylate buffered glutaraldehyde, post-fixing in 1% osmium tetroxide, dehydrating through a graded ethanol solution and embedding in Epon as described by Schaer-Zammaretti and Ubbink.[101] Ruthenium red (0.15%) and phosphate buffer were added to both fixative and wash solutions to stabilize the capsule material.[101] Ultra-thin sections were stained in aqueous uranyl and lead salts and examined by using a Philips / FEI (Morgagni) TEM.

3.8 Contact Angle Measurements

Contact angle measurements were used to quantify the hydrophobicity of both bacterial species and also to calculate their Hamaker constants. Bacteria were harvested at early stationary growth phase and washed two times with phosphate buffer and resuspended in the same solution. Four milliliters of the bacterial cell suspension was applied to a 0.45 μm filter (membrane filters; Millipore, Billerica, MA) and vacuum filtered. The filters were partially dried and contact angles were determined on lawns of bacterial cells using the sessile drop

technique. The measurements were carried out at room temperature by depositing a 20 μ l droplet of the probe liquid. Five contact angle measurements were obtained immediately following deposition of the liquid droplet. Water and diiodomethane (HPLC grade, Sigma-Aldrich) were used as the probe liquids, as they have well known surface tension properties. Eight filters were prepared for each bacterial species, and contact angle values were averaged and used for surface free energy calculations.

4. Atomic Force Microscopy Measurement of Heterogeneity in Bacterial Surface Hydrophobicity²

4.1 Introduction

The use of microorganisms in hydrocarbon processing or remediation of oil spills is a promising technology considered to be the most environmentally sound, least intrusive and cheapest of the new technologies in these fields.[36] However, the chemical complexity and water insolubility of crude oil present challenges to microorganisms using petroleum as a growth substrate. Attachment of bacteria to the oil/water interface, at the surface of oil droplets suspended in water, is a common adaptation for overcoming the poor aqueous solubility of the hydrocarbons.

Macroscopic surface properties of microbial cells have been extensively investigated starting with the pioneering observations by Mudd and Mudd [8, 9] of bacterial partitioning at oil/water interfaces. These studies suggest that, depending on their surface hydrophobicity, bacteria can be positioned on one side or the other of the oil/water interface. Macroscopic cell-surface properties have been commonly inferred from water contact angle measurements on bacterial lawns deposited on membrane filters [10, 11] or from bacterial adhesion to hydrocarbons.[12] The results of these measurements were based on average cell surface hydrophobicity, and do not provide information about the forces governing the adhesion process at the molecular scale.[14]

² A version of this chapter was published previously:

Dorobantu, L.S., Bhattacharjee, S., Foght, J.M., and Gray, M.R. 2008. *Langmuir* 24: 4944-4951.

To enhance the bioavailability of an insoluble substrate and promote adhesion, we need to understand how the behavior of microbial cells at an oil/water interface depends on the morphology and physicochemical properties of the cell surface. The morphology of the bacterial cells has traditionally been observed via electron microscopy. While this technique can provide high-resolution images, the extensive sample processing such as treatments with heavy metals to provide the necessary contrast to make structures visible and the need for the sample to be under vacuum limits its application in visualization under physiological conditions.[135] It has been shown that bacterial interactions can be mediated by extracellular layers, such as capsules or slime layers of polysaccharides, or protein-based appendages such as pili.[21] The structure of these appendages and their specific chemistry facilitate the microorganism's attachment to different types of surfaces and interfaces.[20] The presence and properties of these cell surface constituents depends on the bacterial species and the growth and environmental conditions.

Atomic force microscopy (AFM) offers a facile alternative for obtaining microscopic physicochemical properties and morphology of biological surfaces. [15, 16] AFM allows probing of surface hydrophobicity, surface charges, and mechanical properties of living bacterial surfaces in their physiological environments, without chemical preparation and with nanometer resolution, providing information that is complementary to that obtained using other structure-determination techniques.[17] AFM also allows the quantitative determination of the nanoscale interaction forces between the probe tip and a cell. A force-distance curve or a force-volume map can be exploited to gain insights into a variety of physicomechanical and physicochemical properties of the cell and its surface structures.[18]

Most commercially available AFM tips are made of silicon nitride and have a unique surface chemistry which provides a limited range of parameters for quantitative force measurements.[93] One method for obtaining probes of well-defined chemistry and geometry is to attach a particle such as a microsphere to the AFM cantilever. However, the use of a large colloidal probe of micrometer dimension is not an effective solution for mapping the chemically heterogeneous surface of a bacterial cell because of the loss of resolution. A large AFM tip cannot probe local interactions on an area a few tens of square nanometers or give high-resolution imaging.[19] Other methods include the modification of AFM probes with different chemicals or biological molecules. Emerson et al. [116] studied the interaction of *S. epidermidis* immobilized on AFM probes with functionalized planar surfaces. This technique provides useful information on bacterial interactions with different materials, but it cannot be used to probe the heterogeneity of the cell surface. The most common and versatile approach is based on the formation of self-assembled monolayers of alkanethiols onto gold-coated probes.[96] The thiols form ordered self-assembled monolayers that are tightly bound to the gold surface via chemisorption of the sulfur atoms. The monolayers are stabilized further by the lateral hydrophobic interactions of the alkyl chains. By derivatizing the surface of the AFM tips with such well-defined chemical groups, we can learn more about the local distribution of cell surface properties such as surface hydrophobicity across single cells. Furthermore, by changing the terminal groups of these self-assembled monolayers, specific interactions between regions of a bacterial cell surface and different functional groups may be elucidated.

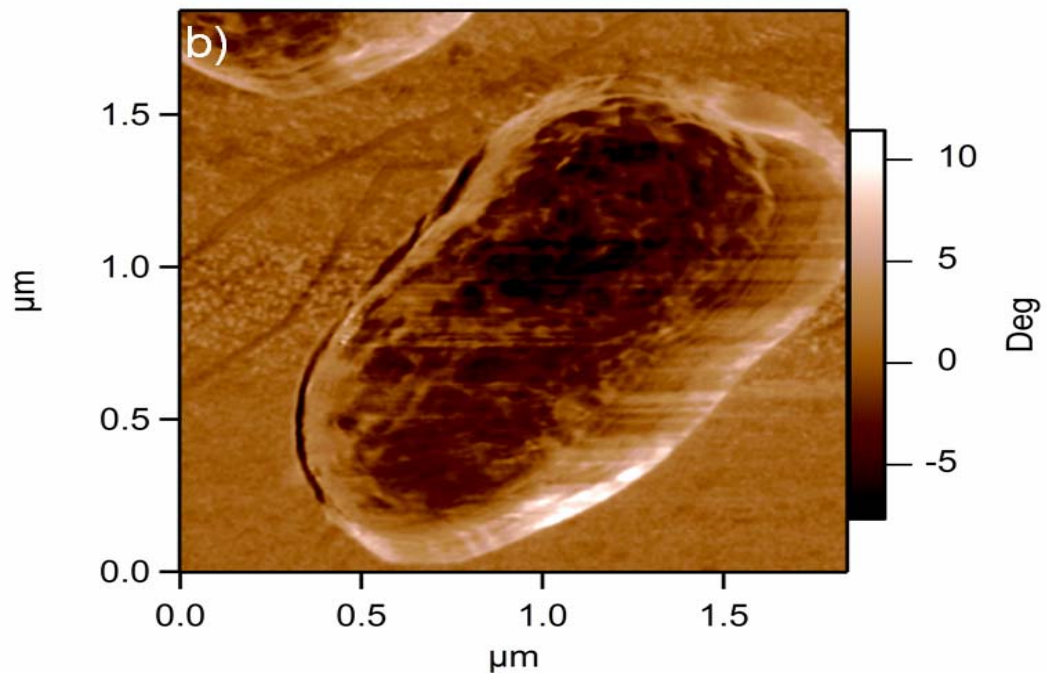
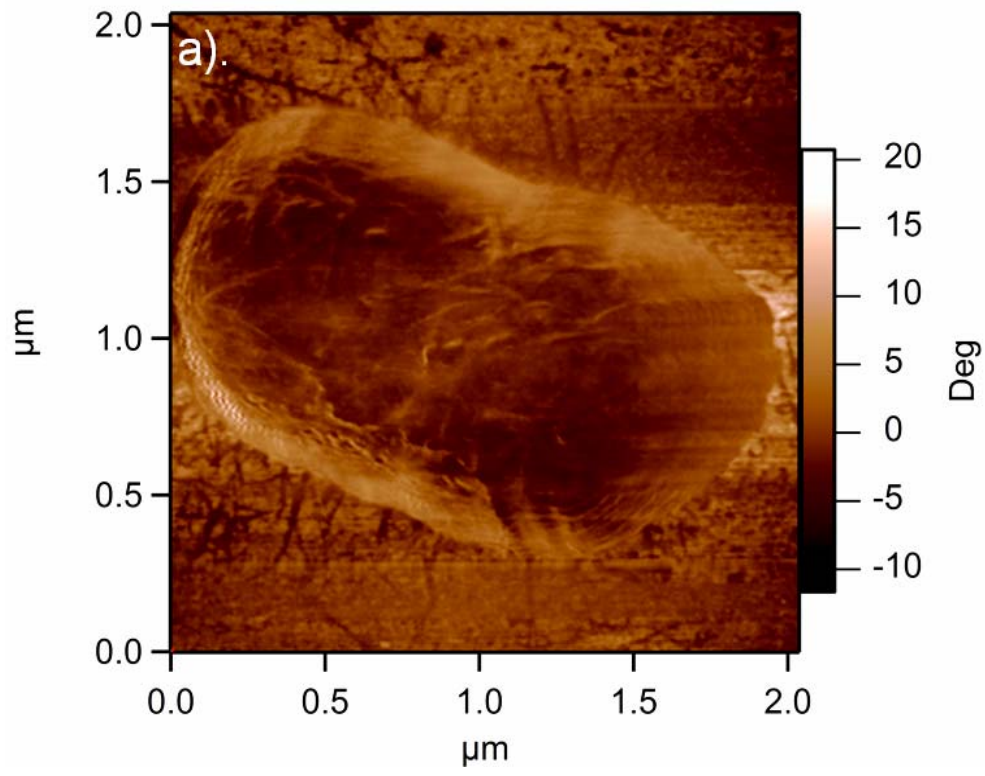
In this study, we used AFM to visualize the morphological details of two bacterial strains with different surface hydrophobicity under native conditions and measure the interaction force between these microbial cells and chemically modified AFM tips. By AFM imaging, we investigated the correlation of the bacterial cell dimensions to the results obtained by transmission electron microscopy. The shape and magnitude of the interaction forces determined from the AFM retraction force curves were used to define the heterogeneity of the cell surfaces. Results from the AFM force curves were used to define the relationship between the heterogeneous bacterial surface properties and the three-phase contact angle of hexadecane and water at the cell surfaces.

4.2 Microbial Characterization: Ultrastructure and Morphology

The AFM height images provide information on sample surface topography, whereas phase and amplitude images reveal a high sensitivity to fine surface details. Moreover, phase images can provide insight regarding adhesion interactions between the heterogeneous cell surface and the chemically modified tips whose surface modification procedure is presented in Section 3.3 of Chapter 3.

Fig. 4.1 presents AFM phase images, recorded in AC mode, of the surface of *A. venetianus* RAG-1 taken with the hydrophilic (a) and hydrophobic (b) modified tips, respectively, in phosphate buffer. Images of *A. venetianus* RAG-1 acquired using the hydrophilic tip show the cells surrounded by pili (thin fibrils in Fig. 4.1a), in comparison to the image of another RAG-1 cell acquired with the hydrophobic tip (Fig. 4.1b), which does not show the presence of any extracellular structures. Figure 4.1c shows the amplitude image taken on *A. venetianus* RAG-1 surface with the hydrophobic tip. The amplitude image

provides information about the topography of the cell surface. The bacterium appears covered by a compact granular layer, which resembles a capsular structure. It is worth mentioning that the fine surface features were not detectable from the height image obtained by direct topographical scan of the bacterium as can be seen in Figure A.8. The phase and amplitude images provide considerable details regarding the organization of the cell surface in terms of the distribution of highly adhesive regions and the nanoscale roughness of the surface. With the hydrophobic tips, an adhesive region was mapped toward the right hand side of the images giving a halo-like appearance in the phase image (Fig. 4.1b) and a smooth extended profile in the amplitude image (Fig. 4.1c).



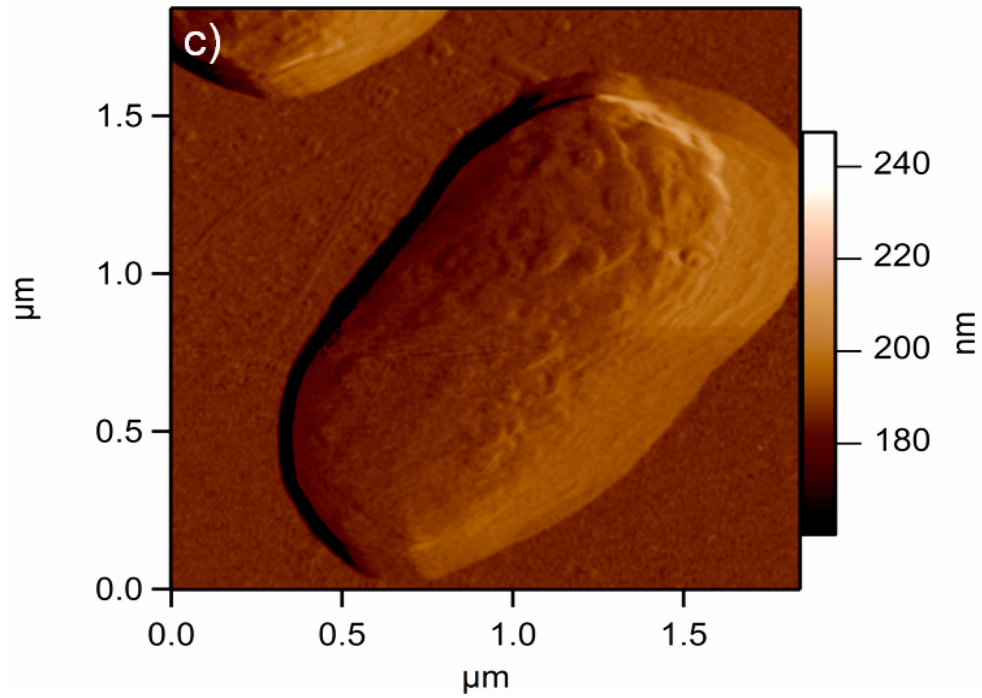
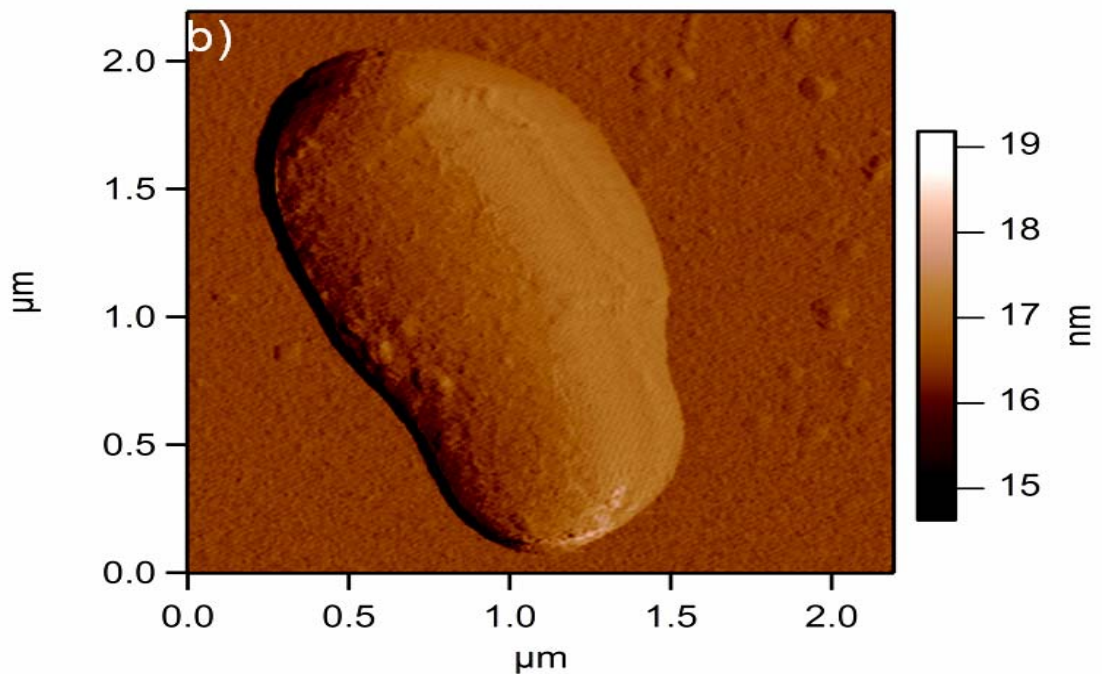
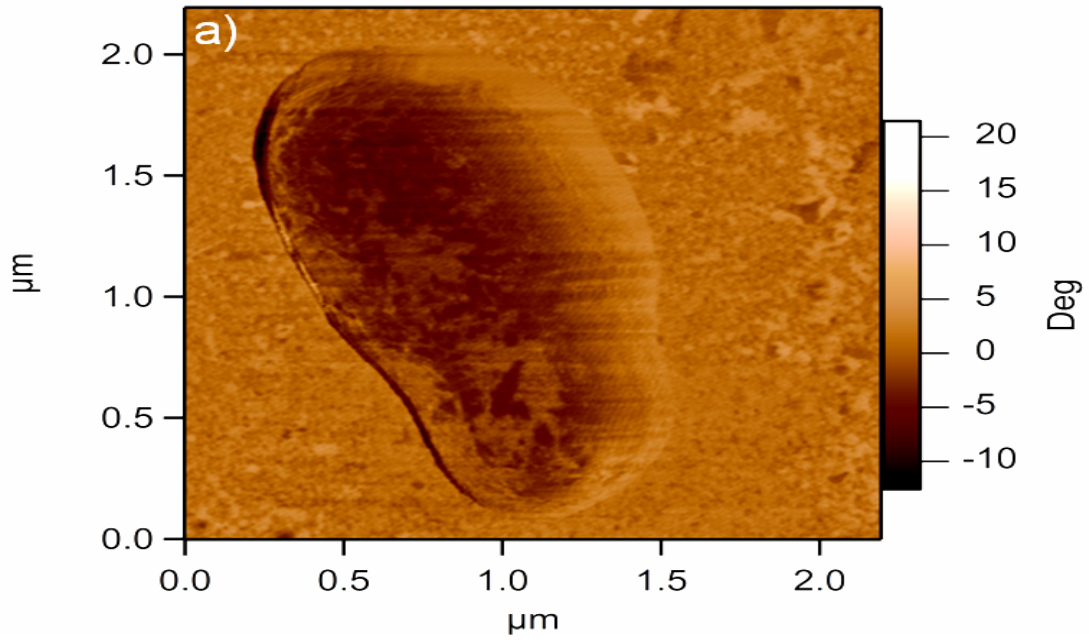


Figure 4.1 (a) *A. venetianus* RAG-1 AFM phase image taken in phosphate buffer with the hydrophilic tip; (b) and (c) *A. venetianus* RAG-1 AFM phase and amplitude images, respectively, taken in phosphate buffer with the hydrophobic tip. The axes represent cell dimensions (in μm).

Fig. 4.2a shows the AFM phase image, recorded in AC mode, of the surface of *R. erythropolis* 20S-E1-c taken with the hydrophobic modified tip. While no extracellular structures were observed on the surface of this bacterium, a lighter phase contrast could be seen at the pole of the cell. The amplitude image (Fig. 4.2b) shows a rough surface, possibly representing capsule. As in the case of *A. venetianus* RAG-1, we once again observe a halo like adhesive zone toward the right hand side of the phase image, and a smooth extended profile in the amplitude image. It is worth noting that the phase image provides a fairly detailed view of the chemically heterogeneous surface, as manifested by the distribution of adhesiveness.

The amplitude image, on the other hand, provides the nanoscale roughness of the bacterial surface. Fig. 4.2c, which is a contour plot calculated from point-by-point measurements of adhesion forces, presents a map of adhesive forces on the surface of *R. erythropolis* 20S-E1-c. Comparing Fig. 4.2a and 4.2c, we notice that the lighter contrast in the phase image corresponds to the higher forces in the adhesion force map.



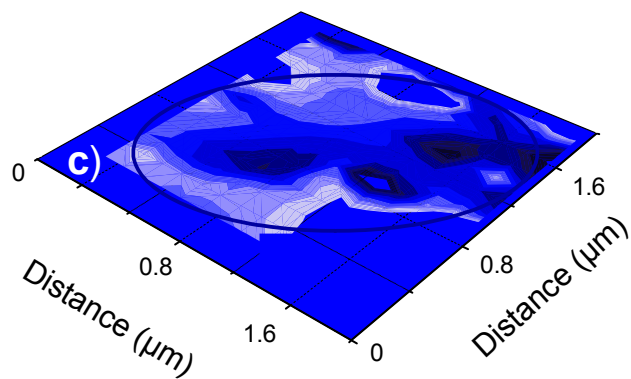
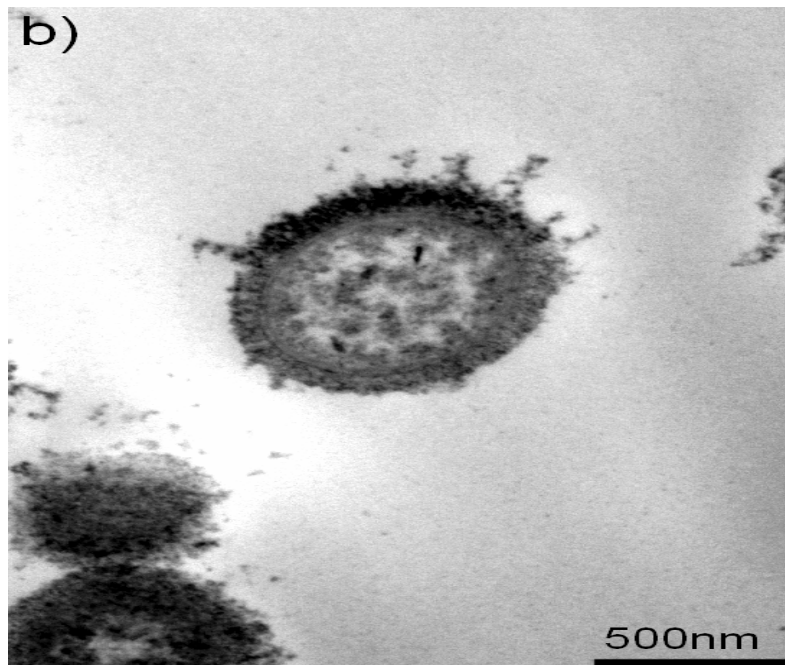
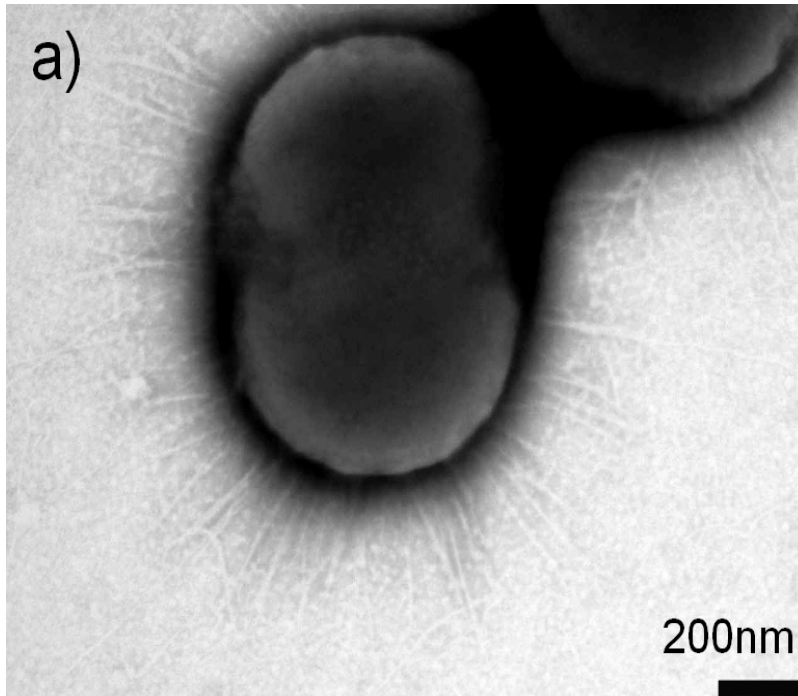


Figure 4.2 (a) *R. erythropolis* 20S-E1-c AFM phase image; (b) *R. erythropolis* 20S-E1-c AFM amplitude image. (c) Adhesion force map for the surface of one cell of *R. erythropolis* 20S-E1-c. Contours are from point measurements and the darker color in this image represents stronger adhesion forces. All images were taken in phosphate buffer with the hydrophobic tips. The axes represent cell dimensions (in μm).

Figure 4.3 shows some representative TEM images of the two types of bacteria employed in this study. The existence of pili on the surface of *A. venetianus* RAG-1 was confirmed by TEM in Fig. 4.3a where pili of 0.1 to 0.7 μm length and 5-8 nm diameter can be clearly seen surrounding the cell. The presence of a capsule surrounding *A. venetianus* RAG-1 surface was also confirmed by TEM in Fig. 4.3b, which displays a capsule of ~ 100 nm thickness. Finally, the presence of a capsule surrounding *R. erythropolis* 20S-E1-c surface was also confirmed by TEM, as depicted in Fig. 4.3c, where the capsule material seems to be unevenly distributed.



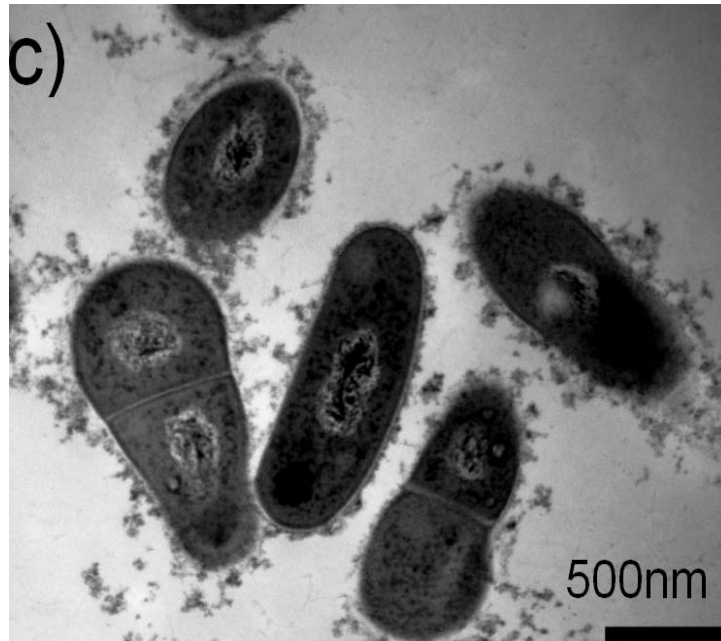


Figure 4.3 Transmission electron micrographs; (a) Thin sections of *A. venetianus* RAG-1, negatively stained, with pili extending from the cell surface (scale bar = 200 nm); *A. venetianus* RAG-1 (b) and *R. erythropolis* 20S-E1-c (c) surrounded by capsule (scale bars = 500 nm)

The dimensions of the *A. venetianus* RAG-1 and *R. erythropolis* 20S-E1-c obtained during AFM imaging in liquid were comparable to TEM measurements. *A. venetianus* RAG-1 cells were 1.72 ± 0.09 μm long, 1.10 ± 0.05 μm wide, and their height was 0.66 ± 0.03 μm , Figure A6 and A7 in Appendix A. *R. erythropolis* 20S-E1-c cells were 2.44 ± 0.02 μm in length, 1.50 ± 0.23 μm in width, and 0.71 ± 0.05 μm in height (mean \pm 1 standard deviation; $n = 10$), Figure A9 and A10 in Appendix A.

The measurements of *A. venetianus* RAG-1 and *R. erythropolis* 20S-E1-c were done only on non-dividing cells; therefore, the variation in size is relatively small.

Although the measurements were taken using both unmodified as well as functionalized tips, there was not a significant variation in the key dimensions of the cells. In all cases, the attachment of the cells to the surface was sufficiently robust to allow an individual bacterium to be repeatedly imaged.

4.3 Force Measurements

Figure 4.4 depicts typical force distance measurements consisting of approach (Fig. 4.4a) and retraction curves (Fig. 4.4b) obtained on a silanized glass substrate (blue trace), *A.venetianus* RAG-1 (red trace), and *R. erythropolis* 20S-E1-c (green trace). In all cases, the measurements were conducted with hydrophobic tips immersed in phosphate buffer. The data for the hydrophobic tips interacting with the cell surfaces are representative of results obtained on at least five cells, using fresh AFM tips and independent preparations (a collection of retraction force curves for each bacterium is presented in Appendix A). Multiple force curves recorded at the same location yielded reproducible behavior (data presented in Appendix A). Force curves were also measured on the silanized

glass substrate (Figs. 4.4a and 4.4b, blue trace), before and after measurement on the cells, to confirm that there was no contamination on the AFM tip that may have caused nonspecific adhesion between the tip and the cell surface.

The approach curves for the hydrophobic tip toward the silanized glass (Fig. 4.4a, blue trace) and *A.venetianus* RAG-1 (Fig. 4.4a, red trace) are almost identical, indicating a sharp short range repulsion, followed by a short range attraction (resembling a jump-to-contact), and a virtually negligible long-range interaction.

In case of *R. erythropolis* 20S-E1-c, the approach curve (Fig. 4.4a, green trace) does not show any short range attraction. Overall, all the approach curves are quite similar for the three types of surfaces indicating a very short range (~10 -20 nm) interaction between the approaching tip and the substrate.

The retraction curves, on the other hand, are strikingly different for the three types of substrates. The retraction curves for the interaction between the silanized glass substrate and the hydrophobic tip displayed the snap-off effect (Fig. 4.4b, blue trace), which occurred over a length of only a few nanometers. During retraction, the attractive interaction between the *A. venetianus* cell and the AFM tip was manifested over a considerably larger distance, generally exhibiting an irregular pattern with multiple adhesion peaks. Eventually, the retracting tip snapped off at a distance between 0.6 – 0.7 μm (Fig. 4.4b, red trace). The retraction curves for *R. erythropolis* 20S-E1-c also exhibited long-range attraction (Fig. 4.4b, green trace), although the snap-off appeared to take place at a shorter separation compared to *A. venetianus* RAG-1, after a smooth decrease in the force.

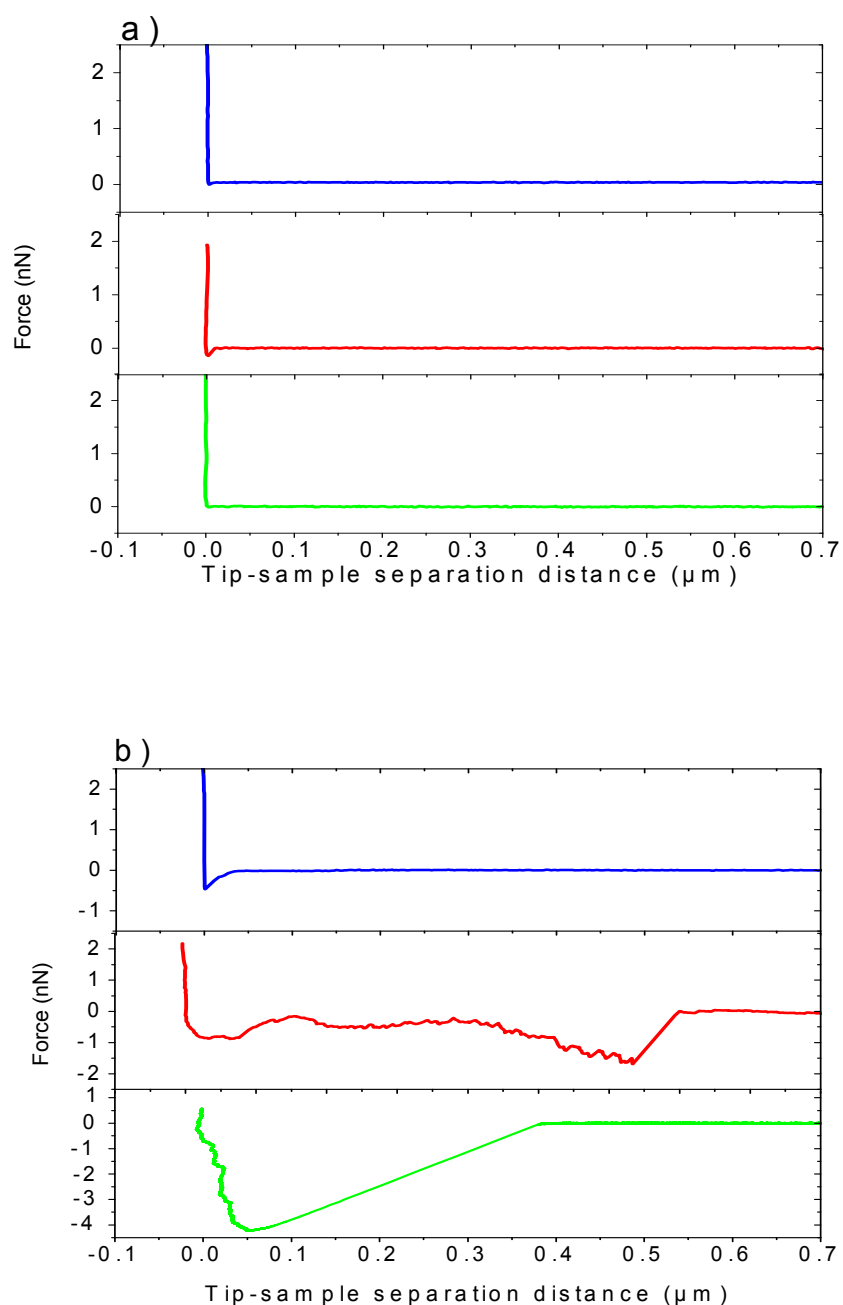


Figure 4.4 Typical results from AFM force measurements. Panel (a) represents the approach curves while panel (b) indicates the retraction curves. Example of force-distance curves taken on bare substrate (blue trace), *A. venetianus* RAG-1 (red trace), and *R. erythropolis* 20S-E1-c (green trace) with hydrophobic tips in phosphate buffer.

The local adhesion forces, measured from the retraction curves for *A. venetianus* RAG-1, ranged from 0.10 ± 0.03 nN to 1.50 ± 0.09 nN (mean \pm 1 standard deviation, $n = 3$, where n represents the number of extension/retraction force curves measured at the same location). *R. erythropolis* 20S-E1-c exhibited much higher adhesion forces, ranging from 0.40 ± 0.05 nN to 4.0 ± 0.4 nN. These error bounds represent standard deviations and indicate the typical repeatability of force measurements at a single point. In the case of *A. venetianus* RAG-1, the local adhesion forces extended up to 620 nm from the cell surface, consistent with the observed lengths of the pili (Figs. 4.1a and 4.3a).

The magnitude of the adhesion forces and their frequency is displayed in the adhesion histograms in Fig. 4.5 for *A. venetianus* RAG-1 (a) and *R. erythropolis* 20S-E1-c (b), respectively. With the hydrophobic tip, the mean adhesion force for *A. venetianus* RAG-1 was 0.63 ± 0.08 nN and for *R. erythropolis* 20S-E1-c 1.82 ± 0.18 nN. The adhesion forces for *A. venetianus* RAG-1 were smaller and more heterogeneous than those measured for *R. erythropolis* 20S-E1-c.

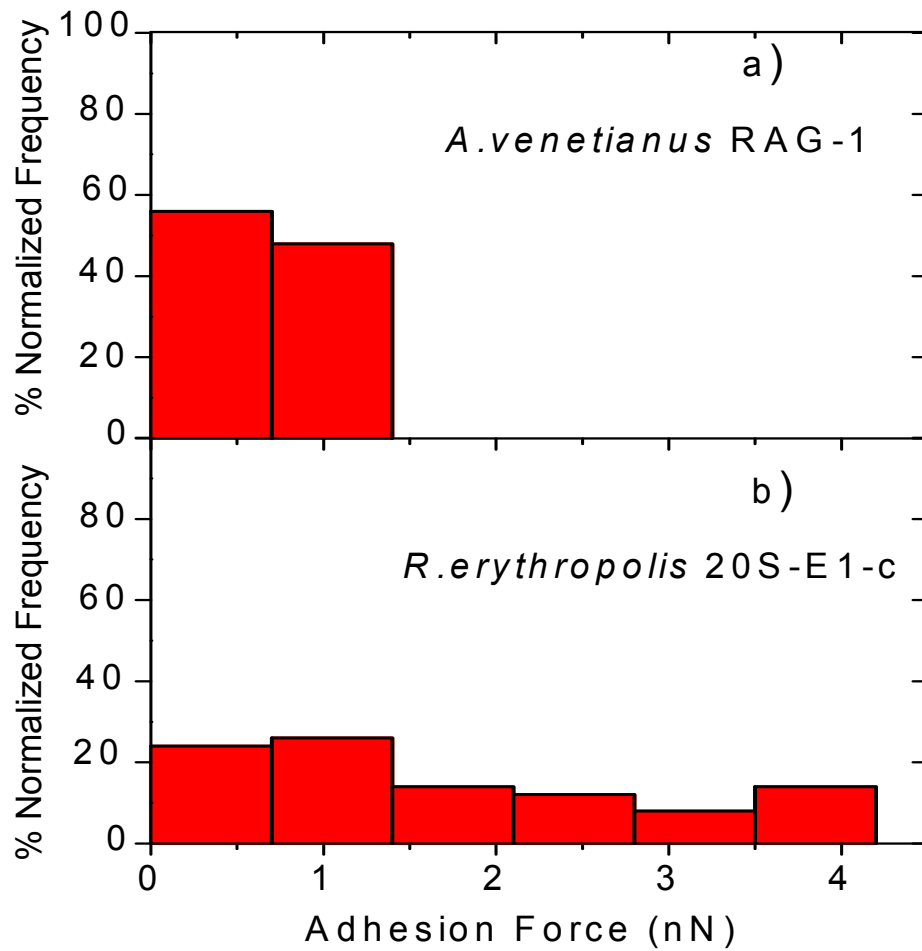
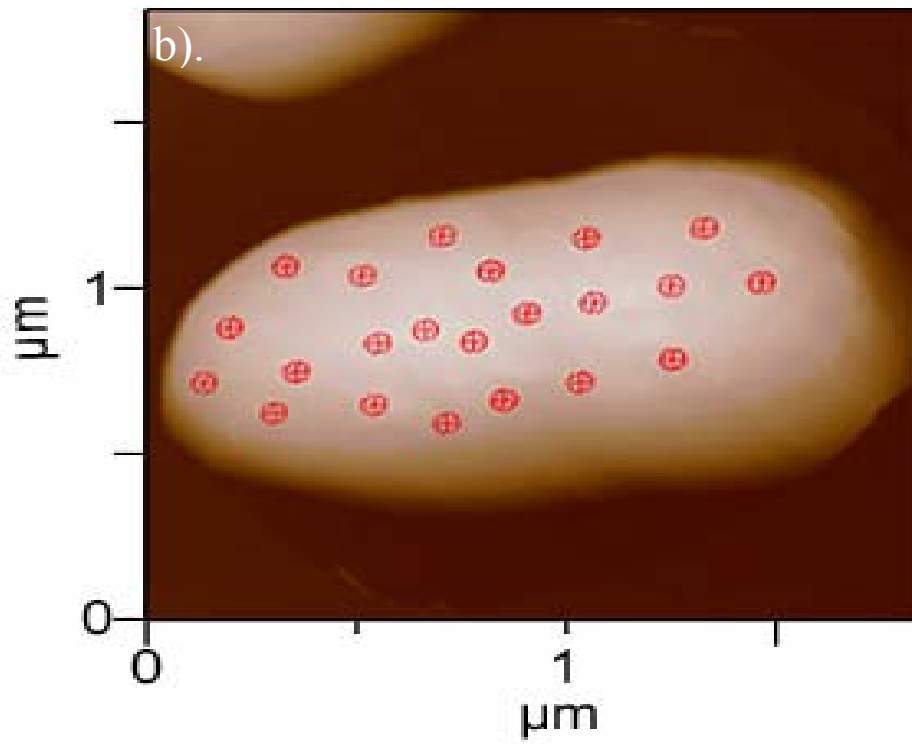
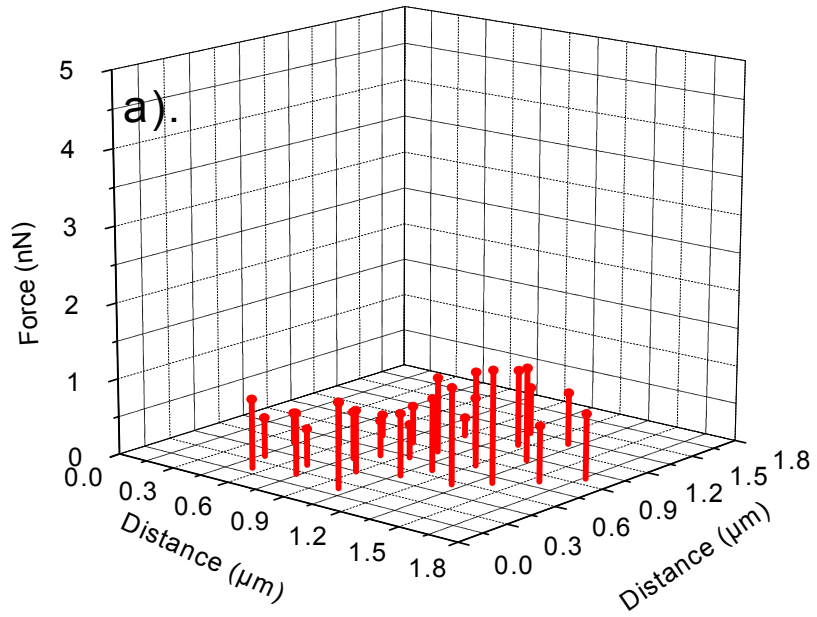


Figure 4.5 Force distribution histogram for *A. venetianus* RAG-1 (a) and *R. erythropolis* 20S-E1-c (b) interacting with the hydrophobic tips in phosphate buffer, as derived from Figure 4.4.

Figures 4.6a and 4.6b show the distribution of the adhesion forces at different x-y positions on the surface of *A. venetianus* RAG-1 (panel 4.6c) and *R. erythropolis* 20S-E1-c (panel 4.6d), respectively. Panels 4.6a and 4.6b show the locations where the forces were measured on the surface of the two bacterial species. In Fig. 4.6a, the surface of *A. venetianus* RAG-1 shows a random distribution of the adhesion forces. In contrast, Fig. 4.6b indicates a patterned distribution of the adhesion forces for *R. erythropolis* 20S-E1-c, with the highest forces grouped at one pole of the cell.



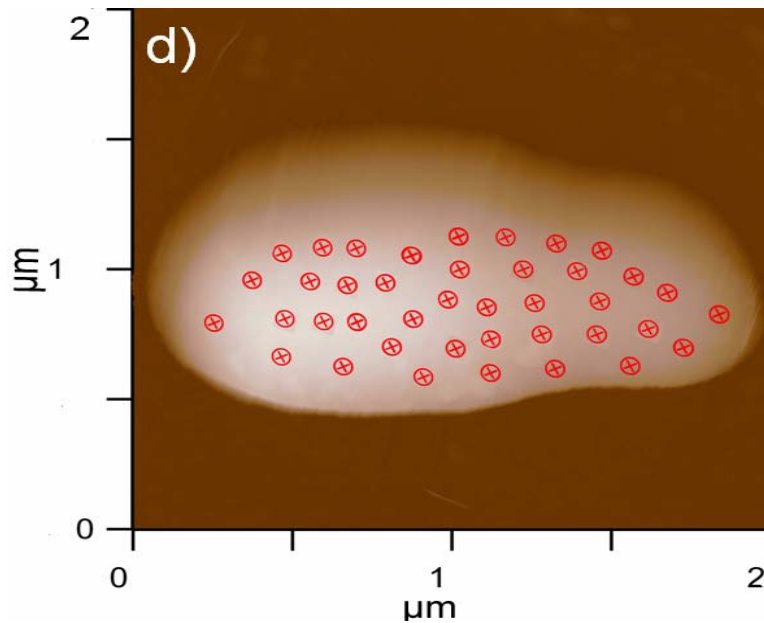
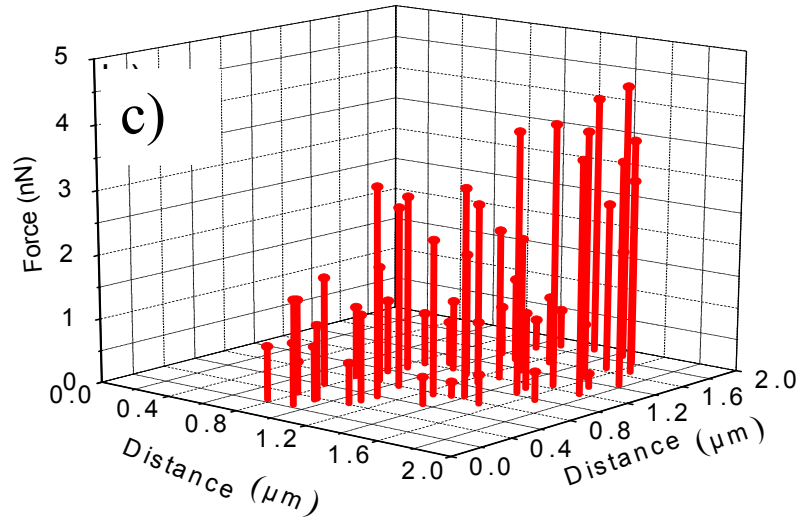


Figure 4.6 (a) Distribution of adhesion forces over *A.venetianus* RAG-1 surface on a representative cell and the corresponding bacterial image (b) showing the locations where the forces were measured. (c) Distribution of adhesion forces over *R. erythropolis* 20S-E1-c surface on a representative cell and the corresponding bacterial image (d) showing the locations where the forces were measured.

In contrast to the data for hydrophobic tips illustrated in Figure 4.4, the interactions between the hydrophilic tips and the two microbes, in both approach and retraction curves, were qualitatively identical to the cell-free control curve in Fig. 4.4a, blue trace (data shown in the appendix; Figure A3). No measurable difference was observed between the approaching and retracting traces in these controls. In general, the force of interaction between the bacterial surface and the hydrophilic tips always gave a monotonic increase in the repulsive force as the separation distance was reduced during tip approach.

4.4 Discussion

In this study, high-resolution AFM imaging was performed on *A. venetianus* RAG-1 and *R. erythropolis* 20S-E1-c, two species previously documented to degrade hydrocarbons, revealing not only the cell surface morphology but also the ultrastructure of the extracellular appendages under physiological conditions (Figures 4.1 and 4.2). As revealed by AFM phase image (Figure 4.1a) and confirmed by TEM negative staining (Figure 4.3a), *A.venetianus* RAG-1 is covered with pili of up to 0.7 μm in length and 5 nm in diameter. The pili are visible when imaging with the hydrophilic tips, but are not revealed during imaging with the hydrophobic tips. These observations strongly suggest that the pili are hydrophobic in nature. When the hydrophilic tip approaches these structures, they remain immobilized on the substrate, and their positions are recorded by the tip. In contrast, when the hydrophobic tip approaches these structures, they adhere to the tip and move with it. In this case, the tip fails to detect the presence of these structures except via the force curves during retraction (Figure 4.4d).

Using TEM, *A. venetianus* RAG-1 was observed by Rosenberg et al. [33] to produce two major types of pili: abundant thin pili and occasional thick pili with diameters of 3.5 and 6.5 nm, respectively. The thin pili were a major factor in adherence to hydrophobic surfaces (hydrocarbon droplets or polystyrene surfaces), and thus presumably have hydrophobic tips. Only one abundant pilus type was observed in the current study, having a diameter of 5 nm and likely corresponding to the thin pili observed by Rosenberg et al.[33]

The amplitude image in Figure 4.1c shows the coverage of *A. venetianus* RAG-1 cells by a compact granular film that likely represents capsule. *A. venetianus* RAG-1 is a Gram-negative bacterium with a conventional lipopolysaccharide outer membrane. It produces an extracellular bioemulsifier (emulsan) that is cell-associated in the early phases of growth but is released from the cells as they enter stationary phase.[136] Cultures of RAG-1 used in the current work were grown to stationary phase and washed before analysis, thus reducing sloughed emulsan and exposing the hydrophilic cell surface and fimbriae. However, TEM observations and glutaraldehyde fixation confirmed the existence of a capsule surrounding this bacterial surface (Figure 4.3b), consistent with observations by Pines et al. [137]

The surface of *R. erythropolis* 20S-E1-c was devoid of pili (Figure 4.2a), but a layer consistent with capsule was observed surrounding the cells in TEM images (Figure 4.3c). The AFM amplitude images also revealed a rough surface for this bacterium (Figure 4.2b) consistent with the presence of a compact capsule layer. Whyte et al. [138] observed loosely associated material external to the *Rhodococcus* cell surface.

It is not clear whether this 'extracellular polymeric substance' [138] or 'surface layer' [139] is hydrophobic, hydrophilic, or amphiphilic, as its chemical composition appears to change depending upon growth conditions [138] and between species; [139] both polysaccharide [138] and lipidic [139] materials have been observed surrounding cells. We have not determined whether the capsule material observed surrounding *R. erythropolis* 20S-E1-c in Figure 4.3c (which appears granular due to fixation and dehydration for TEM) represents noncovalently bound lipidic amphiphiles or polysaccharide or a combination of these moieties.

Images of *A. venetianus* RAG-1 in buffer (Figure 4.1b,c) revealed lines oriented in the scanning direction (forward scanning) that could represent extracellular structures pulled off the bacterial cell. This behavior is also apparent for *R. erythropolis* 20S-E1-c (Figures 4.2a,b) to a lesser extent. The presence of some material apparent along the scan direction of an image of an *E. coli* cell was also observed by Velegol et al., [92, 140] and it was stated to be an imaging artifact introduced by the height of bacteria in conjunction with the pyramidal AFM tip geometry. In contrast, our AFM imaging, performed with both hydrophilic and hydrophobic tips with virtually identical geometry shows different structures of the bacteria. While the images obtained using the hydrophobic tips showed a halo-like extended structure along the forward scan direction, the images using hydrophilic tips did not show any such structural artifacts, suggesting that the imaging artifacts were not due to the geometric interaction of the tip with the substrate.

AFM in the aqueous phosphate buffer phase allowed force measurements on viable cells of *A. venetianus* RAG-1 and *R. erythropolis* 20S-E1-c. Force-distance curves for the interaction of *A. venetianus* RAG-1 with the

hydrophobic tip gave multiple adhesion peaks during retraction (Figure 4.4b, red trace).

This behavior is consistent with pull-off forces from pili attached to the cell surface. The irregular pattern of forces upon retraction of the hydrophobic tip (Figure 4.4) could be caused by two factors: first, multiple pili of different lengths could attach to the AFM tip at the same time and then pull off sequentially; second, a single longer pilus could attach to the tip at several points along its length. Similar retraction curves have been reported in literature for pili of *P. aeruginosa* [77] and with adhesive polymers.[141] The range of separation distances at which these adhesion forces occurred matched the lengths of pili determined in both phase and electron microscopy images. Although these distances may appear to be large, widely varying lengths of bacterial pili have been reported in the literature.[77]

Most of the retraction curves after contact with the surface of *R. erythropolis* 20S-E1-c displayed single rupture events accompanied by pronounced adhesion force peaks (Figure 4b, green trace). These curves are consistent with interaction of the probe tip with an adhesive capsule. The presence of a capsule surrounding this bacterium surface was also confirmed by TEM in Figure 4.3c. The thickness of the capsule cannot be accurately measured from TEM images due to the highly hydrated polymers, composing bacterial capsules, which collapse during the dehydration stages of conventional processing. Consequently, the stabilized capsules are not always representative of native structure and their dimensions rarely correlate well with those determined by other methods.[142] In the AFM images, the hydrophobic cell wall exterior of *R. erythropolis* 20S-E1-c, imparted by mycolic acids, may be masked by the presence of the capsule material. Nevertheless, as illustrated in Figure

4.4b (green trace), the exposed surface was strongly hydrophobic on the basis of the force interaction with the hydrophobic AFM tip, indicating the presence of hydrophobic capsular material surrounding this bacterium.

The interaction forces detected between the two bacterial species and the hydrophobic AFM tips were averaged for each cell into an adhesion force and compared to the hexadecane-water contact angle measured on bacterial lawns by Dorobantu et al.[5] A contact angle of 56.4° for *A. venetianus* RAG-1 was found to correspond to an adhesion force of 0.63 ± 0.08 nN, whereas in the case of *R. erythropolis* 20S-E1-c, a contact angle of 152.9° corresponded to an adhesion force of 1.82 nN. For both bacterial species examined, the contact angle was proportional to the mean adhesion force on the hydrophobic tip of the AFM. Although we cannot extrapolate to all other bacterial cells, similar results were obtained by Pietak et al. [143] using natural polymers and by Vadillo-Rodriguez et al. [144] with two *Lactobacillus* strains. Although Vadillo-Rodriguez et al. [144] reported a correlation between the adhesion force on a hydrophobic AFM tip and contact angle, the limited amount of data on tip properties in their report precludes a quantitative comparison to our force measurements.

For both bacterial species, the adhesion force measurements indicated a patchy surface distribution of interaction forces between the cell surfaces and functionalized tips (Figure 4.6). Surface heterogeneity was also confirmed during AFM phase imaging by different levels of phase contrast as shown in Figures 4.1b and 4.2a. The contrast in the phase image implicitly embeds information on the difference in adhesion properties and is presumably caused by variations in the dominant surface constituents like proteins and polysaccharides.

The arrangement of the adhesion forces for *R. erythropolis* 20S-E1-c typically showed a patterned distribution with the highest forces grouped at one pole of the cell (Figure 4.6b), which coincided with the lighter color in the phase image for this bacterium (Figure 4.2a).

Similar results were observed in measurements on other batches of cells and the end of the cell displaying high forces was independent of the scanning direction. This gradient in adhesion suggests a gradient in composition.

The TEM image of these cells suggests one possible reason for this gradient (Figure 4.3c); as the cells divide, they septate to give two distinct cells with a continuous external surface. The gradient in adhesion force could indicate the differing surface composition between newly formed cell surface near the septum and older cell surface distal to the septum. Many species change cell surface composition from the exponential growth phase to the stationary phase [145] which would reflect age-dependent changes in the cell population.

In contrast, *A. venetianus* RAG-1 showed a random distribution of the adhesion forces (Figure 4.6a), confirmed by the phase image in Figure 4.1b and consistent with presence of pili on the surface of the cells. The adhesion force varied over a wide range (Figure 4.5a), presumably depending on the number of pili interacting with the AFM tip. Given a relatively uniform but random distribution of pili, a probe experiment at a random point on the cell surface could interact with many pili or with few. Consequently, the map of adhesion forces in Figure 4.6a was consistent with the microscopy images of pili surrounding the cells (Figures 4.1a and 4.3a). The differences in cell surfaces could have significant implications for cell attachment to hydrophobic surfaces or interfaces such as crude oil droplets in water.

The uniform heterogeneity of the surface of *A. venetianus* RAG-1 would give no preferred orientation on a surface or interface. The gradient on the surface of *R. erythropolis* 20S-E1-c, however, could give a preferred orientation of attachment of one pole of the cell. As more and more cells attach, the interactions between the cells could alter the preferred orientation with respect to the hydrophobic surface.

A logical extension of this study would be to explore the surface heterogeneities of confluent biofilms associated with hydrophobic surfaces or interfaces. Biofilm growth can give changes in cell surface properties, and heterogeneity in the biofilm surface could be very different from the individual planktonic cells.

Although the individual cells had significant heterogeneities on their surfaces, we did not observe significant differences among adhesive forces of individual bacteria within the populations of early stationary phase cells. Consequently, the cell-average adhesive forces were proportional to the population averaged results for contact angle. We anticipate that cell populations in the exponential growth phase could be more heterogeneous, due to the potential influence of the cell cycle on surface composition.

5. Analysis of Force Interactions between AFM Tips and Hydrophobic Bacteria Using DLVO Theory³

5.1 Introduction

Understanding the fundamental adhesion processes between bacteria and hydrocarbon surfaces is important for many environmental and bioengineering applications, such as *in situ* remediation of oil spills or hydrocarbon processing.[146] The microorganisms attach to the oil/water interface as a common adaptation for overcoming the poor aqueous solubility of the petroleum hydrocarbons. Even though extensive research has been done on bacterial adhesion in the last decade, [5] the fundamental mechanisms governing this process are still poorly understood and have not been well defined.[6] An accurate quantification of the physico-chemical properties of bacterial cell surfaces is essential in order to reach a better understanding of bacterial adhesion to a surface or interface.

Hydrophobicity and electric charge of the microorganisms are influential in bacterial adhesion.[10] Hydrophobicity of microbial surfaces has been commonly inferred from water contact angle measurements on bacterial lawns deposited on membrane filters [11, 12] or from bacterial adhesion to hydrocarbons.[12] The electrical properties of microbial surfaces are often represented by the zeta potential, which is usually determined from their electrophoretic mobilities.[13] The results of these measurements give an

³ A version of this chapter has been accepted for publication:

Dorobantu, L.S., Bhattacharjee, S., Foght, J.M., and Gray, M.R. 2009. Langmuir

average of the cell surface properties, and do not provide information about the forces governing the adhesion process at the molecular scale.[14]

Atomic force microscopy (AFM) offers the opportunity to locally probe molecular forces of hydrated bacterial surfaces by means of force-distance curves.[16] A force–distance curve records the interaction forces as the AFM tip approaches the cell surface, makes contact and then retreats from it and can be exploited to gain insights into a variety of physico-mechanical and physico-chemical properties of the cell and its surface structures.[147]

The AFM tips most commonly used in force-distance measurements are made of silicon nitride and lack the chemical diversity that is needed to probe bacterial surface heterogeneity.[148] In order to overcome this drawback, the AFM probes have been functionalized with a wide range of molecules or particles and used for force-distance measurements to determine the type and magnitude of the interaction forces.[93] One of the methods employed for AFM tip modification consists of attaching cells to the AFM probes. Bowen et al.[149] measured the pull-off force between a single yeast cell immobilized on AFM probes and planar surfaces. This technique provides useful information on bacterial interactions with different materials, but it cannot be used to probe the heterogeneity of the cell surface. A similar method consists of attachment of micrometer-sized spherical particles directly onto the AFM cantilever. This method gives controlled surface chemistry and geometry, but the use of a large colloidal probe of micrometer dimension is not an effective solution for mapping the chemically heterogeneous surface of a bacterial cell because it cannot probe local interactions on an area a few tens of square nanometers.[19] Another approach used to modify AFM tips consists of deposition of organosilane layers

which directly couple to the surface silanol groups of the silicon nitride tips.[150] This method is not as extensively employed for AFM tip modification due to the difficulties encountered in controlling the polymerization process and the film thickness.[150]

The most common and versatile approach is based on the immobilization of alkanethiol-monolayers onto gold-coated probes by chemisorption of the sulfur atoms.[151] The thiol-monolayers are stabilized further by the lateral hydrophobic interactions of the alkyl chains.[152] By derivatizing the surface of the AFM tips with such well-defined chemical groups terminating with a variety of functionalities, we can learn more about the local distribution of cell surface properties such as hydrophobicity across single cells. For example, Alsteens et al.[152] used methyl-terminated tips to measure local hydrophobic forces on *Mycobacterium bovis*. The measured adhesion forces were large (about 3 nN) and uniformly distributed on the bacterial surface suggesting a highly hydrophobic surface consistent with the presence of mycolic acids on the outermost surface.

Owing to their dimensions, bacterial cells in solution may be described as colloidal particles,[5] and hence the process of microbial adhesion can be described by the Derjaguin-Landau-Verwey-Overbeek (DLVO) theory of colloidal stability.[112, 153] The DLVO theory estimates the interaction forces between two surfaces as a sum of the Lifshitz-Van der Waals (LW) and electrostatic double layer interactions between them. LW forces, which are of relatively long range, are always present and not very sensitive to solution ionic strength. The most important parameter determining the LW interaction is the Hamaker constant, which is a material property and whose value is in most cases rather

uncertain.[154] For microbial cell surfaces, it is often estimated from contact angle measurements on bacterial lawns.[155] Electrostatic forces, which are of long range, are very sensitive to the ionic strength and composition of the liquid solution in which measurements are performed. Calculation of electrostatic interactions requires knowledge of the electrostatic surface potential of the interacting surfaces, which is usually approximated by the zeta potential.

The DLVO theory assumes that the interacting surfaces are perfectly smooth, with no asperities or surface structures.[19] However, living organisms such as microbial cells can form specific extracellular structures, and their cell walls are more complex structurally and chemically than the surface of synthetic colloidal particles. Therefore, one would expect that the force curves taken on bacterial surfaces would involve specific biological polymer interactions.[22] As DLVO theory has only been marginally successful in describing interactions of biological systems, [119] other forces, including acid-base and steric interactions, have been considered to account for the discrepancy between measurements and theory [156] and corresponding enhanced models have been proposed.

Van Oss et al. [122] extended the DLVO model by accounting for the acid-base interactions, which determine the hydrophobicity (or hydrophilicity) of the involved surfaces. This approach, generally known as the extended DLVO (XDLVO) model, has been successful in predicting the interactions between largely uncharged colloidal entities in aqueous media. The acid-base interactions can be attractive or repulsive and range up to *ca.* 5 nm from the surface into the surroundings.[157] However, in many instances, the extended XDLVO model failed to describe bacterial adhesion.[158] Discrepancies between the results of adhesion experiments and calculated extended XDLVO interactions have been

attributed to interactions between bacterial surface polymers and solid surfaces, which interfere with the extended XDLVO interactions.[25, 111]

Surface structures such as fimbriae, flagella, [159, 160] and capsules [21] are believed to be involved in bacterial adhesion to different types of surfaces and interfaces.[161] The presence and properties of these cell surface constituents depends on the bacterial species and the growth conditions.[162]

Both Gram-negative and Gram-positive bacteria have been shown to possess surface layers and appendages which can range in length from short filaments to rigid or flexible structures up to several times the diameter of the cell. [81]

The presence of polymeric structures on bacterial cell surfaces has motivated the introduction of steric forces in addition to the DLVO interactions for interpretation of AFM force measurements.[23] The steric force arises from contact between the AFM tip and the extracellular polymeric chains extending from the microorganism surface into solution; as the AFM probe pushes down on the cell, the polymers are forced into a more compact spatial arrangement.[19] These steric interactions can be attractive or repulsive. Steric repulsion has been observed to arise from the higher affinity of the bacterial surface polymers for the interacting medium than for the solid surface (e.g., the AFM probe tip).[163] Polymer attraction has been proposed to occur when the bacterial surface polymers have a higher affinity for the solid surface than for the liquid medium and are sufficiently long to bridge the distance from the non-adhered cell to the solid surface.[163] In general, polymer bridging is observed for solids and microbes that are both hydrophobic.[114]

In this study, we analyzed the AFM force-distance data acquired during approach of AFM tips to bacterial surfaces. The interactions were measured between each of two bacterial strains possessing different surface hydrophobicity and chemically functionalized AFM tips, terminating in hydrophobic or hydrophilic groups. The experimental force-distance curves were compared with predictions based on classical DLVO theory and two extended DLVO models incorporating acid-base and steric interactions. The fitting parameters from the extended DLVO models were used to define the component of the force curves between AFM tips and bacteria that could not be explained by LW and electrostatic double layer mechanisms.

5.2 Mathematical Modeling

To help explain the force measurements, the classical DLVO model and two variations of the extended DLVO (denoted by XDLVO and EDLVO) model were employed. The XDLVO model accounts for acid-base interactions between the microorganisms and the chemically modified AFM probes, whereas the EDLVO model combines the effects of the acid-base and long-range steric interactions into a bi-exponential semi-empirical force form. These models were each considered for their ability to predict the experimental force measurements. Using nonlinear regression software OriginPro 7.5 (OriginLab Corporation, Northampton, MA, USA), the models were fitted to the recorded AFM approach curves.

5.2.1 Determination of Hamaker Constant

The contact angle of an apolar fluid on a substrate (here, the microbial lawn) provides its apolar surface tension component, γ_i^{LW} . The apolar surface tension component is related to the Hamaker constant of the microbial surface by equation 2.7 in Chapter 2 .[119]

The γ_s^{LW} surface tension component of the microbial cells, used in equation 2.7, can be obtained through contact angle measurements using the van Oss–Chaudhury–Good equation [106] adapted for the case of apolar liquid ($\gamma^+ = \gamma^- = 0 \text{ mJ.m}^{-2}$),

$$(1 + \cos \theta) \gamma_L = 2 \left(\sqrt{\gamma_s^{LW} \gamma_L^{LW}} \right) \quad 5.1$$

where θ is the contact angle, γ_L is the total surface tension of the liquid, γ_i^{LW} is the Lifshitz-van der Waals (LW), or apolar surface tension component of material (i), and the subscripts S and L refer to the bacterial and liquid phases, respectively.

5.2.2 DLVO Model

The AFM tip was modeled as a sphere with a radius of 40 nm, whereas the bacterial surface was assumed to be planar. The system geometry was modeled as a sphere interacting with a flat plate. The total DLVO interaction force (F_t) between the two interacting substrates was calculated as the sum of Lifshitz-van der Waals and electrostatic interactions,

$$F_t = F_{LW} + F_e \quad 5.2$$

where F_e is the electrostatic force and F_{LW} is the interaction force due to Lifshitz-van der Waals forces.

The expression for the nonretarded van der Waals force between a sphere and an infinite planar surface, based on Hamaker's approach and Derjaguin's approximation used in this study, is given by [110]

$$F_{LW} = \frac{A_{132}}{6} \left[-\frac{a}{h^2} - \frac{a}{(h+2a)^2} + \frac{2a}{h(h+2a)} \right] \quad 5.3$$

where A_{132} is the effective Hamaker constant of interaction between the bacteria (1) and the tip material (2) in phosphate buffer medium (3), a is the radius of the AFM tip, and h is the surface-to-surface distance between the substrate and the AFM tip.

The effective Hamaker constant for the system is related to the Hamaker constants of the individual components of the system by equation 2.5 in Chapter 2.

When two charged surfaces approach each other in an electrolyte solution, their diffuse double layers overlap, resulting in the electrostatic double layer interaction. Assuming constant surface potential on the substrates, the well-known Hogg, Healy, and Fuerstenau (HHF) [109] expression for the electrostatic force is used in fitting the data:

$$F_e = 4\pi\epsilon\epsilon_0(\kappa a) \left(\frac{kT}{ze} \right)^2 \psi_t \psi_s \left[\frac{\exp(-\kappa ah)}{1 + \exp(-\kappa ah)} - \frac{(\Psi_t - \Psi_s)^2}{2\Psi_t \Psi_s} \times \frac{\exp(-2\kappa ah)}{1 - \exp(-2\kappa ah)} \right] \quad 5.4$$

In the above formula, Ψ_t and Ψ_s are the scaled surface potentials ($\Psi = ze\psi/kT$) of the tip and the substrate, respectively, h is the separation distance between the two substrates, and κ is the inverse Debye length, given by the equation 2.2 in Chapter 2.

5.2.3 Extended DLVO Models

The approach part of a force distance curve was fitted to the sum of DLVO and an exponentially decaying function in which F_0 is the force at the minimum equilibrium cut-off separation distance l_0 , and λ is the characteristic decay length (separation distance over which F decays from F_0 to F_0/e). According to the XDLVO model,[113] this newly added force is of acid-base nature.

$$F_{XDLVO} = F_{DLVO} + F_0 \exp(-h/\lambda) \quad 5.5$$

A bi-exponential term extension to the classical DLVO theory was formulated for the microbial surfaces covered by extracellular structures of different length. This can be represented mathematically by

$$F_{EDLVO} = F_{DLVO} + F_{hi} \exp(-h/\lambda_{hi}) + F_{ho} \exp(-h/\lambda_{ho}) \quad 5.6$$

To distinguish this model from the conventional XDLVO theory, we denote the force obtained using this model as EDLVO. Here, F_{hi} and λ_{hi} represent the contact value of the force and the decay length of the shorter range force, and F_{ho} and λ_{ho} represent the corresponding parameters for the longer range force. It is evident that the shorter range exponential force in Eq. 5.6 can also be

represented as the acid-base force from the XDLVO model. Thus, Eq. 5.6 may either represent a combination of an acid-base and a long range force or other types of short and long ranged exponential forces.

5.2.4 Steric Model

A model developed for grafted polymers at relatively high surface coverage was used to model steric interactions between the AFM tip and bacterial extracellular structures. The interaction force between two parallel flat surfaces, F_{St} , only one of which is coated with polymer, has been modeled following the work of Alexander [123] and de Gennes.[164] This model was modified by Butt et al. [125] to describe the forces between a spherical AFM tip and a flat surface by integrating the force per unit area over the tip surface, to produce the interaction force given by equation 2.8 in Chapter 2.

For all the calculations, the tip radius was assumed to be 40 nm. L_0 and Γ serve as fitting parameters for the model. Note that Eq. 2.8 represents an exponentially decaying force, which can be represented by either exponential decay terms of Eq. 5.6.

5.3 Physicochemical Surface Properties Used for DLVO Interaction Calculations

The results of zeta potential measurements ξ are shown in Figures A.4 and A.5 in the Appendix as a function of ionic strength. They agree closely with results from Jones et al.[165] who concluded that the electrophoretic behavior of *C. albicans* in solution can be approximated by a simple colloidal suspension.

The zeta potential measurements recorded in 0.1M phosphate buffer showed that *R. erythropolis* 20S-E1-c is more electrostatically negative than *A. venetianus* RAG-1 (Table 5.1). These results are consistent with other studies which give values in the range -10 mV to -50 mV for the zeta potential of microbial cells at neutral pH.[13]

Table 5.1 Summary of parameters used for DLVO interaction calculations.

Substrate	Zeta potential (mV, n = 3)	$\Theta_{\text{diiodomethane}}$ ($^{\circ}$)	Hamaker constant ($\text{J} \times 10^{20}$)
<i>A. venetianus</i> RAG-1	-13.7 ± 0.4	30 ± 1	8.18
<i>R. erythropolis</i> 20S-E1-c	-32.3 ± 2.3	NA	NA
C ₁₈ thiol	-24[131]	55 ± 1.1	6.06
C ₁₁ -OH thiol	-64[131]	31 ± 1.9	7.97

NA, value could not be estimated, nor obtained from the literature

The contact angle values were measured with diiodomethane on different substrates and used to calculate the individual Hamaker constants (Table 5.1) from the apolar surface tension component (γ_i^{LW} in Eq. 2.7). *A.venetianus* RAG-1 had an average contact angle of $30^\circ \pm 1.2$ and a Hamaker constant of $8.18 \pm 0.12 \times 10^{-20}$ J, in good agreement with reported values of similar bacterial strains.[24] The contact angle and Hamaker constant of *R. erythropolis* 20S-E1-c could not be experimentally determined because the diiodomethane spread on its surface.

The contact angle of diiodimethane on the hydrophilic modified substrate was $31^\circ \pm 1.9$, yielding a Hamaker constant of $7.97 \pm 0.03 \times 10^{-20}$ J, whereas the contact angle measured on the hydrophobic modified substrate had a value of $55^\circ \pm 1.1$ and a Hamaker constant of $6.06 \pm 0.07 \times 10^{-20}$ J. The values of the contact angle measured on these thiol-derivatized surfaces are in good agreement with literature values.[129]

The individual Hamaker constants were used to calculate the effective Hamaker constants for the different systems according to Eq. 2.5. A value of 2.90×10^{-21} J was obtained for the combination *A. venetianus* RAG-1-water- $C_{17}CH_3$ and 5.71×10^{-21} J for the *A. venetianus* RAG-1-water- $C_{11}OH$ system. The systems comprising *R. erythropolis* 20S-E1-c-water- $C_{17}CH_3$ and *R. erythropolis* 20S-E1-c-water- $C_{11}OH$ were modeled using two different Hamaker constants with values of 3×10^{-21} and 6×10^{-21} ; to demonstrate that the model performance was insensitive to the exact value. These values of the Hamaker constant for the bacterial systems are in good agreement with literature values.[166]

5.4 Modeling of the AFM Approach Curves

We always observed continuous, monotonically increasing repulsive forces during the approach of the modified AFM probes to the two bacterial surfaces. The force curves for interaction of *A. venetianus* RAG-1 with both the hydrophilic and hydrophobic modified probes showed distinct repulsive profiles (Figures 5.1a and 5.1b, red circles). Measurable forces were recorded at distances as large as 50 nm from the cell surface for the case of the hydrophobic AFM tip and reached a magnitude of approximately 0.6 nN at the cell surface (Figure 5.1a, red circles). The interaction of the bacterium with the hydrophilic tip began at 10 nm from the cell surface and reached a magnitude of about 0.5 nN at the cell surface (Fig. 5.1b, red circles).

The interaction forces between *R.erythropolis* 20S-E1-c and the hydrophobic or hydrophilic AFM tips were of comparable magnitude and of shorter range than observed with *A. venetianus* RAG-1. With the hydrophobic AFM tip (Figure 5.1c, red circles), interactions began at 15 nm from the cell surface and reached a magnitude of approximately 0.45 nN at the cell surface, whereas *R.erythropolis* 20S-E1-c interacting with the hydrophilic AFM tip (Figure 5.1d, red circles) gave interactions starting at 5 nm from the cell surface and reaching a magnitude of 0.4 nN at the cell surface.

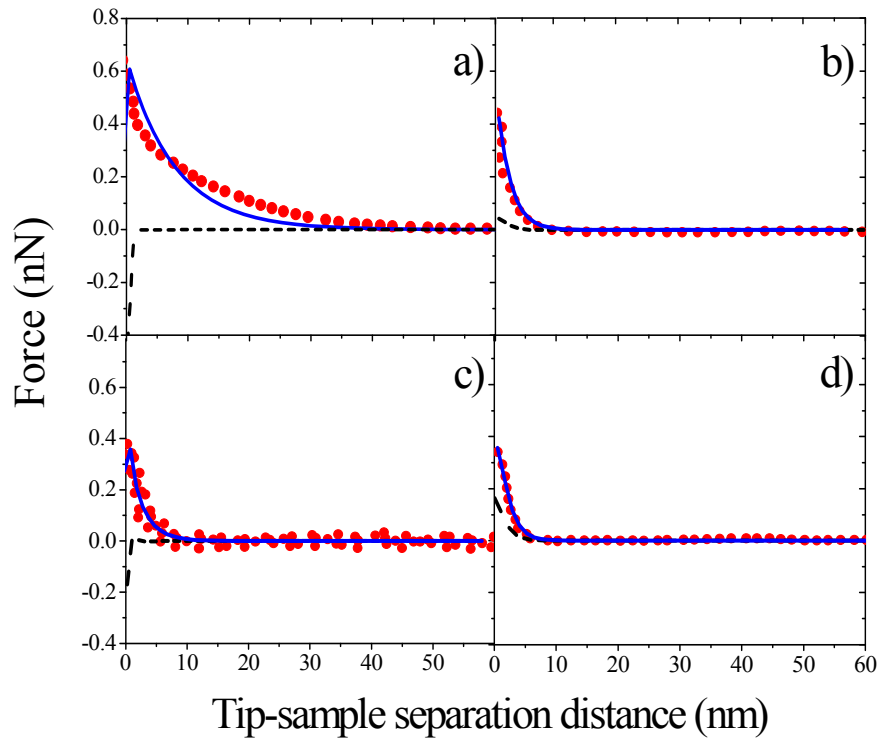


Figure 5.1 Modeling of the approach curves for *A. venetianus* RAG-1 and *R. erythropolis* 20S-E1-c interacting with the hydrophobic (a and c) or the hydrophilic (b and d) AFM probes in 0.1M PBS. Data points are in red; dashed line represents classical DLVO theory (Eq. 5.2) and blue line the fitting of the extended XDLVO theory (Eq. 5.5). The resulting model parameters are shown in Table 5.2.

5.4.1 Glass Interaction with the Gold AFM Tip in 0.001M KCl Solution

In order to test the application of the DLVO theory to the AFM force distance curves, we modeled the interaction between the unmodified AFM tip (gold) and bare glass slides in 0.001M KCl solution. The surface potential of the glass substrate was taken from the literature as -30 mV at the experimental pH.[105] The Hamaker constant for the system was computed from the Hamaker constants of the individual components, which were taken from literature, giving a value of 2.5×10^{-20} J.[105] The results of the simulation are shown in Figure 5.2, using the potential of the gold surface as the only fitting parameter for the system. The Debye length was computed independently using Eq. 2.2. A good agreement between the DLVO model and AFM force curve for the control system can be observed in the following figure.

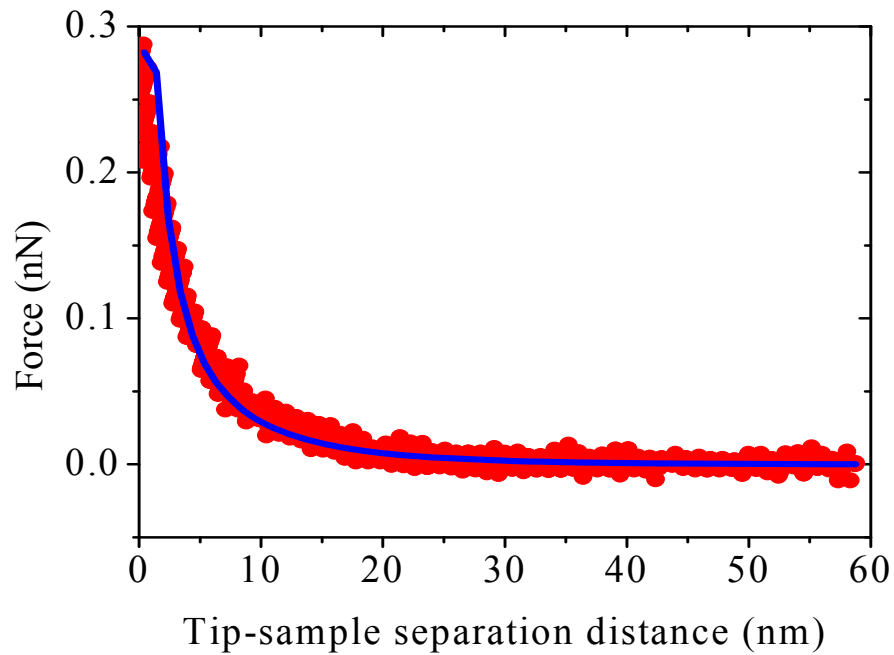


Figure 5.2 Approach curve between unmodified AFM probe and cleaned glass surface in 0.001M KCl solution (Debye length of 0.96×10^{-9}). Interactions begin at 20 nm from the glass surface and are repulsive in nature. The blue line is from DLVO theory (Eq. 5.2) with a zeta potential of -50 mV for the gold surface and -30mV for the glass surface.

5.4.2 Modeling of Interactions between Bacteria and Modified AFM Tips in 0.1M Phosphate Buffer

The predictions of the DLVO theory, Eq. 5.2, for all the four bacteria-AFM tip interaction combinations deviated considerably from the experimental measurements. The DLVO theory predicted attraction for the interaction of *A. venetianus* RAG-1 and *R. erythropolis* 20S-E1-c with the hydrophobic AFM probe (Figures 5.1a and 5.1c, dashed line) whereas the experimental force curve showed long range repulsion for both systems (Figures 5.1a and 5.1c, red circles). In the case of *A. venetianus* RAG-1 and *R. erythropolis* 20S-E1-c interacting with the hydrophilic AFM probe (Figures 5.1b and 5.1d, dashed line), the classical DLVO theory predicts a much lower and a shorter ranged repulsive interaction than the experimental observations.

Figure 5.1 also superimposes the fitted XDLVO interaction force (Eq. 5.5, blue line) on the experimental force distance approach curves in all four cases. It is evident that incorporation of a short range acid-base repulsive interaction can lead to very good fits to the approach curves for both microbes interacting with the hydrophilic AFM tip (Figures 5.1b and 5.1d, blue line). The corresponding fits of the XDLVO model to the experimental force-distance curves for the interaction of the bacteria with hydrophobic tips are not as promising. Whereas the extended DLVO model provided good agreement with the experimental data for the interaction of *R. erythropolis* 20S-E1-c with the hydrophobic AFM tip, it showed poor agreement with the experimental data for *A. venetianus* RAG-1 interacting with the hydrophobic tip. While the acid-base interaction improves the agreement between the theory and experiment, there are qualitative discrepancies between the XDLVO and the experimental force profiles. In Figure 5.1a, the experimental

decay behavior is not adequately captured by the XDLVO model, and the interaction force at contact was smaller than the experimental values.

We next show the fitting of the experimental force distance data for *A. venetianus* RAG-1 interacting with the hydrophobic tips to the EDLVO model, which comprises a bi-exponential term added to the classical DLVO theory (Eq. 5.6). The model comprising the bi-exponential term (Eq. 5.6) provides a good fitting for *A. venetianus* RAG-1 interacting with the hydrophobic AFM probe indicating long range repulsion followed by short range repulsion (Figure 5.3). The parameters obtained from fitting the interaction curve between *A. venetianus* RAG-1 and the hydrophilic tip (F_{hi} and λ_{hi}) were used to investigate the potential interaction mechanisms between *A. venetianus* RAG-1 and the hydrophobic tip.

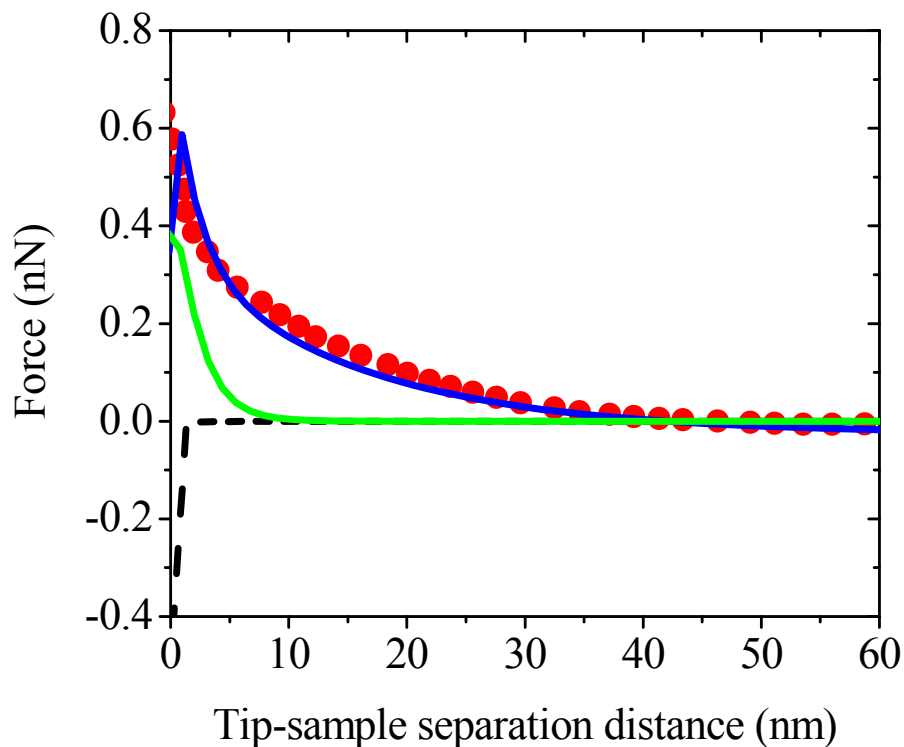


Figure 5.3 Modeling of the approach curves for *A. venetianus* RAG-1 interacting with the hydrophobic AFM probe. Data points are in red; the dashed line represents classical DLVO theory (Eq. 5.2), the blue line shows the fitting of Eq. 5.6 which comprises a bi-exponential term and the green line emphasizes the fitting of the XDLVO theory accounting for *A. venetianus* RAG-1 interacting with the hydrophilic AFM probe (Eq. 5.5). In Eq. 5.6, F_{hi} and λ_{hi} represent the fitting parameters obtained through modeling the interaction of *A. venetianus* RAG-1 with the hydrophilic AFM probe and were inserted as known values when modeling *A. venetianus* RAG-1 interaction with the hydrophobic AFM probe. F_{ho} and λ_{ho} are the unknowns of the bi-exponential model.

5.4.3 Significance of the Parameters Obtained from the Extended DLVO Fitting to the Steric Model

The parameters obtained from the fitting of XDLVO theory (Eq. 5.5) to the approach force curves for the interaction of *A. venetianus* RAG-1 and *R. erythropolis* 20S-E1-c with both hydrophobic and hydrophilic coated AFM tips are presented in Table 5.2. The force at zero separation distance (F_0) varies in the narrow range from 0.39 nN to 0.55 nN for the four cases. Whereas the decay length for the interaction of *A. venetianus* RAG-1 with the hydrophobic AFM probe has a value of 11.64 nm, the other interactions of the microbes with both hydrophilic and hydrophobic AFM probes give a decay length of approximately 2 nm.

In order to determine the significance of the additional exponential term in the XDLVO model, we evaluated the polymer brush thickness (L_0) and the grafted polymer density (Γ) from the steric model using the values of the force at zero separation distance (F_0) and the decay length (λ) in Table 5.2. Whereas the polymer layer thickness ($L_0 = 2\pi\lambda$) for the interaction of *A. venetianus* RAG-1 with the hydrophobic AFM probe showed a thickness of 73 nm, all the other combinations of bacteria and AFM probes resulted in comparable values for the polymer layer thickness in the range 12 to 15 nm. *A. venetianus* RAG-1 had the lowest grafting polymer density (Γ) when measured with the hydrophobic AFM tip ($0.94 \times 10^{-16} \text{ m}^{-2}$); all the other tip-bacterium combinations gave a grafting polymer density of approximately $2.5 \times 10^{-16} \text{ m}^{-2}$. The interaction of *A. venetianus* RAG-1 with the hydrophobic AFM probe was characterized by a longer polymer brush with a low grafting density, in contrast to all the other interactions which suggested short brushes of much higher density.

When the interaction of *A. venetianus* RAG-1 with the hydrophobic AFM tip was modeled using EDLVO theory (Eq. 5.6), the force at zero separation distance (F_{ho}) had a value of 0.57 nN and the decay length (λ_{ho}) was 19 nm. The polymer layer thickness (L_o) showed a value of 119 nm and the grafting polymer density (Γ) was $0.47 \times 10^{-16} \text{ m}^{-2}$.

Table 5.2 Summary of quantitative data resulted from fitting the XDLVO theory to the experimental AFM force curve (approach) for *A. venetianus* RAG-1 and *R. erythropolis* 20S-E1-c interacting with both hydrophobic and hydrophilic AFM tips. These data include the force at zero separation distance (F_0) and the decay length (λ). The equilibrium polymer length (L_0) and polymer grafting density (Γ) were calculated from F_0 and λ using Eq. 2.8.

Bacterial strain	AFM tip coating	F_0 (nN)	λ (nm)	L_0 (nm)	Γ ($\text{m}^{-2} \times 10^{16}$)
<i>A.venetianus</i> RAG-1	C ₁₇ CH ₃	0.55 ± 0.01	11.6 ± 0.5	73.1 ± 0.9	0.94 ± 0.12
	C ₁₁ OH	0.48 ± 0.06	2.1 ± 0.3	13.5 ± 2.2	2.65 ± 0.13
<i>R.erythropolis</i> 20S-E1-c	C ₁₇ CH ₃	0.41 ± 0.02	2.5 ± 0.2	15.7 ± 0.2	2.12 ± 0.14
	C ₁₁ OH	0.39 ± 0.07	1.9 ± 0.3	12.0 ± 2.4	2.49 ± 0.16

5.5 Discussion

A Gram positive and a Gram negative environmental isolate, possessing different degrees of hydrophobicity and previously documented to degrade hydrocarbons,[126, 128] were selected to investigate the connection between the hydrophobic nature of their surfaces and the attachment to AFM tips presenting different surface chemistry. AFM was used as our investigation tool since it can simultaneously provide information on local surface properties and interaction forces. Modeling of the AFM approach force curves for *A. venetianus* RAG-1 and *R. erythropolis* 20S-E1-c can give quantitative information on forces to aid our understanding of bacterial adhesion.

The macroscopic measurements of zeta potential of the bacteria (Table 5.1) were in good agreement with the water contact angle results previously measured by Dorobantu et al.[11] The highly hydrophobic surface of *R. erythropolis* 20S-E1-c ($\Theta = 153^\circ$) had the most negative surface charge whereas the intermediate hydrophobicity surface of *A. venetianus* RAG-1 ($\Theta = 56^\circ$) had a less negative surface charge. These observations suggest that high hydrophobicity cells have high negative electrostatic potentials and are consistent with observations by van Loosdrecht et al.[167] The net negative charge present on the two bacterial strains investigated here may have originated from the lipopolysaccharides of the Gram-negative cell envelope and/or acidic functional groups on the proteins of the pili of the *Acinetobacter* cells [4, 82], and the mycolic acids of the acid-fast *Rhodococcus* cell surface.[82, 129]

DLVO force predictions suggested attraction at short separation distance for interaction of *R. erythropolis* 20S-E1-c and *A. venetianus* RAG-1 with the

hydrophobic AFM probes (Figures 5.1a and 5.1c, dashed line). This attraction was not observed experimentally (Figures 5.1a and 5.1c, red circles); instead a strong repulsion was recorded. Other interactions, such as steric forces, masked any attraction in the AFM approach curves when the two microorganisms were interacting with the hydrophobic probe.

DLVO theory provided poor agreement with experimental observations for *R. erythropolis* 20S-E1-c and *A. venetianus* RAG-1 interaction with the hydrophilic AFM probes. In this case, we suspected that other interactions such as hydration forces associated with the presence of a biopolymeric-rich coat around the cell surface or steric forces may be responsible for the behavior observed in the experimental curves. Therefore, the extended DLVO models were further considered.

An extended XDLVO model, comprising an exponential term in addition to the Lifshitz-Van der Waals and electrostatic forces, was added for the interaction of *A. venetianus* RAG-1 and *R. erythropolis* 20S-E1-c with the hydrophilic AFM tip. In this case the model fitted the experimental data (Fig. 1b and 1d, blue line) with a decay length of 2.1 nm for *A. venetianus* RAG-1 cells and 1.9 nm for *R. erythropolis* 20S-E1-c (Table 5.2). These large decay lengths suggest that steric repulsion and not acid-base type interactions, which should range up to 0.6 nm from the cell surface into the surrounding medium,[168] are involved in the interaction of *A. venetianus* RAG-1 and *R. erythropolis* 20S-E1-c with the hydrophilic AFM tip.[25, 111] Camesano and Logan [114] modeled the AFM approach curves between *Pseudomonas putida* KT2442 and *Burkholderia cepacia* G4, and unmodified silicon nitride AFM tips in MOPS buffer. They fitted the force curves to the classic DLVO theory and to the steric model separately.

Whereas the experimental approach forces were much larger in magnitude and extended over longer distances than predicted by the DLVO theory, they were represented well by the steric repulsion model.

When *R. erythropolis* 20S-E1-c interacts with the hydrophobic AFM tip, XDLVO theory provides good agreement with the experimental force curve. The surface of *R. erythropolis* 20S-E1-c is devoid of pili as reported by Dorobantu et al.[11], but a layer consistent with a capsule can be observed surrounding these cells in TEM images. Whyte et al.[138] also observed loosely associated material external to the *Rhodococcus* cell surface. The force F_0 at contact for *R. erythropolis* 20S-E1-c interacting with the hydrophobic AFM tip is larger than that for the interaction of *R. erythropolis* 20S-E1-c with the hydrophilic tip, 0.41 nN vs 0.39 nN (Table 5.2), suggesting that hydrophobic interactions are not present in this case.

For the case of *A. venetianus* RAG-1 interacting with the hydrophobic AFM tip, XDLVO theory provided poor agreement with the experimental curve (Figure 5.3). Therefore, an EDLVO model, which accounts for polymeric structures of different length on the bacterial surface, was considered (Eq. 5.6). The theoretical curve obtained in this case had an inflection point at a separation distance of about 5 nm from the bacterial surface (Figure 5.3), suggesting the possibility that two polymer layers of different length may be involved in the interaction. This observation is consistent with the work of Dorobantu et al.[4] that describes the presence of pili and capsule surrounding *A. venetianus* RAG-1 cells. These extracellular structures were visible during AFM phase imaging with the hydrophobic AFM probe. Moreover, Rosenberg et al.[33] observed in TEM images that *A. venetianus* RAG-1 surface was covered by two major types of pili:

abundant thin pili and occasional thick pili with diameters of 3.5 and 6.5 nm, respectively. The thin pili played a major role in adherence to hydrophobic surfaces (hydrocarbon droplets or polystyrene surfaces), and thus presumably have hydrophobic tips. The existence of a capsule surrounding this bacterium was also emphasized by Pines et al.[137]

When *A. venetianus* RAG-1 surface was approached by the hydrophobic tip, long range repulsion was first observed in the force-distance curve (Figure 5.3, blue line), which is consistent with the compression of pili. This first step is characterized by a decay length of 18.9 nm. As the tip came into closer contact with the cell, the compression of the exopolymeric capsule was consistent with a decay length of 2.13 nm (Table 5.2). The force F_0 at contact between *A. venetianus* RAG-1 and the hydrophobic AFM tip was larger than that detected for *A. venetianus* RAG-1 interaction with the hydrophilic AFM tip suggesting that hydrophobic forces were not involved in this case (Table 5.2).

The experimental values of the interaction forces of both bacteria at the point of contact with the hydrophobic tips (i.e. a tip separation distance of zero in Figure 5.1) were larger than those with the hydrophilic tips. If acid-base interactions were dominant as incorporated in the XDLVO model, then this result implies that the acid base interaction free energy per unit area at contact between the bacteria and the hydrophobic tips must be more repulsive than that of the bacteria and the hydrophilic tips. This implication seems to be fundamentally incorrect and inconsistent with the measured contact angles and the estimated interfacial tension parameters of these substrates. In particular, hydrophobic attraction between the bacteria and the hydrophobic AFM tips should imply a negative acid-base free energy of adhesion, which is clearly not

evident in the experimental plots (Figures 5.1a and 5.1c). As a result, hydrophobic forces are not involved in the interaction of *A. venetianus* RAG-1 and *R. erythropolis* 20S-E1-c with the hydrophobic AFM tip.

Bridging forces likely played an important role in the interaction of both bacteria with the hydrophobic AFM probe. The considerable strength of the bridging interactions leading to an irreversible bacterial adhesion has been suggested to originate from the formation of polymer bridges.[119] As described by Jucker et al., the bridging facilitates irreversible adhesion due to strong short-range interactions such as hydrogen bonds between the polymers and the substrates.[25] Van Oss has suggested that the hydrophobic groups associated with bacterial surface appendages have the ability to remove the vicinal water film by dehydration, resulting in small areas of direct contact between protuberant parts of the cell surface and the substratum.[119] Jucker et al.[111] showed that polymers that are long enough to bridge the distance between cells and the surface may cause adhesion even when the cells do not experience attraction.

The schematic in Figure 5.4 depicts the interaction between a thiol modified AFM tip and a microbial surface featuring extracellular structures. When the surface of *A. venetianus* RAG-1 was approached by the hydrophobic AFM tip, the pili, which may be hydrophobic in nature, adhered to the AFM tip [4] and were compressed as the tip came into closer contact with the cell surface (Figure 5.4). At smaller separation distance, the compression of the exopolymeric capsule occurred. As the hydrophobic AFM tip approached *R. erythropolis* 20S-E1-c surface, the polymer brush compressed (Figure 5.4). As the tip came in closer contact with the cell wall, the hydrophobic mycolic acids interacted with the tip leading to irreversible adhesion.

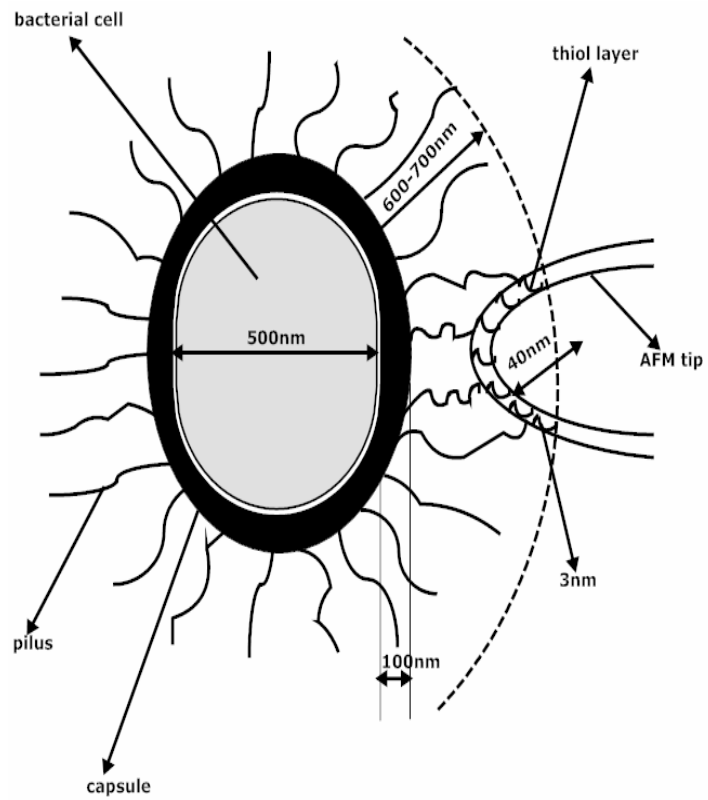


Figure 5.4 Schematic representation (not to scale) of the interaction between an adhering cell possessing exopolymeric capsule and pili, and the thiol coated AFM probe. The thiol layer ranges from 1 to 3 nm in length.

The AFM force distance measurements were conducted under dynamic conditions in a liquid medium. Consequently, the measured forces should not be considered identical to the DLVO force. In a kinematic situation, where the tip is approaching the substrate at a constant speed, the total resistive force on the probe includes at least a combination of hydrodynamic and colloidal repulsive forces. The hydrodynamic repulsion certainly becomes the dominant repulsive force felt by the tip during the final nanometer of approach. For this reason, we conducted the DLVO fittings using force data obtained for separation distances above 1 nm.

The retraction curves showed in every case that once the tip was forced into contact with the substrate, there was always an attraction.[4] Despite the importance of bacterial extracellular structures in influencing adhesion and the fact that these biopolymers can lead to steric repulsion, the presence of steric interactions does not prevent the attachment of bacteria to surfaces and interfaces. Bridging interactions are of particular importance in modeling the AFM approach curves because they are believed to be one of the driving forces for the adhesion of microbes to the oil/water interface for bioremediation and bioprocesses. This study represents a step forward in predicting cell association with hydrophobic pollutants, because the forces as the bacteria approach the oil water interface can be predicted on the basis of the presented results.

In this study, we examined two microbes exhibiting different surface hydrophobicity and characterized their interactions with hydrophobic and hydrophilic terminating AFM probes. Although modeling the interactions using DLVO theory of colloid stability usually leads to a quantitative framework for the interpretation of the AFM results, it was insufficient to explain our results.

The interaction forces presented in Fig. 5.1 and Fig. 5.3 demonstrate the importance of steric repulsion in addition to traditional DLVO interactions when characterizing microbial cells possessing extracellular structures.

Based on the theoretical predictions, the observed distance at which the repulsive forces become effective, and the forces at contact, we conclude that force-distance curves for approach can be described in terms of the extended XDLVO and EDLVO theories accounting for steric/bridging interactions in the case of bacteria possessing extracellular appendages. Our results emphasize that bacterial adhesion is indeed strongly influenced by the presence of extracellular structures.

6. IMPLICATIONS OF THE CURRENT STUDY

This study enables the estimation of the bacterial positioning at the oil/water interface from both a macroscopic and a microscopic point of view. Knowledge of the distance at which microorganisms reside from the oil/water interface has importance in bioprocesses where the hydrocarbon flux towards microbial cells can be optimized by minimizing the resistance to mass transfer. The results of this research allow us to identify the most desirable bacterial surface properties to enhance the rate of transport of hydrophobic species to the cell.

As previously described [11], both bacteria from this study attach readily to the oil/water interface. *A. venetianus* RAG-1 cells, characterized by a contact angle θ of 56° , are found partially immersed in the oil or totally in the water phase. Marshall mentioned in his book that regardless of the presence or absence of capsular material, non-acid-fast bacteria such as *A. venetianus* RAG-1 remained in the aqueous phase.[115] *R. erythropolis* 20S-E1-c cells, whose contact angle θ has a value of 152° , can be found at the interface almost entirely immersed in the oil phase, and also completely immersed in the oil phase. In the case of acid-fast bacteria such as *R. erythropolis* 20S-E1-c they can readily pass through the interface into the oil phase with only small numbers remaining at the interface.[115]

We expect a bacterium at the oil-water interface to have two characteristic dimensions that are significant for mass transfer. Assuming that the bacteria attach along their long axis [169], then one length scale is the fraction of the bacterium cross section that lies within the oil phase. The macroscopic analysis, based on contact angle measurements, allows the computation of the bacterial

height immersed in oil or water and the extent of deformation of the interface by the bacterium as shown in Figure 6.1.

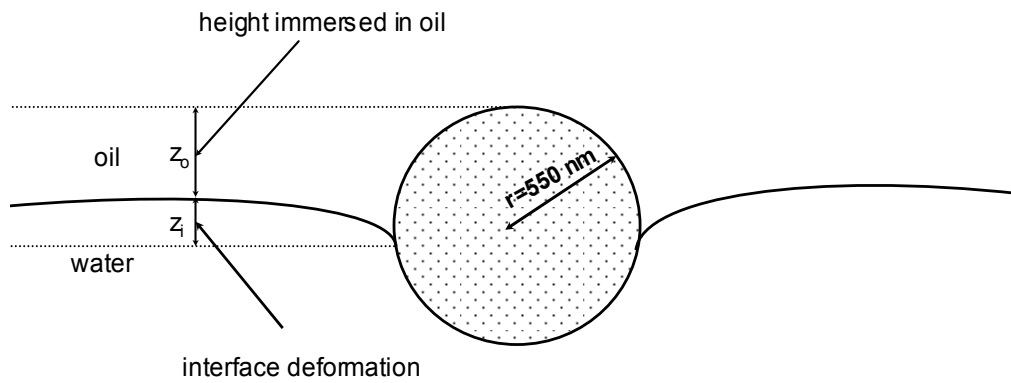


Figure 6.1 Schematic showing the deformation of the interface z_1 and particle height immersed in the oil phase z_0 . The bacterium radius r has a value of $5.50 \times 10^{-7} \text{ m}$.

The second length scale is the distance from the oil phase to the cell wall, δ , which is determined by the mechanical properties of the material on the cell surface. This distance will be related to the forces determined by AFM approach and retraction curves. Based on these dimensions, a model for diffusion across the external layer of thickness δ can be used to obtain the maximum hydrocarbon flux towards the microbial cell.

6.1 Bacterial Positioning at the Oil/Water Interface

We approach this question by first measuring the three phase contact angle on bacterial lawns of *A. venetianus* RAG-1 and *R. erythropolis* 20S-E1-c. The contact angle is the parameter that determines the position of a particle at the interface, and the fraction that will be immersed. For setting up a simple force analysis, we approximated the bacterium as a spherical particle with radius r in mechanical equilibrium at the oil/water interface.

R. erythropolis 20S-E1-c, which has a θ of 152° , resides mostly in the oil phase as shown in Figure 6.2. Far from the bacterium, the oil/water interface is flat and leveled at $z = 0$; the z -axis points upwards (against gravity) normal to the flat liquid interface. The three-phase contact line describes a circle with radius r_i and is located at a distance z_i below the zero level, while its position with respect to the bacterium centre is measured by the angle φ , hence $r_i = r \sin \varphi$.

There are three forces involved in determining the equilibrium position at the oil/water interface; the particle weight acting downwards (mg), the vertical capillary force F_v due to the vertical component of the oil/water interfacial tension, and the vertical resultant of the hydrostatic pressure distribution around the entire bacterium F_p acting also upwards.

In the case of *R. erythropolis* 20S-E1-c, F_y acts upwards and the force balance is represented by the following equation:

$$F_y + F_p = mg \quad 6.1$$

The vertical component of the capillary force is given by equation 6.2:

$$F_\gamma = -2\pi r \gamma_{ow} \sin \varphi \sin(\varphi + \theta) \quad 6.2$$

The vertical resultant of the hydrostatic pressure distribution around the entire microbial cell can be obtained by integrating the hydrostatic pressure distribution around the cell.[178] The result can be written in the form:

$$F_b = \rho_w V_{bw} g + \rho_o V_{bo} g - (\rho_w - \rho_o) g z_i A_i \quad 6.3$$

where $V_{bw} = \frac{\pi r^3 (2 - 3 \cos \varphi + \cos^3 \varphi)}{3}$ and $V_{bo} = \frac{4\pi r^3}{3} - V_{bw}$ are the volumes of the bacterium immersed in water and in oil, respectively and $A_i = \pi (r \sin \varphi)^2$ is the area of the contact line circle. The mass of the bacterium is $m = \frac{\rho_b 4\pi r^3}{3}$.

Substituting equations 6.2 and 6.3 into 6.1 allows the computation of z_i by performing a sensitivity analysis on φ . The obtained value of z_i is 8.83×10^{-10} m for $\varphi = 28^\circ$ and the resulting $z_0 = 8.78 \times 10^{-8}$ m, which, in this case, represents the bacterium height immersed in water. The interface deformation, z_i , is negligible due to the low weight of the bacterial cells.

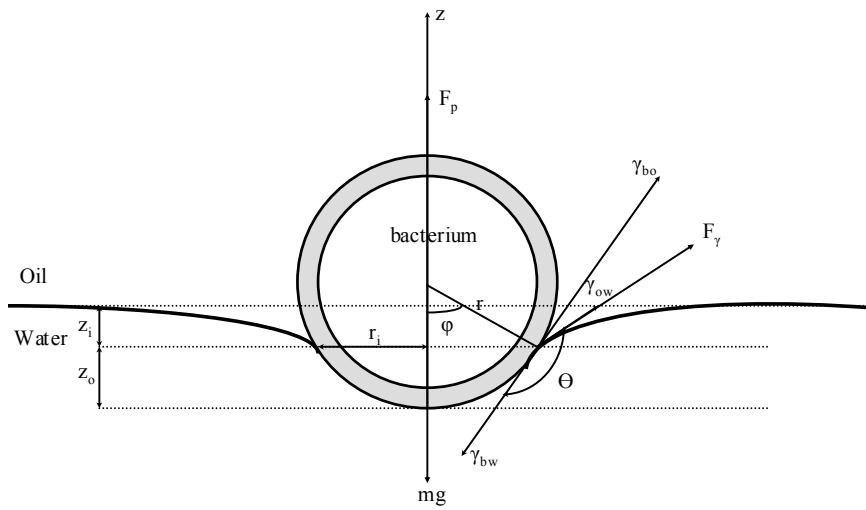


Figure 6.2 *R. erythropolis* 20S-E1-c assumed to be spherical with radius r and contact angle θ in equilibrium at the oil/water interface leveled at $z = 0$ far from the microorganism. The three-phase contact line with radius r_i is depressed at depth z_i below the zero level. The bacterium radius r equals 7.50×10^{-7} m. Adapted from reference [179].

A. venetianus RAG-1, which has a θ of 56° , resides mostly in the water phase (Figure 6.3). The three-phase contact line describes a circle with radius r_i and is located at a distance z_i above the zero level, its position with respect to the bacterium centre is measured by the angle φ , hence $r_i = r \sin\varphi$.

In the case of *A. venetianus* RAG-1, F_y acts downwards and the force balance is given by the following equation:

$$F_p = mg + F_y \quad 6.4$$

The obtained value of z_i is 9.02×10^{-10} m for a $\varphi = 55.99^\circ$ and the resulting $z_o = 2.42 \times 10^{-7}$ m which in this case represents bacterium height immersed in oil. The knowledge of the bacterium height immersed in the oil phase allows the calculation of the microbial interfacial area that resides in the hydrocarbon and through which the mass transfer takes place.

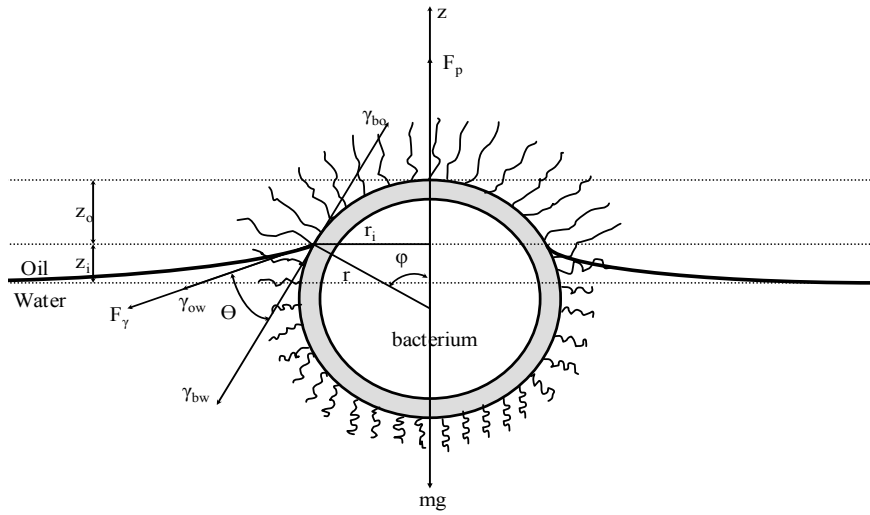


Figure 6.3 *A. venetianus* RAG-1 assumed to be spherical with radius r and contact angle θ in equilibrium at the oil/water interface leveled at $z = 0$ far from the microorganism. The three-phase contact line with radius r_i is depressed at depth z_i above the zero level. The bacterium radius r equals 5.50×10^{-7} m. Adapted from reference [179].

6.2 Separation of Bacteria from the Oil/Water Interface Revealed by AFM Experiments

The AFM force-distance curves give us the opportunity to estimate the thickness of the extracellular water layer, δ , surrounding the two bacterial species investigated in this study.

The approach and retraction AFM force curves allow the calculation of two bounding values for δ . The lower bound was estimated from the AFM approach force curve as the point where the repulsive force starts to increase in magnitude. In order to find the upper bound for δ , the AFM retraction force-distance curve was converted into energy versus distance. This transformation was done based on the well known relationship between energy and force,

$$U = -\int F_{(x)} dx \quad 6.5$$

and by performing numerical integration of the force-distance curve using the trapezoidal rule. The points of equilibrium were read from the graph and used as the upper bound for δ .

In the case of *A. venetianus* RAG-1, the lower limit of δ was set at 0.05 μm based on the data shown in Figure 6.3. At smaller separation distances, the repulsive force increases, which will tend to push the interface further away from the cell wall.

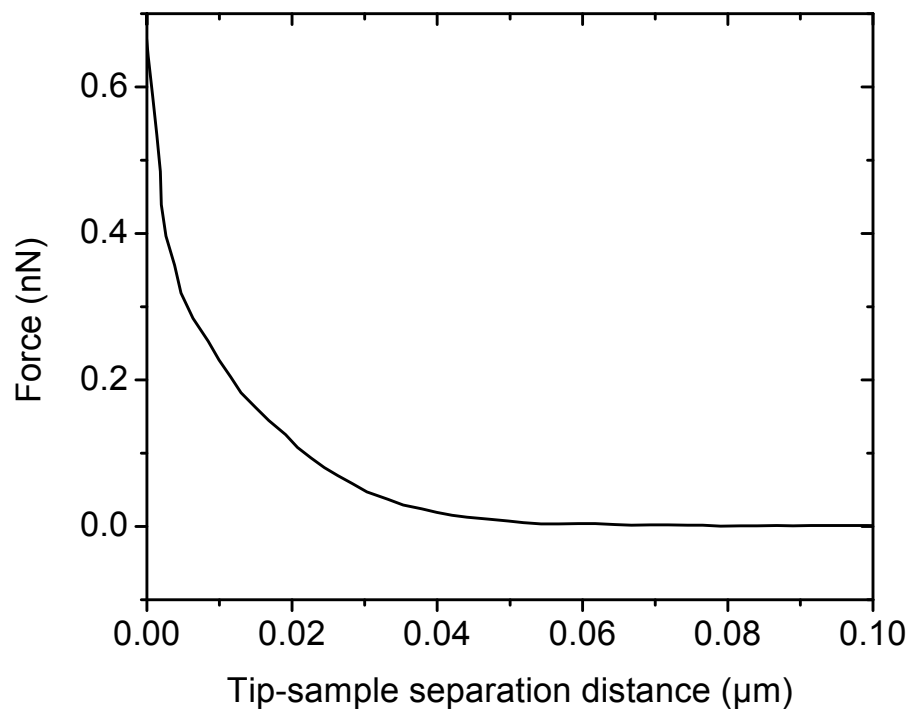


Figure 6.4 Representative *A. venetianus* RAG-1 approach curve used to set the lower limit for δ .

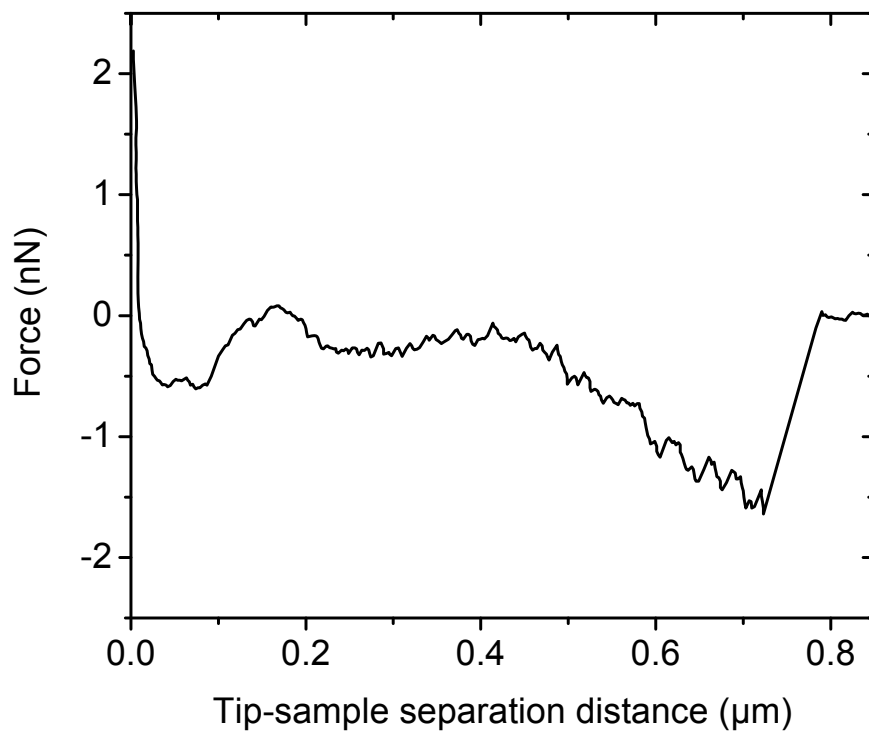


Figure 6.5 Representative *A. venetianus* RAG-1 retraction curve used for conversion into energy.

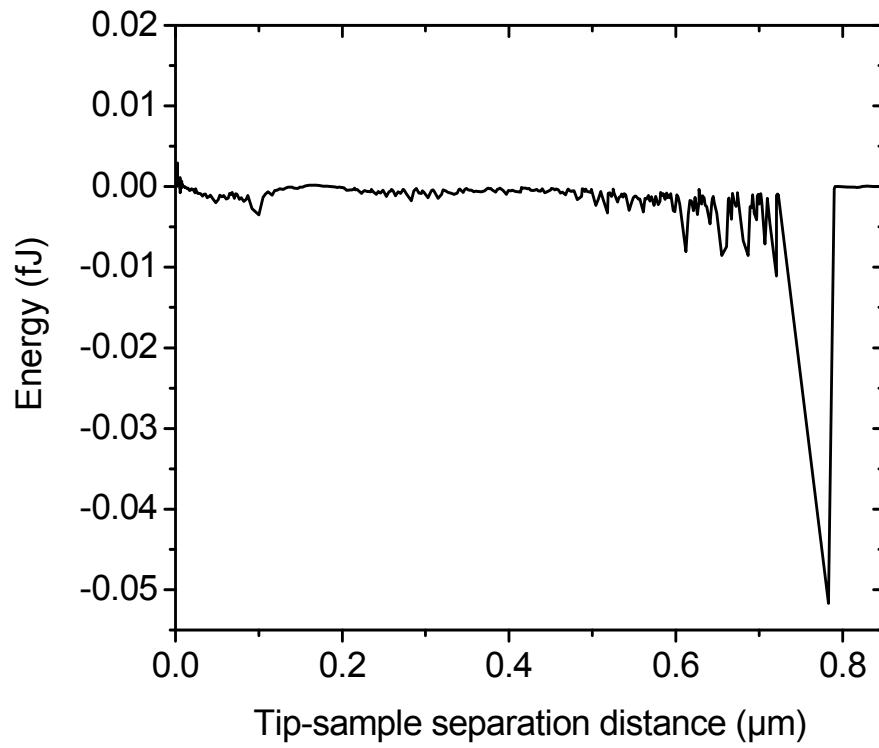


Figure 6.6 Energy versus separation distance for *A. venetianus* RAG-1, calculated from the data of Figure 6.5 using equation 6.5.

In Figure 6.6, the first energy minimum occurs at a separation distance of 0.1 μm , therefore we set up the upper limit of δ in the case of *A. venetianus* RAG-1 to be 0.1 μm . Even though other energy minima were present at distances between 0.5 to 0.8 μm , they were not included in our calculations. These minima reflect the longer-range interactions of the AFM tip with the fimbriae attached to the cell and extending out into the liquid medium.

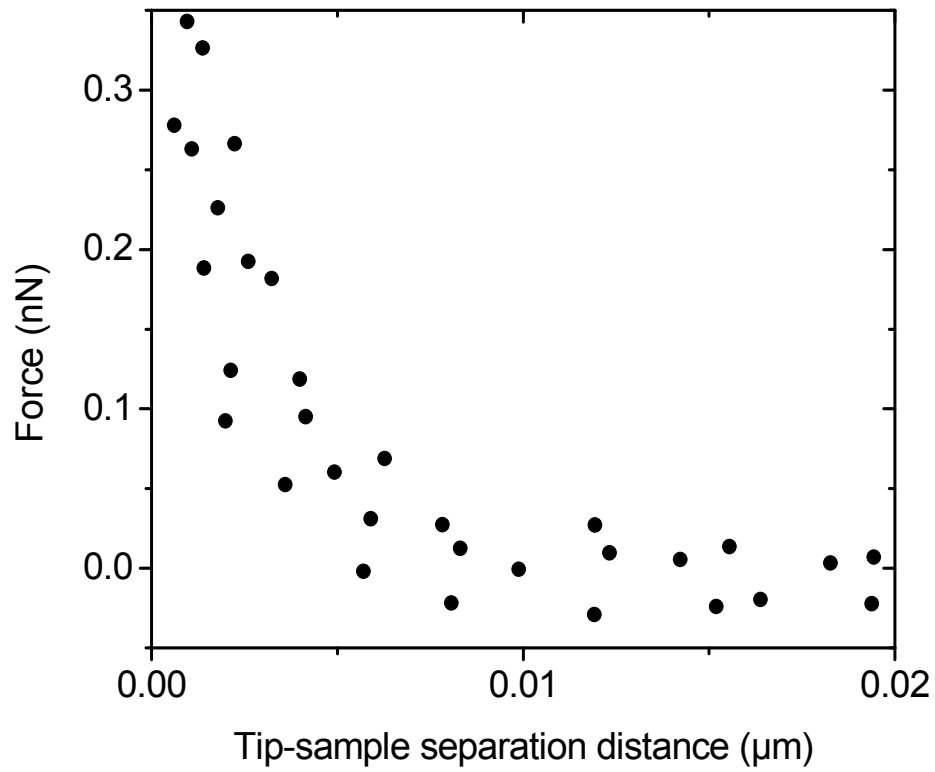


Figure 6.7 Representative approach force curve for *R. erythropolis* 20S-E1-c used to determine the lower bound for δ .

In the case of *R. erythropolis* 20S-E1-c, the lower limit of δ was set at 0.01 μm based on the data of Figure 6.7.

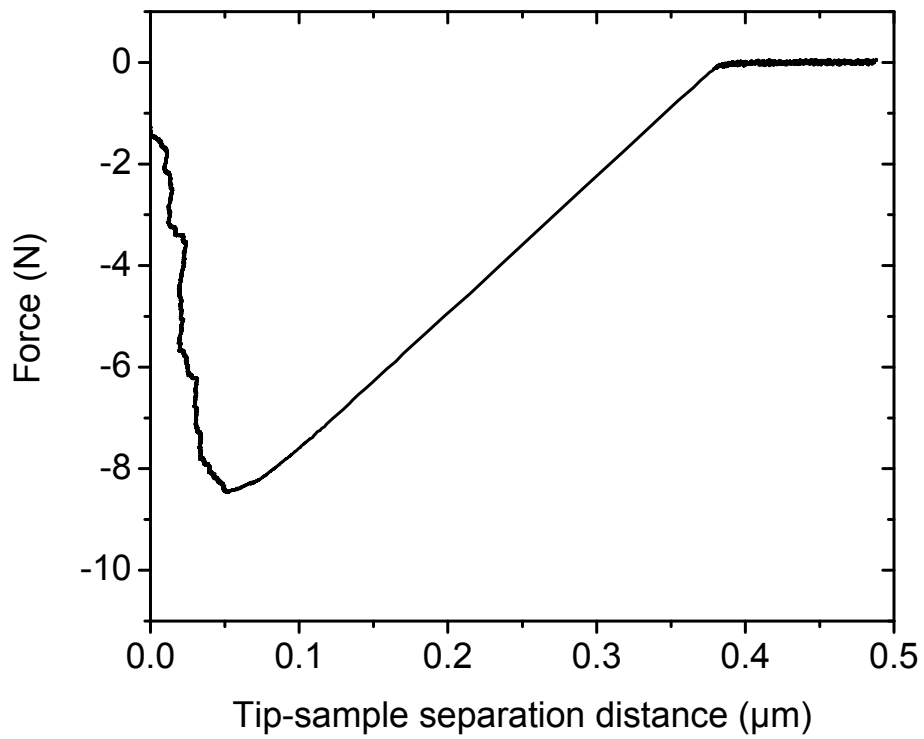


Figure 6.8 Representative retraction force curve for *R. erythropolis* 20S-E1-c used for conversion into energy.

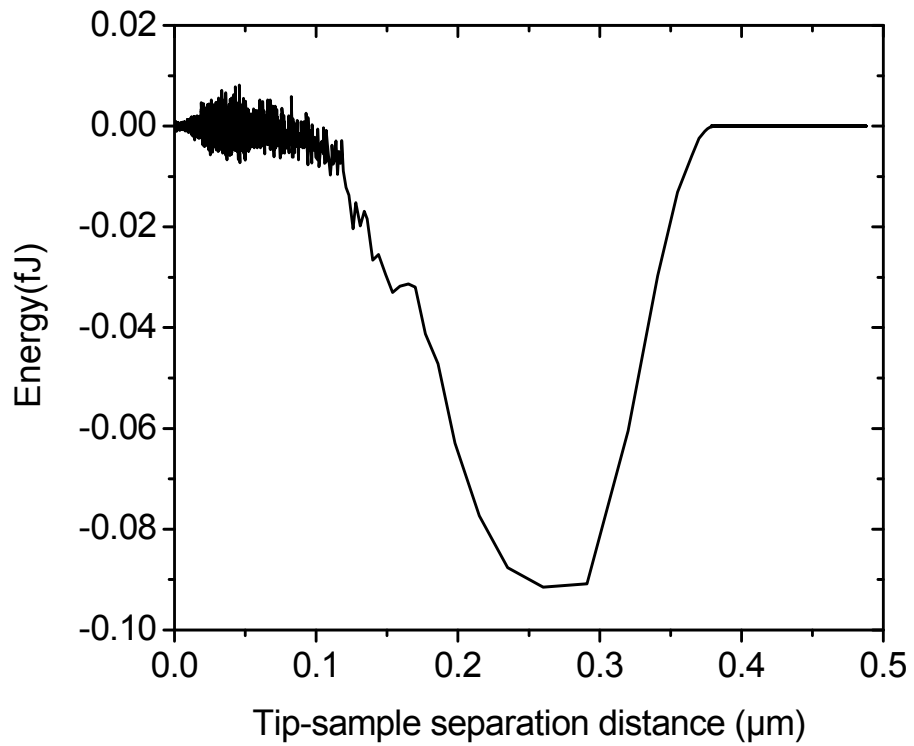


Figure 6.9 Energy versus distance curve for *R. erythropolis* 20S-E1-c from the data Figure 6.8 and equation 6.5.

In Figure 6.9, the energy minimum occurs at 0.25 μm , therefore we set up the upper limit of δ in the case of *R. erythropolis* 20S-E1-c to be 0.25 μm .

6.3 Mass Transfer Across the Oil/Water Interface

The study of hydrocarbon mass transfer across an oil/water interface towards a microbial cell is important for the fundamental understanding of how different parameters influence the mass transfer and how it can be improved.

6.3.1 Bacterial Colonization of an Oil/Water Interface

Microbial colonization of an oil/water interface may occur by diffusive transport, convective transport, or active movement. Each of these processes is described in detail in the following paragraphs.

(1) Diffusive transport is a slow process responsible for bacterial transport towards interfaces. In general, bacteria exhibit a non-negligible Brownian motion (average displacement about 40 $\mu\text{m h}^{-1}$ [170]) that has been observed under the microscope. This motion accounts for random contacts of microorganisms with interfaces even under quiescent conditions and is responsible for crossing any diffusion layer across which no convection can take place.[156] Diffusive transport is slow compared with transport by convective flow or transport of motile cells.

(2) Convective transport of cells is the result of flowing liquid and may be several orders of magnitude faster than diffusive transport, but there may exist situations in which the final part of the distance to the surface is diffusion

controlled.[156] An extensive overview of convective bacterial transport is given by Characklis in reference [171].

(3) Active movement of the cells is the result of cellular structures such as flagella that allow microorganisms to propel themselves.[145]

Once a motile bacterium is in the close vicinity of a surface, it may encounter the surface by chance or chemotactically respond to any concentration gradient that may exist in the interfacial region.[156]

6.3.2 Hydrocarbon Transport towards Microbial Cells

After the microbial cells have reached and attached to an interface, the transport of the hydrocarbon pollutants from the bulk phase towards them involves the mass transfer pathways presented in Figure 6.10.

Resistance to mass transfer can be encountered at three possible locations:

- (1) transport of hydrocarbon from the bulk oil phase to the stagnant liquid region surrounding the microorganism;
- (2) diffusion through the boundary liquid layer associated with the cells;
- (3) transport across the cell envelope and to the intracellular reaction site;

These resistances occur in series and the largest of them controls the rate of transport. Thus the entire mass transfer pathway can be modeled using a single mass transfer relation.

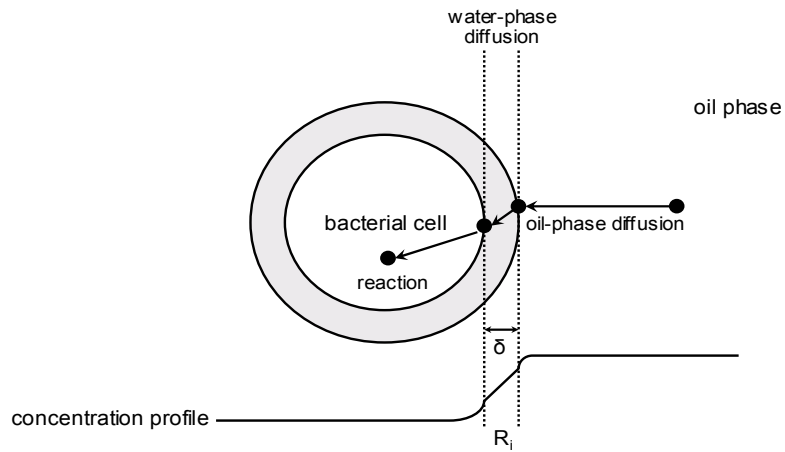


Figure 6.10 Schematic of mass transfer resistances encountered during transport of hydrocarbons to a bacterial cell.

The two microorganisms studied in this thesis have the tendency to adsorb at the oil/water interface due to the hydrophobic nature of their surfaces. Therefore, the major limitation to transport is at the interface in the form of a stagnant aqueous layer through which the transport occurs solely by diffusion. Although this layer will contain biopolymers and other structures attached to the exterior of the bacteria, we can model the mass transfer as occurring through a stagnant, water-rich layer. The rate controlling equation in this case is the hydrocarbon diffusion through the stagnant layer associated with the cells.

As shown in Figure 6.10, the hydrocarbon diffuses towards the microbial cell due to the difference in concentration between the bulk oil phase and the surface of microorganism. Diffusion of the hydrocarbon generates a net flux of mass from regions of high concentration to those of low concentration.

In general, the molar rate of hydrocarbon transport from the bulk liquid phase to the oil-bacterium interface, J (mol h⁻¹), can be described based on the following equation:

$$J = k_l a_b (C_b - C_i) \quad 6.6$$

The rate of diffusion of the substrate from the bulk hydrocarbon phase to the surface of bacteria, J , may be considered to be proportional to the area a_b across which mass transfer takes place (m²), and the driving force for mass transfer which is the concentration difference, $C_b - C_i$, between the bulk and bacterial surface. The constant of proportionality k_l is defined as the mass transfer coefficient (m s⁻¹) and characterizes the mass transfer through the diffusive layer around the cell.

For the case when the microorganisms partition at the oil/water interface the octanol-water partition coefficient K_{OW} has to be introduced in equation 6.6 leading to the following expression:

$$J = k_l a_b \left(\frac{C_b}{K_{OW}} - C_i \right) \quad 6.7$$

As reported by Bressler and Gray [172], the oil/water partition coefficient ($K_{oil/water}$) is typically 1/10 of the octanol-water partition coefficient (K_{OW}) which for the case of hexadecane has a value of 17.78×10^7 . [173]

For the case of $\delta \ll r$, the mass transfer coefficient can be expressed as the ratio of the diffusion coefficient to the film thickness

$$k_l = \frac{D_l}{\delta} \quad 6.8$$

where δ represents the thickness of the boundary fluid layer (m) surrounding the cells, and D_l the diffusion coefficient of hydrocarbon in water ($\text{m}^2 \text{s}^{-1}$).

Substituting equation 6.8 in 6.7 gives

$$J = \frac{D_l}{\delta} a_b \left(\frac{C_b}{K_{oil/water}} - C_i \right) \quad 6.9$$

In the above equation a_b represents the area exposed to the hydrocarbon phase.

The hydrocarbon concentration C_i at the interface can be assumed to be negligible as compared to the concentration in the bulk phase for the case where the bacterium is actively transforming the hydrocarbon.

The concentration of the hexadecane in the bulk aqueous phase can be taken as the aqueous solubility of hexadecane at saturation.[173]

The equation for steady-state transport then simplifies to:

$$J = \frac{D_l}{\delta} a_b \frac{C_{aq}^{sat}}{K_{oil/water}} \quad 6.10$$

where C_{aq}^{sat} is the aqueous solubility of hexadecane at saturation

In all the following mass transfer calculations, we consider two model systems for bioremediation comprised of either *A. venetianus* RAG-1 or *R. erythropolis* 20SE-1-c and *n*-hexadecane. The bulk hydrocarbon concentration C_b used in this study was modeled based on a laboratory scale bioremediation experiment that uses 12 g *n*-hexadecane per liter of MSM₄ (vitamin supplemented mineral salt medium).[174] This quantity of hydrocarbon is used to achieve a concentration similar to natural conditions of concentration of *n*-alkane in crude oil.

The diffusion coefficient for *n*-hexadecane in water was measured by Geerdink et al. and found to be $D_l = 4 \times 10^{-10} \text{ m}^2 \text{ s}^{-1}$. [175]

a). *A. venetianus* RAG-1 partitioning at the oil/water interface

For the case of *A. venetianus* RAG-1 attached to the oil/water interface, the bacteria had a three-phase contact angle of 56° . In this case the bacterium will position at the oil/water interface as shown in Figure 6.11:

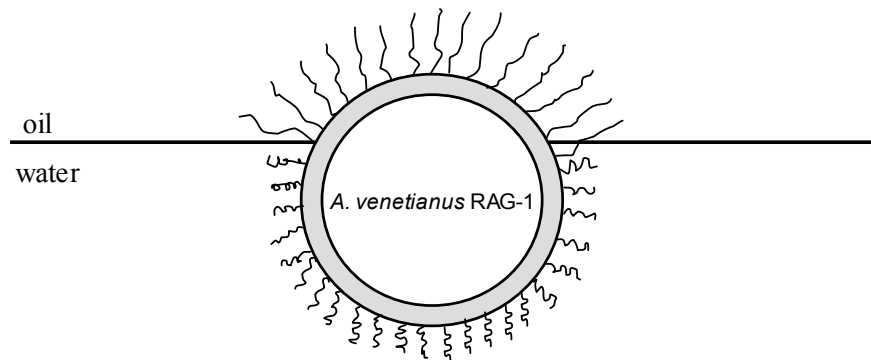


Figure 6.11 *A. venetianus* RAG-1 positioning at the oil/water interface based on a contact angle of 56° .

The extracellular layer surrounding *A. venetianus* RAG-1 would have a thickness δ ranging from 0.05×10^{-6} to 0.1×10^{-6} m as presented in Figures 6.4 and 6.6. With a hexadecane diffusion coefficient in water D_l of $4 \times 10^{-10} \text{ m}^2 \text{ s}^{-1}$, the resulting mass transfer coefficient, k_l , ranges in value from 4×10^{-3} to $8 \times 10^{-3} \text{ m s}^{-1}$. The interfacial area of *A. venetianus* RAG-1 available for hydrocarbon transfer is $2\pi r z_0$ and with a radius r of 5.50×10^{-7} m and a bacterial height immersed in oil z_0 of 2.42×10^{-7} m, as previously determined, a value of $83.62 \times 10^{-14} \text{ m}^2$ is obtained for the interfacial area. Substituting all the above values in equation 6.9 gives a maximum hydrocarbon transfer rate J per cell between 0.51×10^{-12} to $0.10 \times 10^{-11} \text{ g h}^{-1}$ for the two limiting cases of δ .

b). *A. venetianus* RAG-1 immersed in the water phase

The second approach ignores the contact angle of *A. venetianus* RAG-1 and considers the bacterium completely immersed in water with the pili extending into the oil phase as shown in the following figure:

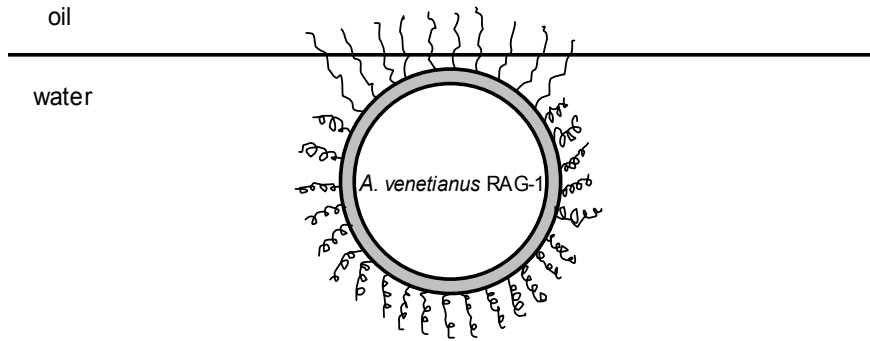


Figure 6.12 *A. venetianus* RAG-1 immersed in water with pili extending in the oil phase.

The hexadecane mass transport rate towards the bacterial cell can be described by the following equation

$$J = \frac{D_l}{\delta} A \frac{C_{aq}^{sat}}{K_{oil/water}} \quad 6.11$$

where A represents the closed packed projected area of a single *A. venetianus* RAG-1 cell (Figure 6.13) on a planar surface, $2\sqrt{3}r^2$, with r being the radius of *A. venetianus* RAG-1 cell.[176] In equation 6.11, δ represents an average distance between the sum of the bacterium radius 5.50×10^{-7} and bound values δ_1 and δ_2 , previously determined from the AFM retraction force curve in Figure 6.6, and the sum of the bacterium radius 0.55×10^{-6} and maximum length of pili of 0.70×10^{-6} m, determined from the same figure. We obtain a value of 0.93×10^{-6} m for δ_1 and 0.95×10^{-6} m for δ_2 .

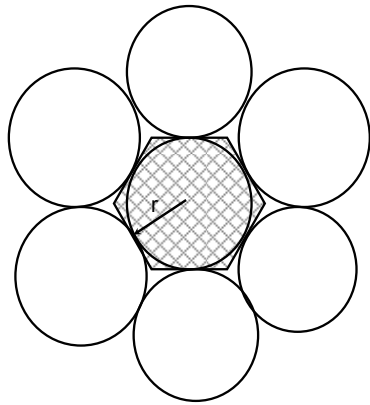


Figure 6.13 Spherical cells packed on a plane surface.

In this case, we assume that the cells are closed packed at the interface and the cell population is high enough to keep the bulk hydrocarbon concentration very low, relative to the equilibrium interfacial concentration.

Substituting the value for the hexadecane diffusion coefficient in water D_i of $4 \times 10^{-10} \text{ m}^2 \text{ s}^{-1}$, the partitioning coefficient of 17.78×10^6 , the values of δ of 0.93 and $0.95 \times 10^{-6} \text{ m}$, and the closed packed projected area of a single bacterial cell $1.05 \times 10^{-12} \text{ m}^2$ in equation 6.11, we obtain maximum hydrocarbon transfer rates of $0.68 \times 10^{-13} \text{ g h}^{-1}$ per cell and 0.67×10^{-13} for the two limiting cases of δ .

a). *R. erythropolis* 20SE-1-c partitioning at the oil/water interface

In the case of *R. erythropolis* 20SE-1-c, the three phase contact angle measured at the *R. erythropolis* 20SE-1-c/oil/water interface had a value of 152° . In this case the bacterium will position at the oil/water interface as shown in Figure 6.13:

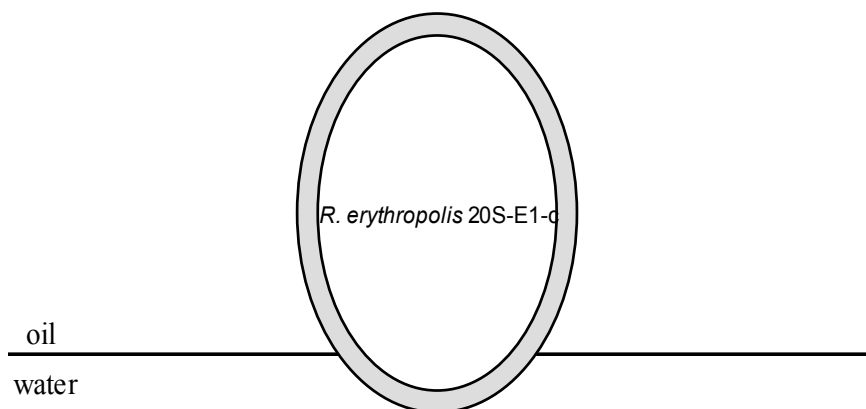


Figure 6.14 *R. erythropolis* 20SE-1-c positioning at the oil/water interface based on its contact angle.

In the case of *R. erythropolis* 20SE-1-c, the extracellular layer surrounding the cells has a thickness δ ranging from 0.01 to 0.24×10^{-6} m as determined from Figures 6.7 and 6.9 respectively. With a hexadecane diffusion coefficient in water D_l of $4 \times 10^{-10} \text{ m}^2 \text{ s}^{-1}$ the resulting mass transfer coefficient, k_l , varies from 1.7×10^{-3} to $40 \times 10^{-3} \text{ m s}^{-1}$.

The interfacial area of *R. erythropolis* 20SE-1-c available for hydrocarbon transfer, is $4\pi r^2 - 2\pi r^2(1-\cos\phi)$ and substituting $r = 7.50 \times 10^{-7}$ and $\phi = 28^\circ$ previously determined, gives a value of $665.49 \times 10^{-14} \text{ m}^2$. The hydrocarbon transfer rate through the stagnant layer surrounding *R. erythropolis* 20SE-1-c becomes $0.17 \times 10^{-11} \text{ g h}^{-1}$ for $\delta = 0.24 \times 10^{-6} \text{ m}$ and $0.40 \times 10^{-10} \text{ g h}^{-1}$ per cell for $\delta = 0.01 \times 10^{-6} \text{ m}$.

b). *R. erythropolis* 20SE-1-c immersed in the oil phase

The second approach ignores the contact angle of *R. erythropolis* 20SE-1-c and considers the bacterium completely immersed into the oil phase as shown in Figure 6.14:

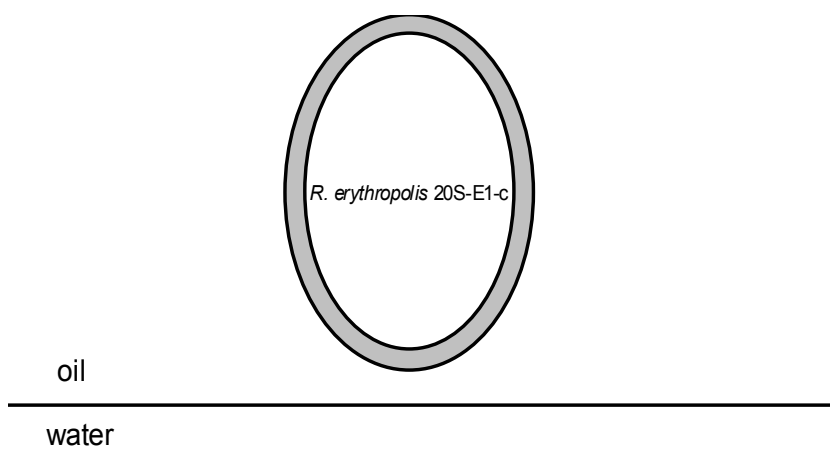


Figure 6.15 *R. erythropalis* 20SE-1-c completely immersed in the oil phase.

In this case the mass transfer resistance is assumed to be in the water layer surrounding the cells suspended in the oil. The diffusivity D_i value remains the same as in the previous case and the stagnant layer δ thickness varies from 0.01 to 0.24×10^{-6} m as shown in Figure 6.9.

The interfacial area available for hydrocarbon transfer changes to $4\pi r^2$, and by substituting $r = 7.50 \times 10^{-7}$ gives a value of 706.50×10^{-14} m². The hydrocarbon transfer rates through the stagnant layer surrounding *R. erythropolis* 20SE-1-c become 0.43×10^{-10} g h⁻¹ and 0.18×10^{-11} g h⁻¹.

In the steady state equation 6.10, the diffusivity and concentration are constant therefore, only the interfacial area and separation distances are relevant for the mass transfer analysis. The key geometric ratio in equation 6.10, a_b/δ , which reflects the only important difference between the two bacteria and the flux estimates are included in Tables 6.1 and 6.2.

The highest hexadecane transfer rate is achieved for *R. erythropolis* 20SE-1-c when it is completely immersed in the oil phase and has the thinnest δ as opposed to the lowest hexadecane transfer rate obtained for *A. venetianus* RAG-1 immersed in the water phase and having the thickest δ .

In order to check the validity of our results, the flux results obtained per cell were compared to the doubling time and wet weight of a single cell of *A. venetianus* RAG-1 and *R. erythropolis* 20SE-1-c. As the wet weight of a cell can be approximated to 6.8×10^{-14} kg and considering the doubling time of each studied bacterium (30 minutes for *A. venetianus* RAG-1 and 60 minutes for *R. erythropolis* 20SE-1-c), the flux values presented in Tables 6.1 and 6.2 look reasonable.

It is evident that the more hydrophobic the surface is, the better the rate of mass transfer. Based on the mass transfer analysis presented in this chapter, we should increase the hydrophobicity of the cells in order to get the optimal biodegradation rate.

Table 6.1 Parameters obtained for the case when *A. venetianus* RAG-1 and *R. erythropolis* 20SE-1-c partition at the oil/water interface

Bacterial species	a_b/δ_1 m	a_b/δ_2 m	Flux per cell, J_1 $g\ h^{-1}$	Flux per cell, J_2 $g\ h^{-1}$	Flux J_1 relative to J_1 for immersed <i>R. erythropolis</i>	Flux J_2 relative to J_1 for immersed <i>R. erythropolis</i>
<i>A. venetianus</i> RAG-1	16.72×10^{-6}	8.36×10^{-6}	0.10×10^{-11}	0.51×10^{-12}	0.23×10^{-1}	1.18×10^{-2}
<i>R. erythropolis</i> 20SE-1-c	665.49×10^{-6}	27.72×10^{-6}	0.40×10^{-10}	0.17×10^{-11}	0.93	0.39×10^{-1}

Table 6.2 Parameters obtained for the case when *A. venetianus* RAG-1 is immersed in the water and *R. erythropolis* 20SE-1-c is immersed in the oil phase

Bacterial species	A/δ_1 m	A/δ_2 m	Flux per cell, J_1 g h^{-1}	Flux per cell, J_2 g h^{-1}	Flux J_1 relative to J_1 for immersed <i>R. erythropolis</i>	Flux J_2 relative to J_1 for immersed <i>R. erythropolis</i>
<i>A. venetianus</i> RAG-1	1.12×10^{-6}	1.10×10^{-6}	0.68×10^{-13}	0.67×10^{-13}	1.58×10^{-3}	1.55×10^{-3}
<i>R. erythropolis</i> 20SE-1-c	706.85×10^{-6}	29.45×10^{-6}	0.43×10^{-10}	0.18×10^{-11}	1	0.41×10^{-1}

7. CONCLUSIONS AND RECOMMENDATIONS

7.1 Conclusions

This thesis has focused on understanding how microorganisms possessing various extracellular structures and different hydrophobicity interact with model substrates such as hydroxyl ($C_{11}OH$, hydrophilic) and methyl ($C_{17}CH_3$, hydrophobic) terminating AFM probes. Two microbial surfaces, *A. venetianus* RAG-1 and *R. erythropolis* 20S-E1-c, isolated from hydrocarbon-contaminated sites were probed by AFM imaging and force curves under physiological conditions.

This study highlights the ability of AFM to provide images and force curves in three dimensions for viable bacterial cells at high resolution under native conditions. This work was motivated by the importance of bacterial adhesion in bioremediation.

AFM imaging was used to determine the morphology of *A. venetianus* RAG-1 and *R. erythropolis* 20S-E1-c and to correlate these findings to the results obtained through electron microscopy techniques. The presence of pili surrounding the cells of *A. venetianus* RAG-1 was detected by AFM phase imaging recorded with the hydrophilic AFM tip and confirmed by TEM images. Moreover, AFM amplitude imaging detected a compact granular layer resembling a capsule surrounding these cells, which was emphasized by TEM, as well. In contrast, the surface of *R. erythropolis* 20S-E1-c was devoid of pili, but a layer consistent with capsule was observed surrounding the cells in TEM images. The proof of existence of bacterial external structures of different hydrophobicity

probed with AFM tips of well-defined chemistry is a novel contribution to the research in the area of bacterial adhesion.

AFM in the aqueous phosphate buffer phase allowed force measurements on viable cells of *A. venetianus* RAG-1 and *R. erythropolis* 20S-E1-c. Force distance curves for the interaction of *A. venetianus* RAG-1 with the hydrophobic tip gave multiple adhesion peaks during retraction suggesting pull-off forces from pili attached to the cell surface. The range of separation distances at which these adhesion forces occurred matched the lengths of pili determined in both phase and electron microscopy images. Most of the retraction curves after contact with the surface of *R. erythropolis* 20S-E1-c displayed single rupture events accompanied by pronounced adhesion force peaks consistent with interaction of the probe tip with an adhesive capsule.

The adhesion forces measured upon the retraction of the hydrophobic AFM tips from the bacterial surfaces were averaged and compared to the three-phase hexadecane-water contact angle measured on lawns of *A. venetianus* RAG-1 and *R. erythropolis* 20S-E1-c. In general, small interaction forces between *A. venetianus* RAG-1 and the hydrophobic tip were found to coincide with low contact angles and strong interactions, as in the case of *R. erythropolis* 20S-E1-c, with high contact angles.

Multiple adhesion force measurements over the microbial surfaces confirmed their heterogeneity at a length scale of 50-100 nm. The arrangement of the adhesion forces for *R. erythropolis* 20S-E1-c typically showed a patterned distribution with the highest forces grouped at one pole of the cell. This is similar to the work of Marshall and Cruikshank [177] who observed that *Flexibacter* and

Hyphomicrobium cells attached to the oil/water interface with a perpendicular orientation suggesting the existence of hydrophobic poles. The gradient in adhesion suggests a gradient in composition. In contrast, *A. venetianus* RAG-1 showed a random distribution of the adhesion forces.

The differences in the cell surfaces could have significant implications for cell attachment to hydrophobic surfaces or interfaces like crude oil droplets in water. The uniform heterogeneity of the surface of *A. venetianus* RAG-1 would give no preferred orientation on a surface or interface. The gradient on the surface of *R. erythropolis* 20S-E1-c, on the other hand, could give a preferred orientation of attachment of one pole (hydrophobic) of the cell.

This first part of my work highlighted the importance of using probes of well-defined chemistry to determine the heterogeneity in bacterial surface hydrophobicity which may have direct implications in bioremediation of hydrophobic contaminants in the environment.

In the second part of this study, the approach AFM force curves taken on *A. venetianus* RAG-1 and *R. erythropolis* 20S-E1-c surfaces with hydrophilic and hydrophobic derivatized AFM tips, were modeled using classical DLVO theory of colloidal stability enhanced by two additional terms accounting for hydrophobic and/or steric interactions.

Although modeling the interactions using DLVO theory of colloid stability usually leads to a quantitative framework for the interpretation of the AFM results, it was insufficient to explain our results. DLVO theory provided poor agreement with experimental observations for *R.erythropolis* 20S-E1-c and *A. venetianus* RAG-1 interaction with both hydrophobic and hydrophilic AFM probes. DLVO

force predictions suggested attraction at short separation distance for interaction of both microorganisms with the hydrophobic AFM probes and short range repulsion for the interaction with the hydrophilic AFM probes.

Two extended DLVO models, XDLVO and EDLVO accounting for acid-base type interactions and steric forces, were considered for the case of *R.erythropolis* 20S-E1-c and *A. venetianus* RAG-1 interaction with both hydrophobic and hydrophilic AFM probes. These models demonstrated the importance of steric forces in addition to traditional DLVO interactions when characterizing microbial cells possessing extracellular structures.

Based on the theoretical predictions, the observed distance at which the repulsive forces become effective, and the forces at contact, we concluded that force-distance curves for approach can be described in terms of the extended XDLVO and EDLVO theories accounting for steric repulsion in the case of bacteria possessing extracellular appendages. Our results emphasize that bacterial adhesion is indeed strongly influenced by the presence of extracellular structures.

7.2 Directions for Future Work

During the course of this study, several unresolved issues that need to be addressed in more details in future projects came to my attention. A brief discussion of these issues is presented below.

The complexity and the duration of the AFM experiments didn't allow us to test a larger range of bacterial cells. For example, it would be interesting to test a hydrophilic microorganism such as *Pseudomonas fluorescense* LP6a, having a

three-phase contact angle of about 20° , and compare the results to those obtained for *A. venetianus* RAG-1 and *R. erythropolis* 20S-E1-c. *P. florescence* LP6a possesses an extracellular capsule as we previously determined (Figure 7.1).

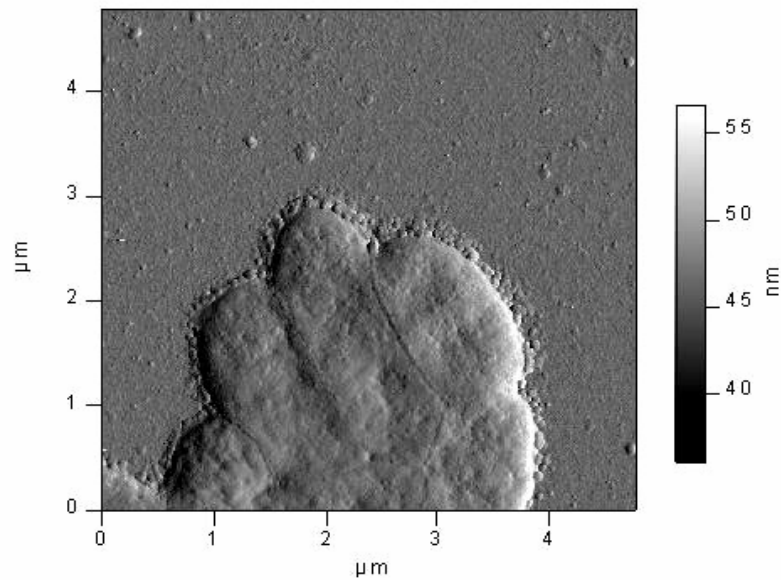


Figure 7.1 Amplitude AFM image of *P. florescence* LP6a surrounded by an extracellular capsule.

Another interesting microorganism to investigate would be one that is devoid of any extracellular structures. It would be interesting to compare the shape of the force curves obtained in this case to those obtained for the bacteria possessing extracellular structures, as probed in this study, and then model the approach force curves using the DLVO theory.

These additional investigations would allow us to create a general picture of bacterial interactions with hydrophobic and hydrophilic substrates.

The study of bacterial heterogeneity and the specific orientation of the cells at the oil/water interface needs more investigation by including the measurements of hydrophobicity on lawn of microorganisms possessing different degrees of hydrophobicity. The results of such experiments would allow the formulation of a general trend followed by microorganisms with regard to their possible orientations at the oil/water interface.

Another possible way of improving our understanding regarding the forces involved in bacterial adhesion to an oil/water interface would be to conduct the AFM force measurements with hydrophobic and hydrophilic modified AFM tips in phosphate buffer of different ionic strength. These series of experiments will allow us to see what happens to the shape of the force curves when the ionic strength varies. Moreover, modeling of the approach force curves obtained for different ionic strength would allow us to better understand the forces involved in bacterial interactions.

Another possible extension to this study would be to approach the AFM tip to the bacterial surface and allow some time for stabilization before retracting the tip. This experiment will allow us to determine if any specific bond is formed during contact by comparing the shape of the retraction force curves to those obtained in this study.

In order to obtain a general view of bacterial adhesion to a surface or interface it would be interesting to investigate the chemical composition of the bacterial surfaces. Fourier transform infrared spectroscopy (FTIR), which is used to identify functional groups in organic molecules based on the vibrational modes at different infrared frequencies, has been successfully applied to elucidate the functional groups on both Gram-positive and Gram-negative bacteria in spite of the complexity of the infrared spectra.[170] Moreover, FTIR microspectroscopy can be used non-destructively down to the micron scale to monitor the chemistry of living cells in vitro and in real time.[70]

REFERENCES

1. Dickinson, R.B., *Bacteria: Surface Behavior* in Encyclopedia of surface and colloid science. ed. Somasundaran, A., 2006, Taylor & Francis.
2. Martinko, M.T.M. *Brock Biology of Microorganisms*. 11th ed. 2005, London: Addison Wesley.
3. Gutnick, D.L., Rosenberg, E. *Oil Tankers and Pollution: A Microbiological Approach*. Annual Review of Microbiology, 1977. **31**: p. 379-396.
4. Dorobantu, L.S., Bhattacharjee, S. Foght, J.M., Gray, M.R., *Atomic Force Microscopy Measurement of Heterogeneity in Bacterial Surface Hydrophobicity*. Langmuir, 2008. **24**: p. 4944-4951.
5. Tegoulia, V.A., Cooper, S.L., *Staphylococcus aureus* adhesion to self-assembled monolayers: effect of surface chemistry and fibrinogen presence. Coll. Surf. B:, 2002. **24**: p. 217-228.
6. Rosenberg, M., *Basic and applied aspects of microbial adhesion at the hydrocarbon: water interface*. Crit. Rev. Microbiol., 1991. **18**(2): p. 159-173.
7. Dorobantu, L.S., Bhattacharjee, S. Foght, J.M., Gray, M.R., *Analysis of Force Interactions between AFM Tips and Hydrophobic Bacteria using DLVO Theory*. Langmuir, 2009.
8. Mudd, S., Mudd, E. B. H., *The penetration of bacteria through capillary spaces. IV. A kinetic mechanism in interfaces*. J. Exp. Med., 1924a. **40**: p. 633-645.
9. Mudd, S., Mudd, E. B. H., *Certain interfacial tension relations and the behavior of bacteria in films*. J. Exp. Med., 1924b. **40**: p. 647-660.
10. Busscher, H.J., Weerkamp, A.H., van der Mei, H.C., van Pelt, A.W.J., DeJong, H.P., Arends, J., *Measurement of the surface free energy of bacterial cell surfaces and its relevance for adhesion*. Appl. Environ. Microbiol., 1984. **48**(5): p. 980-983.
11. Dorobantu, L.S., Young, A.K., Foght, J.M., Gray, M.R., *Stabilization of oil-water emulsions by hydrophobic bacteria*. Appl. Environ. Microbiol., 2004. **70**(10): p. 6333-6336.

12. Rosenberg, M., Gutnick, D., Rosenberg, E., *Adherence of bacteria to hydrocarbons: a simple method for measuring cell-surface hydrophobicity*. FEMS Microbiol. Lett., 1980. **9**(1): p. 29-33.
13. de Kerchove, A.J., Elimelech, M., *Relevance of Electrokinetic Theory for "Soft" Particles to Bacterial Cells: Implications for Bacterial Adhesion*. Langmuir, 2005. **21**(14): p. 6462-6472.
14. Vadillo-Rodriguez, V., Busscher, H.J., Norde, W., de Vries, J., van der Mei, H.C., *On relations between microscopic and macroscopic physicochemical properties of bacterial cell surfaces: an AFM study on Streptococcus mitis strains*. Langmuir, 2003. **19**: p. 2372-2377.
15. Dufrene, Y.F., *Using nanotechniques to explore microbial surfaces*. Nature Rev., 2004. **2**: p. 451-460.
16. Binnig, G., Quate, C.F., *Atomic force microscope*. Phys. Rev. Lett., 1986. **56**(9): p. 930-933.
17. Ubbink, J., Schar-Zammaretti, P., *Probing bacterial interactions: integrated approaches combining atomic force microscopy, electron microscopy and biophysical techniques*. Micron, 2005. **36**: p. 293-320.
18. Razatos, A., Ong, Y-L, Sharma, M.M., Georgiou, G., *Molecular determinants of bacterial adhesion monitored by atomic force microscopy*. Proc. Nat. Acad. Sci. USA, 1998. **95**: p. 11059-11064.
19. Cappella, B., Dietler, G., *Force-distance curves by atomic force microscopy*. Surf. Sci. Rep., 1999. **34**: p. 1-104.
20. Beveridge, T.J., Graham, L.L., *Surface layers of bacteria*. Microbiol. Rev., 1991. **55**(4): p. 684-705.
21. Bullitt, E., Makowski, L., *Bacterial Adhesion Pili Are Heterologous Assemblies of Similar Subunits*. Biophys. J., 1998. **74**: p. 623-632.
22. Poortinga, A.T., Bos, R., Norde, W., Busscher, H.J., *Electric double layer interactions in bacterial adhesion to surfaces*. Surf. Sci. Rep., 2002. **47**: p. 1-32.
23. Ong, Y.-L., Razatos, A., Georgiou, G., Sharma, M.M., *Adhesion forces between E.coli bacteria and biomaterial surfaces*. Langmuir, 1999. **15**: p. 2719-2725.

24. Emerson IV, R.J., Camesano, T.A., *Nanoscale investigation of pathogenic microbial adhesion to a biomaterial*. Appl. Environ. Microbiol., 2004. **70**(10): p. 6012-6022.
25. Jucker, B.A., Harms, H., Zehnder, A.J.B., *Polymer interactions between five gram-negative bacteria and glass investigated using LPS micelles and vesicles as model systems*. Coll. Surf. B:, 1998. **11**: p. 33-45.
26. Rijnaarts, H.H.M., Norde, W., Lyklema, J., Zehnder, A.J.B. *DLVO and steric contributions to bacterial deposition in media of different ionic strengths*. Coll. Surf. B, 1999. **14**: p. 179-195.
27. Rijnaarts, H.H.M., Norde, W., Bouwer, E.J., Lyklema, J., Zehnder, A.J.B., *Bacterial adhesion under static and dynamic conditions*. Appl. Environ. Microbiol., 1993. **59**: p. 3255-3265.
28. Atlas, R.M., Cerniglia, C.E., *Bioremediation of petroleum pollutants*. Bioscience, 1995. **45**(5): p. 332-338.
29. Deziel, E.P., Villemur, G., Lepine, R., Bisailon, J.-G. *Biosurfactant production by a soil Pseudomonas strain growing on polycyclic aromatic hydrocarbons*. Appl. Environ. Microbiol., 1996. **62**: p. 1908-1912.
30. Vater, J.K., B. Wilde, C Franke P., Mehta N. Cameotra S.S. *Matrix-assisted laser desorption ionization-time of flight mass spectrometry of lipopeptide biosurfactants in whole cells and culture filtrates of bacillus subtilis G-1 isolated from petroleum sludge*. Appl. Environ. Microbiol., 2002. **68**: p. 6210-6219.
31. Duarte, G.F.R., Seldin, L. de Araujo. W., van Elsas, J.D. *Analysis of bacterial community structure in sulfurous-oil-containing soils and detection of species carrying dibenzothiophene desulfurization (dszl genes)*. Appl. Environ. Microbiol., 2001. **67**: p. 1052-1062.
32. Churchill, S.A.H., Churchill, P.F. *Isolation and characterization of a Mycobacterium species capable of degrading three- and four-ring aromatic and aliphatic hydrocarbons*. Appl. Environ. Microbiol., 1999. **65**: p. 549-552.
33. Rosenberg, M., Bayer, E.A., Delarea, J., Rosenberg, E. *Role of Thin Fimbriae in Adherence and Growth of Acinetobacter calcoaceticus RAG-1 on Hexadecane*. Appl. Environ. Microbiol., 1982. **44**(4): p. 929-937.
34. Whyte, L.G.H., Zhou, E. Bourbonniere, L. Inniss, W.E. Greer, C.W. *Biodegradation of variable-chain-length alkanes at low temperatures by a*

- Psychrotrophic Rhodococcus sp.* Appl. Environ. Microbiol., 1998. **64**: p. 2578-2584.
35. Baker, K.H., Herson, D.S. *Bioremediation*. 1994, USA: McGraw-Hill, Inc.
 36. Bragg, J.R., Prince, R.C., Harner, E.J., Atlas, R.M., *Effectiveness of bioremediation for the Exxon Valdez oil spill*. Nature, 1994. **368**: p. 413-418.
 37. Coleman, J.M., Baker, J., Cooper, C., Fingas, M., Hunt, G.L., Kvenvolden, K.A., McDowell, J.E., Michel, J., Michel, R.K., Phinney, J., Pond, R., Rabalais, N.N., Roesner, L.A., Spies, R.B. *Oil in the sea-inputs, fates, and effects*. Spill Sci. & Technol. Bulletin, 2002. **7**: p. 197-199.
 38. Rosenberg, E., Legmann, R., Kushmaro, A., Taube, R., Adler, E., Ron, E.Z. *Petroleum bioremediation – a multiphase problem*. Biodegradation, 1992. **3**: p. 337-350.
 39. Bouchez-Naitali, M., Rakatozafy, H., Marchal, R., Leveau, J.-Y., Vandecasteele, J.-P. *Diversity of bacterial strains degrading hexadecane in relation to the mode of substrate uptake*. J. appl. microbiol., 1999. **86**: p. 421-428.
 40. Connell, D.W., Miller, G. J. *Petroleum hydrocarbons in aquatic ecosystems - behaviour and effects of sublethal concentrations:Part 1*. Crit. Rev. Environ. Ctrl., 1981. **11**: p. 37-104.
 41. Atlas, R.M., Pramer, D. *Focus on bioremediation*. ASM News, 1990. **56**(7): p. 13-26.
 42. Alexander, M. *Biodegradation and Bioremediation*, A. Press. 1999, London.
 43. Collins, A.M., Woodley, J. M., Liddell, J. M. *Determination of reactor operation for the microbial hydroxylation of toluene in a two liquid phase process*. J. Ind. Microbiol., 1995. **14**: p. 382-388.
 44. Eirich, L.D., Anderson, K. W., Gates, J. A., Wilson, C. R., Biermann, M., Vice, G. H. *Biooxidation capabilities of Candida sp.* 2005, Cognis Corporation USA.
 45. Fukui, S., Tanaka, A. *Advances in Biochemical Engineering*. 1980, Berlin: Springer. 1-35.

46. Flickinger, M.C., Drew, S.W. *Encyclopaedia of Bioprocess Technology: Fermentation, Biocatalysis and Bioseparation*. 1999: John Wiley and Sons. 2756.
47. Roehr, M., *Biotechnology: Products of Primary Metabolism*. 1996, Weinheim: VCH.
48. Chan, E.C., Cheng, C.S., Hsu, Y.H. *Continuous production of dicarboxylic acid by immobilized Pseudomonas aeruginosa cells*. J. Ferment. Bioeng., 1997. **83**: p. 157-160.
49. Leahy, J.G., Colwell, R.R. *Microbial degradation of hydrocarbons in the environment*. Microbiol. Rev., 1990. **54**: p. 305-315.
50. Atlas, R.M., Bartha, R., *Hydrocarbon degradation and oil-spill bioremediation*. Adv. Microbial. Ecol., 1992. **12**: p. 287-338.
51. Atlas, R.M. *Petroleum Biodegradation and Oil Spill Bioremediation*. Marine Poll. Bul., 1995. **31**: p. 178-182.
52. Gibson, D.T. *Microbial Degradation of Organic Compounds*. 1984, New York, USA: Marcel Decker.
53. Eastcott, L., Shiu, W.Y., Mackay, D. *Environmentally relevant physico-chemical properties of hydrocarbons: A review of data and development of simple correlations*. Oil Chem. Pollut., 1988. **4**: p. 11-216.
54. Walter, M.V., Nelson, E.C., Firmstone, G. *Surfactant enhances biodegradation of hydrocarbons: microcosm and field study*. J. Soil Contam., 1997. **6**: p. 61-77.
55. Hommel, R.K. *Formation and physiological role of biosurfactants produced by hydrocarbon-utilizing microorganisms*. Biodegradation, 1990. **1**: p. 107-110.
56. Beal, R., Betts, W. B. *Role of rhamnolipid biosurfactants in the uptake and mineralization of hexadecane in Pseudomonas aeruginosa*. J. appl. microbiol., 2001. **89**(1): p. 158-168.
57. Rosenberg, E., Navon-Venezia, S., Zilber-Rosenberg, I., Ron, E. Z. *Rate limiting steps in the microbial degradation of petroleum hydrocarbons*, in *Soil and Aquifer Pollution*, H. Rubin, Ed. 1998, Springer-Verlag: Berlin-Heidelberg. p. 159-172.
58. Wieseman, A. *Enzyme and Fermentation Biotechnology*. 1984, New York: Wiley. 11-77.

59. Atlas, R.M. *Microbial Metabolism of Straight-Chain and Branched Alkanes*. 1984, New York: Macmillan. 1-60.
60. Bury, S.J., Miller, C.A. *Effect of micellar solubilization on biodegradation rates of hydrocarbons*. Environ. Sci. Technol., 1993. **27**(1): p. 104-110.
61. Goswami, P.S. *Different Modes of Hydrocarbon Uptake by Two Pseudomonas Species*. Biotech. bioeng., 1991. **37**: p. 1-11.
62. Ron, E.Z. *Biosurfactants and oil bioremediation*. Curr. opinion biotechnol., 2002. **13**: p. 249-252.
63. Noordman, W.H. *Rhamnolipid Stimulates Uptake of Hydrophobic Compounds by Pseudomonas aeruginosa*. Appl. Environ. Microbiol., 2002. **68**(9): p. 4502-4508.
64. Gutierrez, J.R., Erickson, L. E. *Continuous Culture of Candida lipolytica on n-Hexadecane*. Biotechnol. bioeng., 1978. **20**: p. 1833-1847.
65. Prince, R.C. *Petroleum spill bioremediation in marine environments*. Crit. Rev. Microbiol., 1993. **19**(4): p. 217-242.
66. Maier, R.M., Pepper, I.L. and Gerba, C.P. *Environmental Microbiology*. 2000, San Diego: Academic Press.
67. Cole, G.M. *Assessment and Remediation of Petroleum Contaminated Sites*. 1994: Lewis Publishers.
68. Atlas, R.M., Bartha, R. *Hydrocarbon degradation and oil-spill bioremediation*. Adv. Microbial. Ecol., 1992. **12**: p. 287-338.
69. Christenson, B.B., Sternberg, C., Anderson, J.B., Eberl, L., Moller, S., Givskov, M., Molin, S. Appl. Environ. Microbiol., 1998. **64**: p. 2247-2255.
70. Geoghegan, M., Andrews, J.S., Biggs, C.A., Eboigbodin, K.E., Elliott, D.R., Rolfe, S., Scholes, J., Ojeda, J.J., Romero-Gonzalez, M.E., Robert, L.S., Edyvean, G.J., Rutkaite, R., Fernando, R., Pen, Y., Zhanga, Z., Banwart, S.A. *The polymer physics and chemistry of microbial cell attachment and adhesion*. Faraday discuss., 2008. **139**: p. 1-20.
71. Neufeld, R.J., Zajic, J.E., D. F. Gerson, *Cell Surface Measurements in Hydrocarbon and Carbohydrate Fermentations*. Appl. Environ. Microbiol., 1980. **39**(3): p. 511-517.

72. Tufenkji, N. *Modeling microbial transport in porous media: Traditional approaches and recent developments*. Adv. Water Res., 2007. **30**: p.1455-1469.
73. Dickinson, R.B. *Surface behavior of bacteria*. Encyclopedia of surface and colloid science, 2002.
74. Costerton, J.W., Irving, R.T., Cheng, K.-J., *The bacterial glycocalyx in nature and disease*. Annu. Rev. Microbiol., 1981. **35**: p. 299-324.
75. Xu LC, *Interaction forces measured using AFM between colloids and surfaces coated with both dextran and protein*. Langmuir, 2006. **22**: p. 4720-4727.
76. Whitfield, C., Roberts, I.S. *Structure, assembly and regulation of expression of capsules in Escherichia coli*. Mol. microbiol., 1999. **31**(5): p. 1307-1319.
77. Touhami, A., Jericho, M.H., Boyd, J.M., Beveridge, T.J., *Nanoscale Characterization and Determination of Adhesion Forces of Pseudomonas aeruginosa Pili by Using Atomic Force Microscopy*. J. Bacteriol., 2006. **188**(2): p. 370-377.
78. Berkeley, R.C.W., Lynch, J.M., Melling, J., Rutter, P.R., Vincent, B., *Microbial adhesion to surfaces*. 1980, Chichester: Ellis Horwood Limited.
79. Stenstrom, T.A.K. *Fimbriae mediated nonspecific adhesion of Salmonella typhimurium to mineral particles*. Arch. Microbiol., 1985. **143**(1): p. 6-10.
80. McNab, R.F., Handley, P.S. Loach, D.M. Tannock, G.W. Jenkinson, H.F. *Cell wall-anchored CshA polypeptide (259 kilodaltons) in Streptococcus gordonii forms surface fibrils that confer hydrophobic and adhesive properties*. J. Bacteriol., 1999. **181**(10): p. 3087-3095.
81. Busscher, H.J., Weerkamp, A.H., *Specific and non-specific interactions in bacterial adhesion to solid substrata*. FEMS Microbiol. Rev., 1987. **46**: p. 165-173.
82. Bayer, M.E., Sloyer, J.L., Jr. *The electrophoretic mobility of gram-negative and gram-positive bacteria: an electrokinetic analysis*. J. Gen. Microbiol., 1990. **136**(5): p. 867-874.
83. Boonaert, C.J.P., Rouxhet, P.G., *Surface of Lactic Acid Bacteria: Relationships between Chemical Composition and Physicochemical Properties*. Appl. Environ. Microbiol., 2000. **66**(6): p. 2548-2554.

84. Somasundaran, P. *Encyclopedia of Surface and Colloid Science*. 2006: CRC Press.
85. Mangia, A.H.T., L.M.; Costa e Silva Filho, F. *The electrokinetic surface of five enteropathogenic Escherichia coli serogroups*. *Cell Biophysics*, 1995. **26**(1): p. 45-55.
86. Diaspro, A., Rolandi, R. *Atomic force microscopy*. *IEEE Engineering in medicine and biology*, 1997. **16**(2): p. 1-2.
87. Bonnell, D.A., Solomon, I., Rohrer, G.S., Warner, C. *Direct Measurement of Local Properties of Interfaces with Scanning Tunneling Microscopy*. *Acta Metall. Mater.* 1992. **40**: p. S161-S171.
88. Marti O, C.J., Bielefeldt H, Hipp M, Linder A *Scanning Probe Microscopy - Applications in Biology and Physics*. *Microscopy Microanalysis Microstructures* 1993. **4**: p. 429-440.
89. Mate, M.C., *Tribology on the small scale - A bottom up approach to friction, lubrication, and wear*. 2008, New York: Oxford University Press.
90. Janshoff, A., Neitzert, M., Oberdorfer, Y., Fuchs, H., *Force spectroscopy of molecular systems - single molecule spectroscopy of polymers and biomolecules*. *Angew. chem. int. ed.* , 2000. **39**: p. 3212-3237.
91. Bowen, W.R., Hilal, N., Lovitt, R.W., Wright, C.J., *Direct measurement of the force of adhesion of a single biological cell using an atomic force microscope*. *Coll. Surf. A.*, 1998. **136**: p. 231-234.
92. Velegol, S.B., Logan, B.E., *Contributions of bacterial surface polymers, electrostatics, and cell elasticity to the shape of AFM force curves*. *Langmuir*, 2002. **18**: p. 5256-5262.
93. Dufrene, Y.F., *Direct characterization of the physicochemical properties of fungal spores using functionalized AFM probes*. *Biophys. J.*, 2000. **78**: p. 3286-3291.
94. Abu-Lail, N.I., Camesano, T.A., *Elasticity of Pseudomonas putida KT2442 surface polymers probed with single-molecule force microscopy*. *Langmuir*, 2002. **18**: p. 4071-4081.
95. Green, C.P., Lioe, H., Cleveland, J.P., Proksch, R., Mulvaney, P., Sader, J.E., *Normal and torsional spring constants of atomic force microscope cantilevers*. *Rev. Sci. Instrum.*, 2004. **75**(6): p. 1988-1996.

96. Frisbie, C.D., Rozsnyai, L.F., Noy, A., Wrighton, M.S., Lieber, C.M., *Functional Group Imaging by Chemical Force Microscopy*. Science, 1994. **265**: p. 2071-2074.
97. Muller, D.J., Amrein, M., Engel, A., *Preparation techniques for the observation of native biological systems with the atomic force microscope*. Biosens. Bioelect., 1997. **12**(8): p. 867-877.
98. Camesano, T.A., Natan, M.J., Logan, B.E., *Observation of changes in bacterial cell morphology using tapping mode atomic force microscopy*. Langmuir, 2000. **16**: p. 4563-4572.
99. Kasas, S., Ikai, A., *A method for anchoring round shaped cells for atomic force microscope imaging*. Biophys. J., 1995. **68**: p. 1678-1680.
100. Gad, M., Itoh, A., Ikai, A., *Mapping cell wall polysaccharides of living microbial cells using atomic force microscopy*. Cell Biol. Int., 1997. **21**(11): p. 697-706.
101. Schaer-Zammaretti, P., Ubbink, J., *Imaging of lactic acid bacteria with AFM—elasticity and adhesion maps and their relationship to biological and structural data*. Ultramicroscopy, 2003. **97**: p. 199-208.
102. Busscher, H.J., van de Mei, H.C. *Physico-chemical interactions in initial microbial adhesion and relevance for biofilm formation*. Adv Dent Res, 1997. **11**(1): p. 24-32.
103. van Oss, C.J., *Hydrophobicity of biosurfaces - origin, quantitative determination and interaction energies*. Coll. Surf. B: Biointerfaces, 1995. **5**: p. 91-110.
104. Attard, P., *Nanobubbles and the hydrophobic attraction*. Adv. Coll. Interf. Sci., 2003. **104**: p. 75-91.
105. Israelachvili, J.N., *Intermolecular and Surface Forces*. 1991, London: Academic Press.
106. Ducker, W.A., Senden, T.J., Pashley, R.M., *Direct measurement of colloidal forces using an atomic force microscope*. Nature, 1991. **353**(19): p. 239-241.
107. Butt, H.-J., *Electrostatic interaction in scanning probe microscopy when imaging in electrolyte solutions*. Nanotechnology, 1992. **3**: p. 60-68.
108. Moreno-Herrero, F., Colchero, J., Barlo, A. M., *DNA height in scanning force microscopy*. Ultramicroscopy, 2003. **96**: p. 167-174.

109. Hogg, R.H., T. W.; Fuerstenau, D. W. *Mutual coagulation of colloidal dispersions*. Trans. Faraday Soc., 1966. **62**: p. 1638-1651.
110. Smoluchowski, M., *Handbook of Electricity and Magnetism*. Vol. 2. 1921, Leipzig, Germany: Barth.
111. Jucker , B.A., Zehnder , A. J. B., Harms, H., *Quantification of polymer interactions in bacterial adhesion*. Env. Sci. Technol., 1998. **32**: p. 2909-2915.
112. Derjaguin, B., *Analysis of friction and adhesion IV The theory of the adhesion of small particles*. Kolloid Z, 1934. **69**(2): p. 155-164.
113. van Oss, C.J., *Interfacial forces in aqueous media*, ed. Dekker. 1994, New York.
114. Camesano, T. A., Logan, B. E., *Probing bacterial electrosteric interactions using atomic force microscopy*. Environ. Sci. Technol., 2000. **34**: p. 3354-3362.
115. Marshall, K. C., *Interfaces in microbial ecology*. 1976, Cambridge: Harvard University Press.
116. Emerson, R. J., Bergstrom, T.S., Liu, Y.T., Soto, E.R., Brown, C.A., McGimpsey, W.G., Camesano, T.A., *Microscale Correlation between Surface Chemistry, Texture, and the Adhesive Strength of Staphylococcus epidermidis*. Langmuir, 2006. **22**: p. 11311-11321.
117. van Loosdrecht, M.C.M., Norde, N., Lyklema, J., Zehnder, A.J.B., *Hydrophobic and electrostatic parameters in bacterial adhesion* Aquatic Sci., 1990. **52**: p. 103-114.
118. Razatos, A., *Application of atomic force microscopy to study initial events of bacterial adhesion*. Meth.enzymol., 2001. **337**: p. 276-285.
119. Van Oss, C. J., *Acid-base interfacial interaction in aqueous media*. Coll. Surf. A, 1993. **78**: p. 1-49.
120. Sharma, P.H.R., K., *Adhesion of Paenibacillus polymyxa on chalcopyrite and pyrite: surface thermodynamics and extended DLVO theory*. Coll. Surf. B, 2003. **29**: p. 21-38.
121. Jucker , B.A., Harms, H., Hug, S.J., Zehnder , A.J.B., *Adsorption of bacterial surface polysaccharides on mineral oxides is mediated by hydrogen bonds*. Coll. Surf. B 1997. **9**: p. 331-343.

122. van Oss, C.J., *Long-range and short-range mechanisms of hydrophobic attraction and hydrophilic repulsion in specific and aspecific interactions.* J. mol. recogn., 2003. **16**: p. 177-190.
123. Alexander, S., *Adsorption of chain molecules with a polar head A-Scaling description.* J. Phys.(Paris), 1977. **38**(8): p. 983-987.
124. de Gennes, P.G. *Polymers at an interface; a simplified view.* Adv. Coll. Interf. Sci., 1987. **27**: p. 189-209.
125. Butt, H.-J., Kappl, M., Mueller, H., Raiteri, R., *Steric Forces Measured with the Atomic Force Microscope at Various Temperatures.* Langmuir, 1999. **15**: p. 2559-2565.
126. Reisfeld, A.R., E.; Gutnick, D., *Microbial degradation of crude-oil - Factors affecting dispersion in sea-water by mixed and pure cultures* Appl. Microbiol., 1972. **24**(3): p. 363-368.
127. Vanechoutte, M., Tjernberg, I., Baldi, F., Pepi, M., Fani, R. and E.R. Sullivan, van der Toorn, J., Dijkshoorn, L., *Oil-degrading Acinetobacter strain RAG-i and strains described as 'Acinetobacter venetianus sp. nov.' belong to the same genomic species.* Res. Microbiol., 1999. **150**: p. 69-73.
128. Foght, J.M., *Identification of the bacterial isolates comprising the environment Canada freshwater and cold marine standard inocula using 16S rRNA gene sequencing and analysis.*, in *Environmental Protection Service, Environment Canada.* 1999: Ottawa, Canada.
129. Goodfellow, M.M., L. A., *The Families Dietziaceae, Gordoniaceae, Nocardiaceae and Tsukamurellaceae.* . Prokaryotes, 2006. **3**: p. 843-888.
130. Cleveland, J.P., Manne, S., Bocek, D., Hansma, P.K., *A nondestructive method for determining the spring constant of cantilevers for scanning force microscopy.* Rev. Sci. Instrum., 1993. **64**(2): p. 403-405.
131. Vadillo-Rodriguez, V., Busscher, H.J., van der Mei, H.C., de Vries, J., Norde, W., *Role of lactobacillus cell surface hydrophobicity as probed by AFM in adhesion to surfaces at low and high ionic strength.* Coll. Surf. B, 2005. **41**: p. 33-41.
132. Horber, J.K.H., Miles, M.J., *Scanning probe evolution in biology.* Science, 2003. **302**: p.1002-1005.

133. Stark, M., Möller, C., Müller, D.J., Guckenberger, R., *From Images to Interactions: High-Resolution Phase Imaging in Tapping-Mode Atomic Force Microscopy*. Biophys. J., 2001. **80**: p. 3009-3018.
134. Vie, V., Giocondi, M.-C., Lesniewska, E., Finot, E., Goudonnet, J.-P., Le Grimellec, C., *Tapping-mode atomic force microscopy on intact cells: optimal adjustment of tapping conditions by using the deflection signal*. Ultramicroscopy, 2000. **82**: p. 279-288.
135. Graham, L.L., Harris, R., Villiger, W., Beveridge, T.J., *Freeze-substitution of gram-negative eubacteria: general cell morphology and envelope profiles*. J. Bacteriol., 1991. **173**(5): p. 1623-1633.
136. Goodman, F.O., Garcia, N., *Roles of the attractive and repulsive forces in atomic-force microscopy*. Phys. Rev. B, 1991. **43**(6): p. 4728-4731.
137. Pines, O., Bayer, E.A., Gutnick, D.L., *Localization of Emulsan-Like Polymers Associated with the Cell Surface of Acinetobacter calcoaceticus*. J. Bacteriol., 1983. **154**(2): p. 893-905.
138. Whyte LG, S.S., Pietrantonio F, Bourbonniere L, Koval SF, Lawrence JR, Inniss WE, Greer CW *Physiological adaptations involved in alkane assimilation at a low temperature by Rhodococcus sp strain Q15*. Appl. Environ. Microbiol., 1999. **65**(7): p. 2961-2968.
139. Sutcliffe, I.C. *Cell envelope composition and organisation in the genus Rhodococcus*. Antonie van Leeuwenhoek international journal of general and molecular microbiology, 1998. **74**: p. 49-58.
140. Velegol, S.B., Pardi, S., Li, Xu, Velegol, D., Logan, B.E., *AFM imaging artifacts due to bacterial cell height and AFM tip geometry*. Langmuir, 2003. **19**: p. 851-857.
141. Pelling, A.E., Li, Y., Shi, W., Gimzewski, J.K., *Nanoscale visualization and characterization of Myxococcus xanthus cells with atomic force microscopy*. Proc. Nat. Acad. Sci. USA, 2005. **102**(18): p. 6484-6489.
142. Ishii, S., Koki, J., Unno, H., Hori, K., *Two Morphological Types of Cell Appendages on a Strongly Adhesive Bacterium, Acinetobacter sp. Strain Tol 5*. Appl. Environ. Microbiol., 2004. **70**(8): p. 5026-5029.
143. Pietak, A., Korte, S., Tan, T., Downard, A., Staiger, M.P., *Atomic force microscopy characterization of the surface wettability of natural fibres*. Appl. Surf. Sci., 2007. **253**: p. 3627-3635.

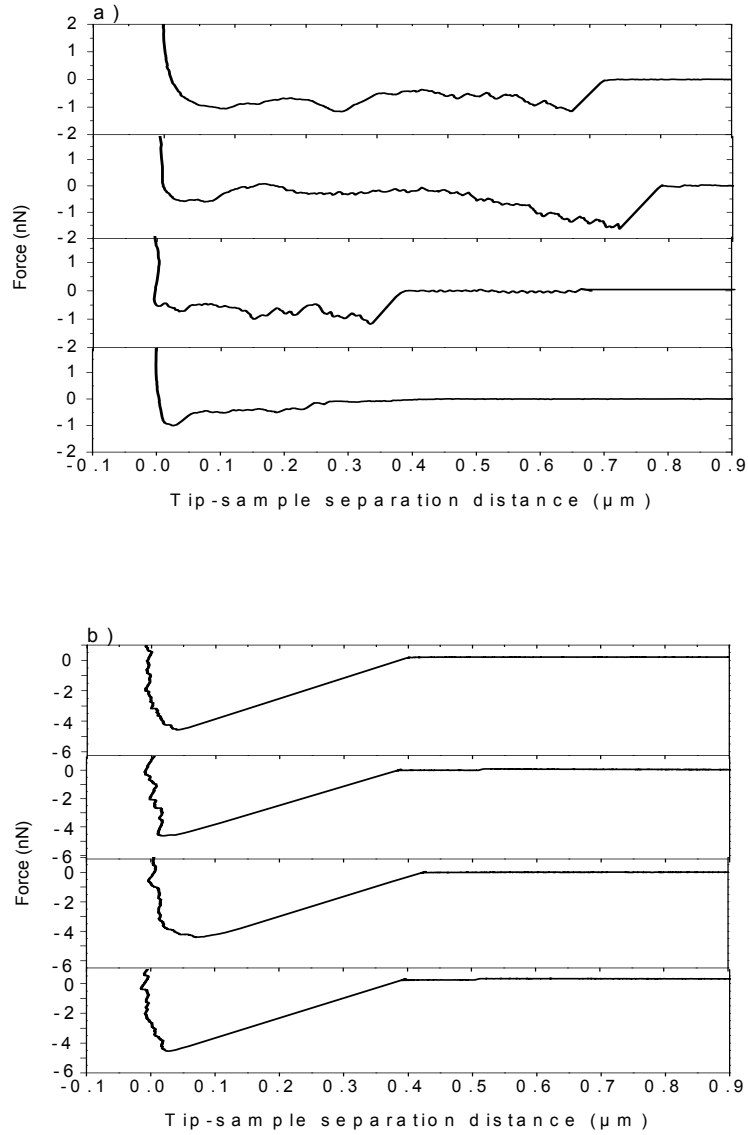
144. Vadillo-Rodríguez, V., Busscher, H.J., Norde, W., de Vries, J., van der Mei, H.C., *Dynamics cell surface hydrophobicity of Lactobacillus Strains with and without surface layer proteins*. J. Bacteriol., 2004. **186**(19): p. 6647-6650.
145. van Loosdrecht, M.C.M., Lyklema, J., Norde, W., Zehnder, A.J.B., *Influence of interfaces on microbial activity*. Microbiol. Rev. 1990. **54**(1): p. 75-87.
146. Bryers, J.D., *Biofilms and the Technological Implications of Microbial Cell Adhesion*. Coll. Surf. B, Biointerfaces, 1994. **2**: p. 9-23.
147. Butt, H.-J., Cappella, B., Kappl, M., *Force measurements with the atomic force microscope: Technique, interpretation and applications*. Surf. Sci. Rep., 2005. **59**: p. 1-152.
148. Headrick, J.E., Berrie, C. L., *Alternative Method for Fabricating Chemically Functionalized AFM Tips: Silane Modification of HF-Treated Si₃N₄ Probes*. Langmuir, 2004. **20**: p. 4124-4131.
149. Bowen, W.R., Lovitt, R.W., Wright, C.J., *Atomic force microscopy study of the adhesion of Saccharomyces cerevisiae*. J. Coll. Interf. Sci., 2001. **237**: p. 54-61.
150. Takano, H., Kenseth, J.R., Wong, S.S., O'Brien, J.C., Porter, M.D., *Chemical and biochemical analysis using scanning force microscopy*. Chem. Rev., 1999. **99**: p. 2485-2890.
151. Muller, D.J., Amrein, M., Engel, A., *Adsorption of biological molecules to a solid support for scanning probe microscopy*. J. Struct. Biol., 1997. **119**: p. 172-188.
152. Ederth, E., *Computation of Lifshitz-van der Waals Forces between Alkylthiol Monolayers on Gold Films*. Langmuir, 2001. **17**: p. 3329-3340.
153. Verwey, E.J.W., Overbeek, J.T.G., *Theory of the Stability of Lyophobic Colloids*. 1948, Amsterdam: Elsevier.
154. Norde, W., *Colloids and Interfaces in Life Sciences*. 2003, NY: Marcel Dekker.
155. Abu-Lail, N.I., Camesano, T.A., *Specific and Nonspecific interaction forces between Escherichia coli and silicon nitride, determined by Poisson Statistical Analysis*. Langmuir, 2006. **22**: p. 7296-7301.

156. van Loosdrecht, M.C.M., Zehnder, A.J.B., *Energetics of bacterial adhesion*. Experientia, 1990. **46**: p. 817-822.
157. Meinders, J. M., van der Mei, H.C., Busscher, H. J. *Deposition efficiency and reversibility of bacterial adhesion under flow*. Coll. Interf. Sci., 1995. **176**: p. 329-341.
158. Abu-Lail L.I., L.Y., Atabek A., Camesano T.A., *Quantifying the adhesion and interaction forces between Pseudomonas aeruginosa and natural organic matter* Environ. sci. technol., 2007. **41**(23): p. 8031-8037.
159. Williams, V., Fletcher, M., *Pseudomonas fluorescens Adhesion and Transport through Porous Media Are Affected by Lipopolysaccharide Composition*. Appl. Environ. Microbiol., 1996. **62**: p. 100-104.
160. Savage, D.C., Fletcher, M., *Bacterial adhesion*. Bacterial cell walls and surfaces ed. A.J. Wickens. 1985, New York: Plenum Press.
161. Beveridge, T.J., *Structures of Gram-Negative Cell Walls and Their Derived Membrane Vesicles*. J. Bacteriol., 1999. **4725-4733**.
162. Bayer, M.E., Carlemalm, E., Kellenberger, E., *Capsule of Escherichia coli K29: Ultrastructural Preservation and Immunoelectron Microscopy*. J. Bacteriol., 1985. **162**(3): p. 985-991.
163. Dufrene, Y.F., *Application of atomic force microscopy to microbial surfaces: from reconstituted cell surface layers to living cells*. Micron, 2001. **32**: p. 153-165.
164. de Gennes, P.G., *Polymers at an interface; a simplified view*. Adv. Coll. Interf. Sci., 1987. **27**: p. 189-209.
165. Jones, L., O'Shea, P. *The Electrostatic Nature of the Cell Surface of Candida albicans: A Role in Adhesion*. Exp. Mycol., 1994. **18**: p. 111.
166. Boonaert, C.J.P., Dufrene, Y.F., Derclaye, S.R., Rouxhet, P.G., *Adhesion of Lactococcus lactis to model substrata: direct study of the interface*. Coll. Surf. B, 2001. **22**: p. 171-182.
167. van Loosdrecht, M.C.M., Lyklema, J., Norde, W. Schraa, G., Zehnder, A. J. B. *The role of bacterial-cell wall hydrophobicity in adhesion*. Appl. Environ. Microbiol., 1987. **53**: p. 1898-1901.
168. Brant, J.A., Childress, A. E., *Colloidal adhesion to hydrophilic membrane surfaces*. J. Membr. Sci., 2004. **241**: p. 235-248.

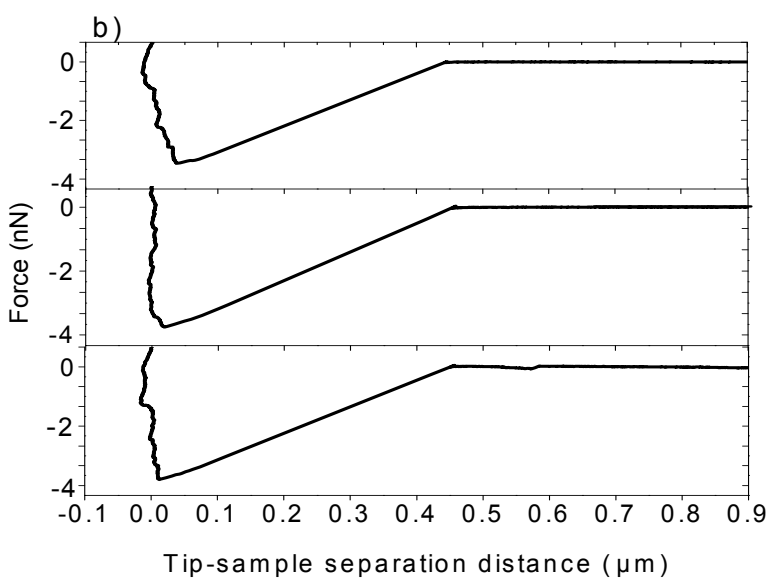
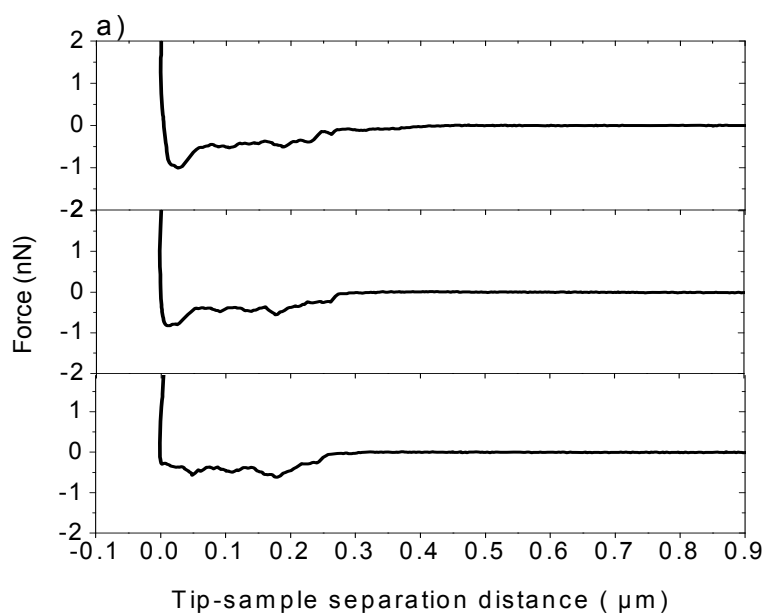
169. Kang, Z., Foght, J.M., Young, A., Gray, M.R. *Mechanical properties of hexadecane-water interfaces with adsorbed hydrophobic bacteria*. Coll. Surf. B, 2008. **62**: p. 273-279.
170. Dittrich, M., Sibler, S., *Cell surface groups of two picocyanobacteria strains studied by zeta potential investigations, potentiometric titration, and infrared spectroscopy*. J. Colloid Interface Sci., 2005. **286**: p. 487-495.
171. Characklis, W.G., *Attached microbial growths - attachment and growth*. Water Res., 1973. **7**: p. 1113-1127.
172. Bressler, D.C., Gray, M.R., *Transport and Reaction Processes in Bioremediation of Organic Contaminants. 1. Review of Bacterial Degradation and Transport*. Int. J. Chem. Reactor Eng., 2003. **1**: p. 1-16.
173. Des W. Connell, M.C., Barron, D.M., *Aqueous Solubility and Octan-1-01 to Water Partition Coefficients of Aliphatic Hydrocarbons*. Environ. Sci. Technol., 1985. **19**: p. 628-632.
174. Bouchez-Naitali, M., Vandecasteele, J.-P., *Biosurfactants, an help in the biodegradation of hexadecane? The case of Rhodococcus and Pseudomonas strains*. World J. Microbiol. Biotechnol, 2008. **24**: p. 1901-1907.
175. Geerdink, M.J., van Loosdrecht, M.C.M., Luyben, K.Ch.A.M., *Model for Microbial Degradation of Nonpolar Organic Contaminants in a Soil Slurry Reactor*. Environ. Sci. Technol., 1996. **30**(3): p. 779-786.
176. Borzani, W., Concone, B. R. V., Vairo, M. L. R., Doin, P. A., Kovacs, J., *Recent advances in microbiology*, A. Perez-Miravete, Editor. 1971, Association Mexicana De Microbiologia. p. 419-425.
177. Marshal, K.C., Cruickshank, R.H., *Cell surface hydrophobicity and the orientation of certain bacteria at interfaces*. Archiv fur Mikrobiol., 1973. **91**: p. 29-40.
178. Binks, B.P., Horozov, T.S. *Colloidal Particles at Liquid Interfaces*. 2006. Cambridge University Press, Cambridge, UK.
179. Kralchevsky, P.A., Nagayama, K. *Particles at Fluid Interfaces and Membranes*. 2001. Elsevier Science, Amsterdam, The Netherlands.
180. Reich, Z., Kapon, R., Nevo, R., Pilpel, Y., Zmora, S., Scolnik, W. *Scanning force microscopy in the applied biological sciences*. Biotech. Adv., 2001. **19**: p.451-485.

181. Hayashi, H., Tsuneda, S., Hirata, A., Sasaki, H. *Soft particle analysis of bacterial cells and its interpretation of cell adhesion behaviors in terms of DLVO theory*. Coll. Surf. B., 2001. **22**(2): p. 149-157.
182. Ohshima, H., Kondo, T., *Approximate analytic expression for the electrophoretic mobility of colloidal particles with surface-charge layers*. J. Colloid Interface Sci., 1989. **130**(1): p. 281-282.
183. Ohshima, H., *Electrophoresis of soft particles*. Adv. Coll. Interf. Sci., 1995. **62**: p. 189-235.
184. McLaine, J. W., Ford, R. M., *Reversal of flagellar rotation is important in initial attachment of Escherichia coli to glass in a dynamic system with high- and low-ionic strength buffers*. Appl. Environ. Microbiol., 2002. **68**: p.1280-1289.
185. de Kerchove, A. J., Elimelech, M. *Relevance of Electrokinetic Theory for "Soft" Particles to Bacterial Cells: Implications for Bacterial Adhesion*. Langmuir, 2005. **21**: p.6462-6472.
186. Bach, H., Berdichevsky, Y., Gutnick, D. *An exocellular protein from the oil-degrading microbe Acinetobacter venetianus RAG-1 enhances the emulsifying activity of the polymeric bioemulsifier emulsan*. Appl. Environ. Microbiol., 2003. **69**: p. 2608-2615.
187. Burks, G. A., Velegol, S. B., Paramonova, E., Lindenmuth, B. E., Feick, J. D., Logan, B. E. *Macroscopic and Nanoscale Measurements of the Adhesion of Bacteria with Varying Outer Layer Surface Composition*. Langmuir, 2003. **19**: p.2366-2371.
188. Heinz, W. F., Hoh, J. H. *Spatially resolved force spectroscopy of biological surfaces using the atomic force microscope*. Trends Biotech., 1999. **17**: p. 143-150.
189. Klein, J. D., Clapp, A. R., Dickinson, R. B. *Direct measurement of interaction forces between a single bacterium and a flat plate*. J, Coll. Int. Sci., 2003. **261**: p. 379-385.

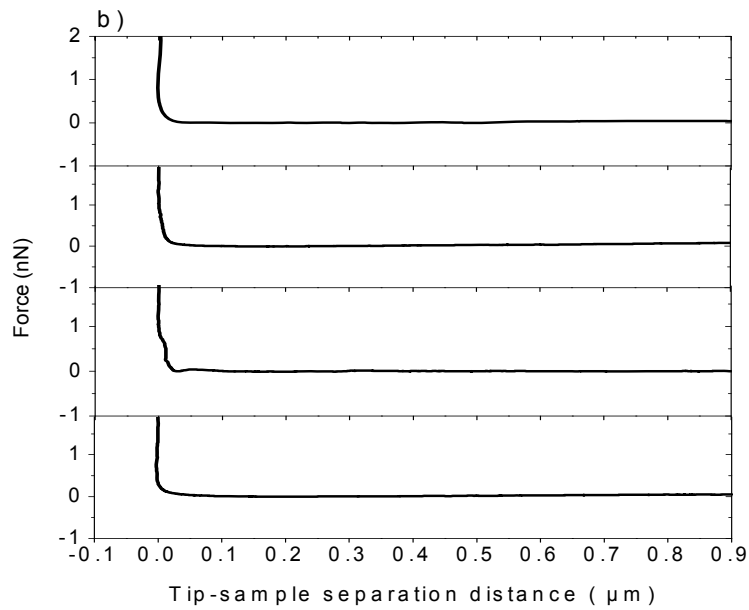
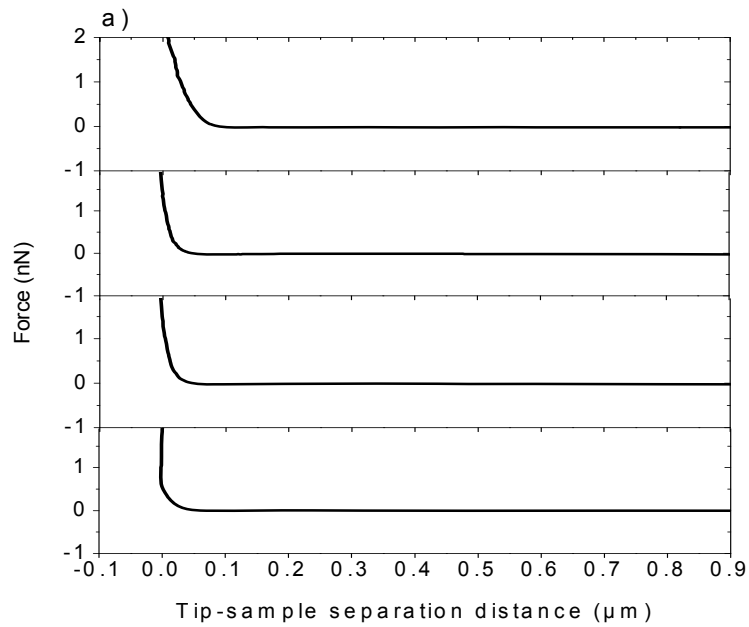
APPENDIX A.



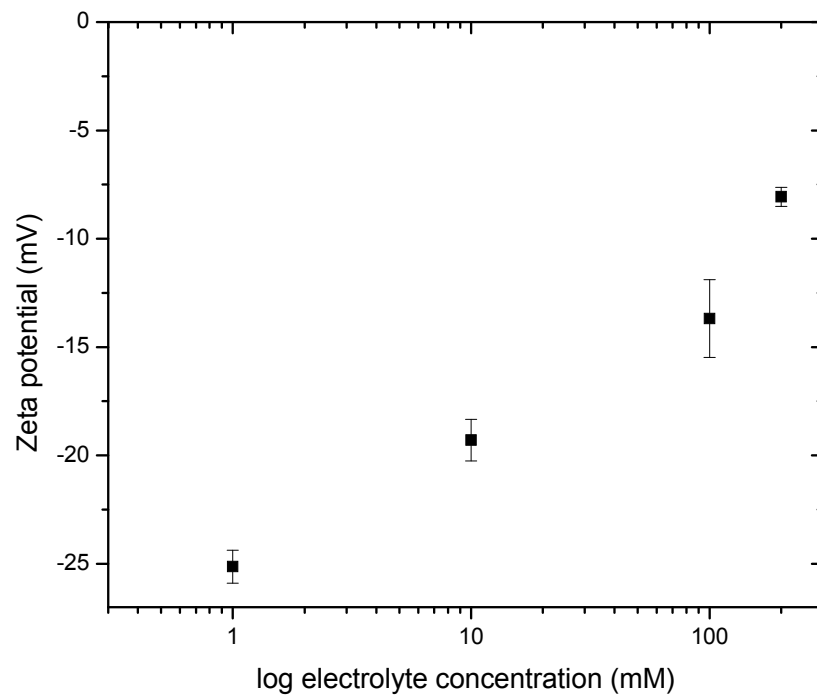
A.1 Representative AFM retraction curves taken on *A. venetianus* RAG-1 (a) and *R. erythropolis* 20S-E1-c (b) surfaces in phosphate buffer with the hydrophobic tip. The four force curves represent data obtained on different areas for the same bacterium.



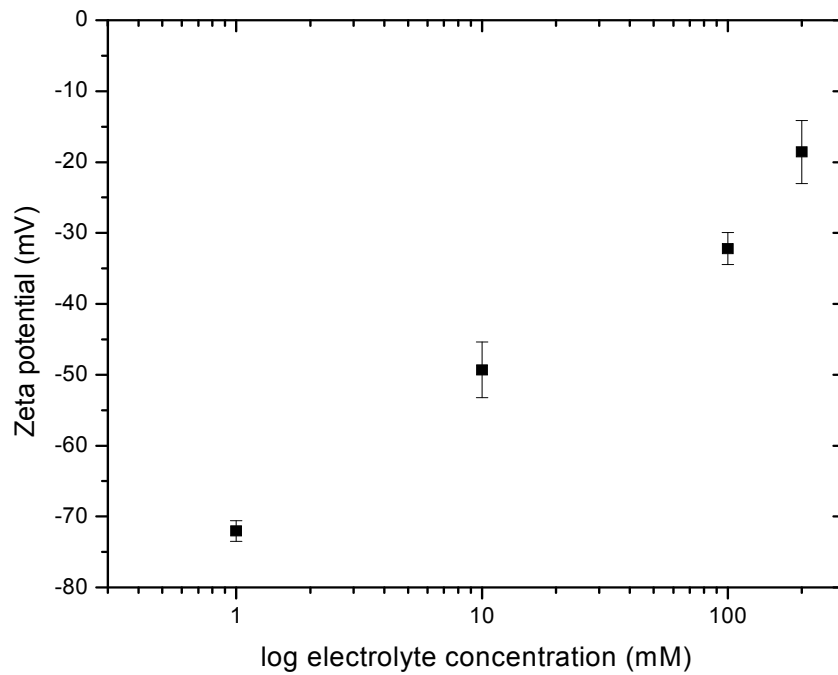
A.2 Representative AFM retraction curves taken on *A. venetianus* RAG-1 (a) and *R. erythropolis* 20S-E1-c (b) surfaces in phosphate buffer with the hydrophobic tip. The three force curves represent the repeatability of measurements at the same point on a bacterium surface.



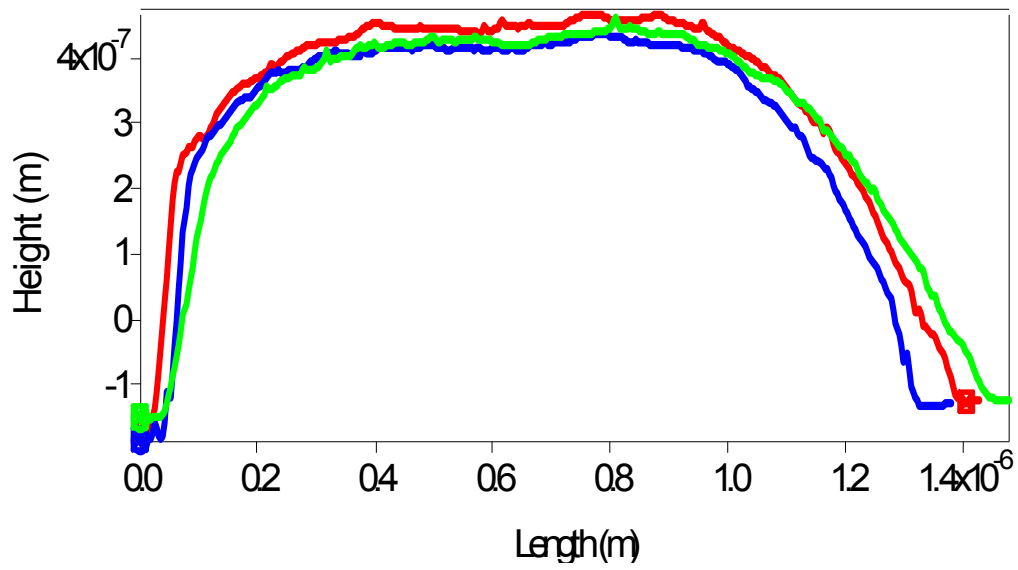
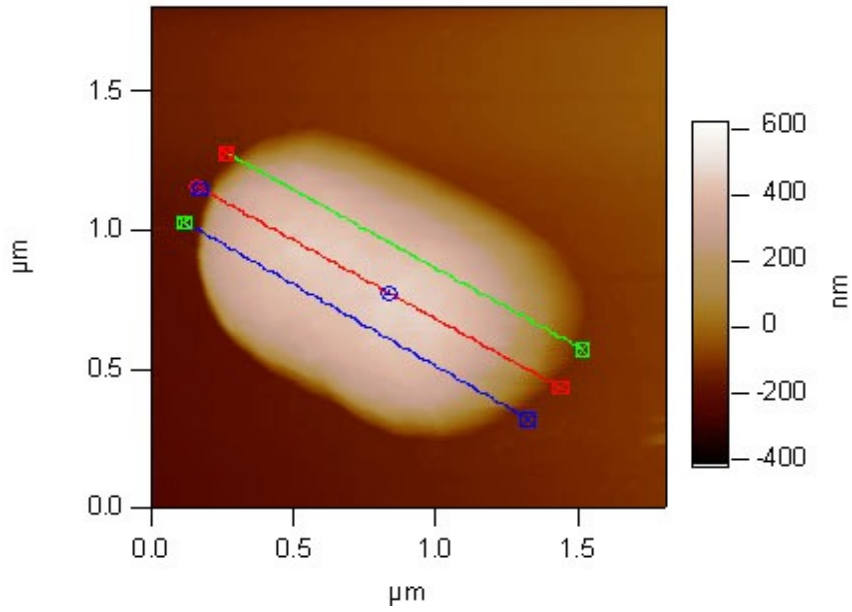
A.3 Representative AFM retraction curves taken on *A. venetianus* RAG-1 (a) and *R. erythropolis* 20S-E1-c (b) surfaces in phosphate buffer with the hydrophilic tip. The four force curves represent data obtained on different areas for the same bacterium.



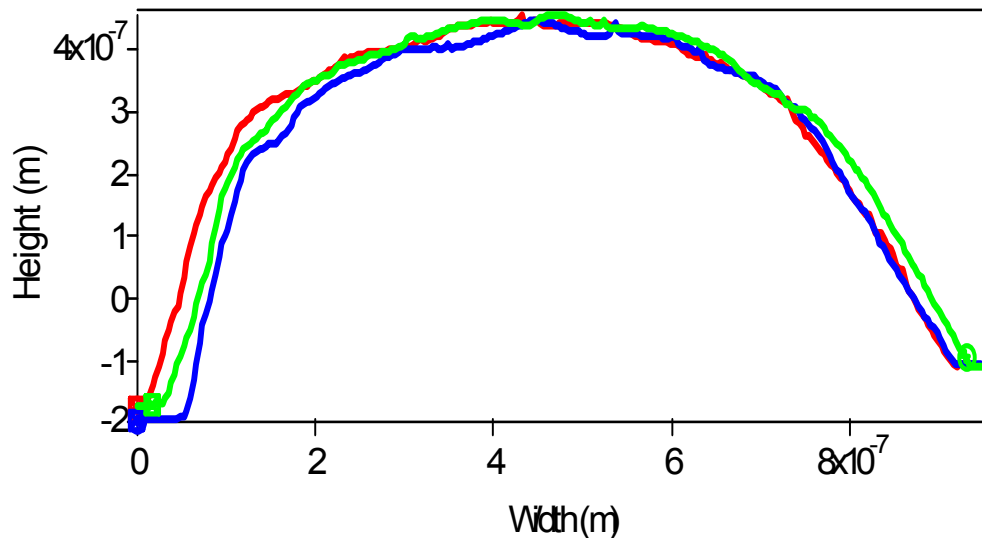
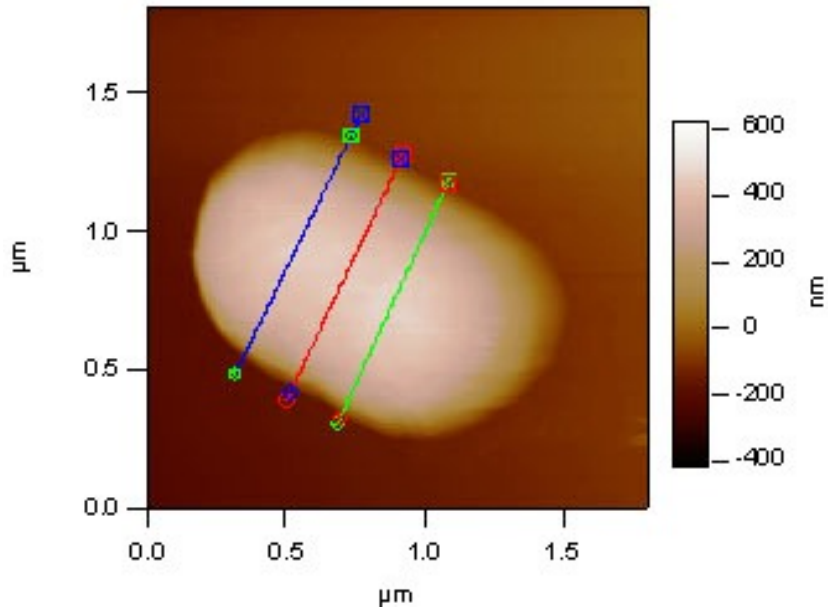
A.4 Zeta potential of *A. venetianus* RAG-1 measured in solutions of various electrolyte concentrations. A minimum of three measurements were taken for each data point.



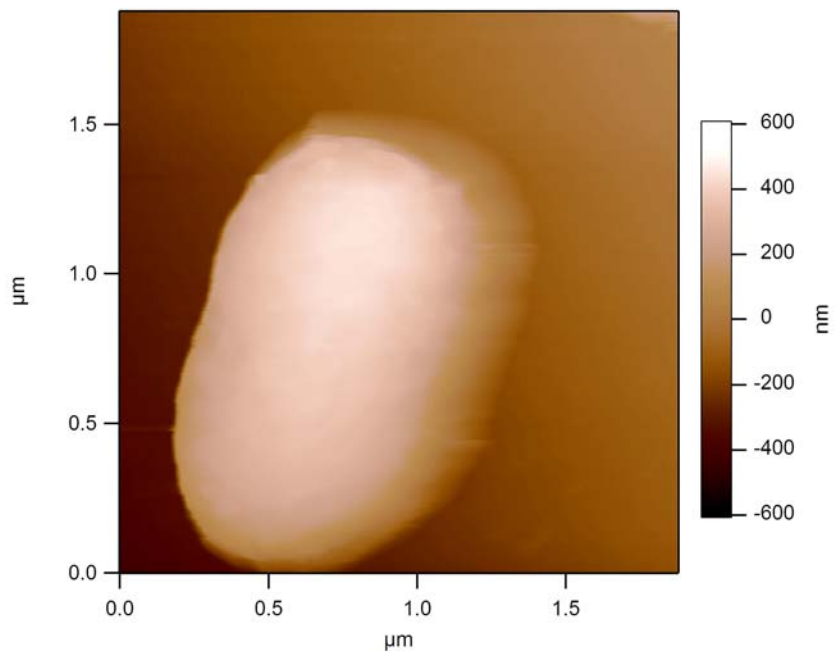
A.5 Zeta potential of *R. erythropolis* 20SE1c measured in solutions of various electrolyte concentrations. A minimum of three measurements were taken for each data point.



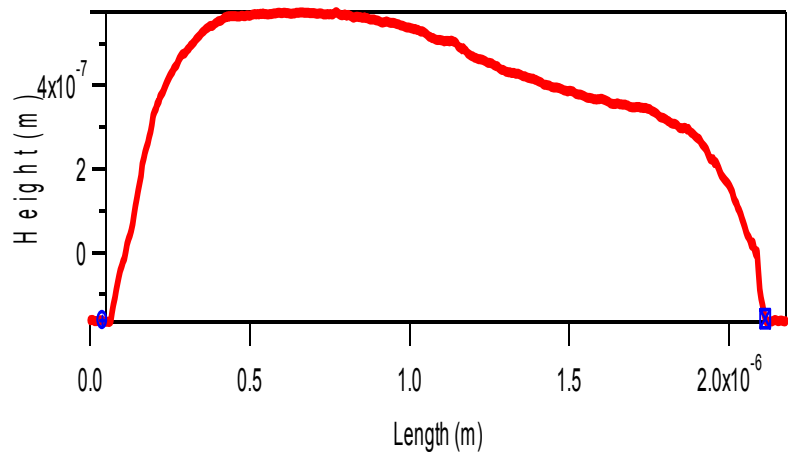
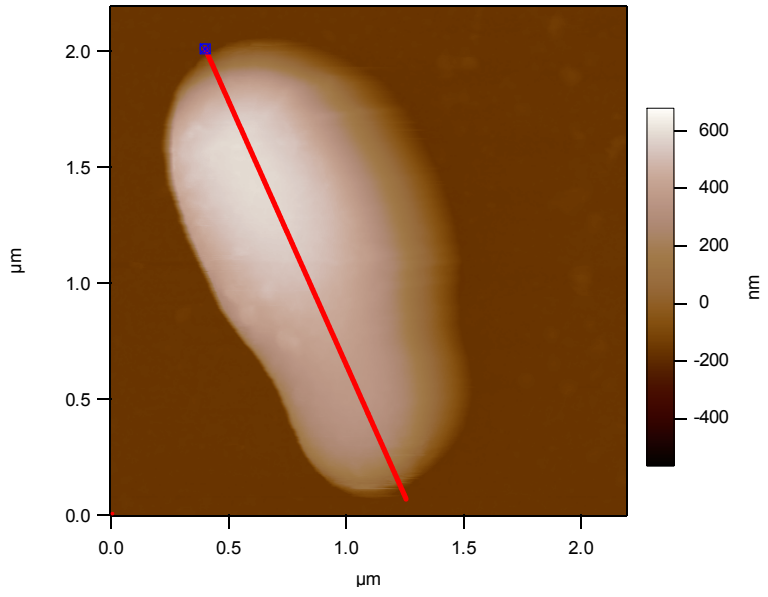
A.6 *A. venetianus* RAG-1 length measured from AFM height images in phosphate buffer.



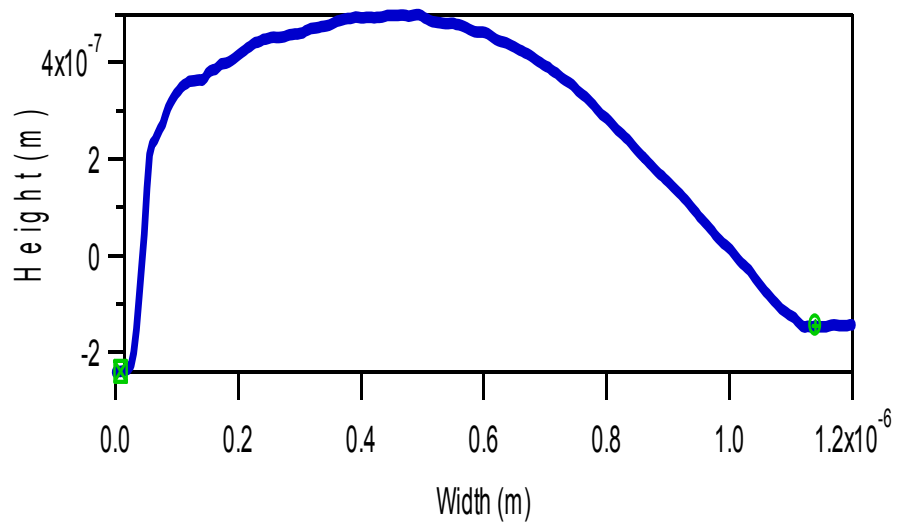
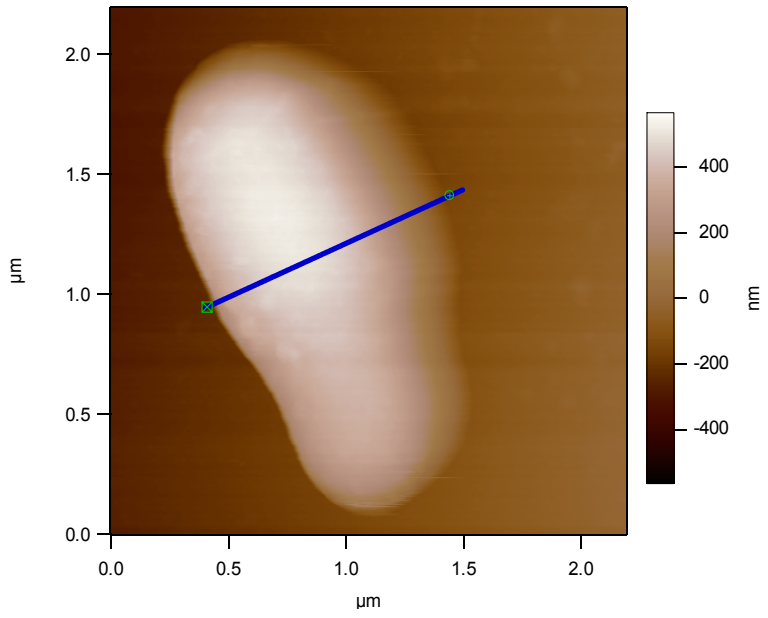
A.7 *A. venetianus* RAG-1 width measured from AFM height images in phosphate buffer.



A.8 *A. venetianus* RAG-1 height image taken in tapping mode in phosphate buffer.



A.9 *R. erythropolis* 20SE1c length measured from AFM height images in phosphate buffer.



A.10 *R. erythropolis* 20SE1c width measured from AFM height images in phosphate buffer.